CHIBA UNIVERSITY

The 20th CEReS International Symposium

# SOMIRES 2013

Symposium on Microsatellites for Remote Sensing

The 231th RISH Symposium

The International Workshop on GPS Radio Occultation Mission with a Microsatellite

# Proceeding

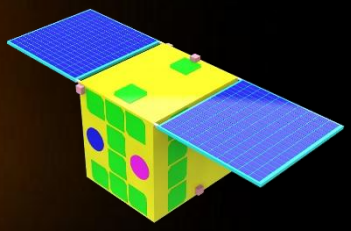

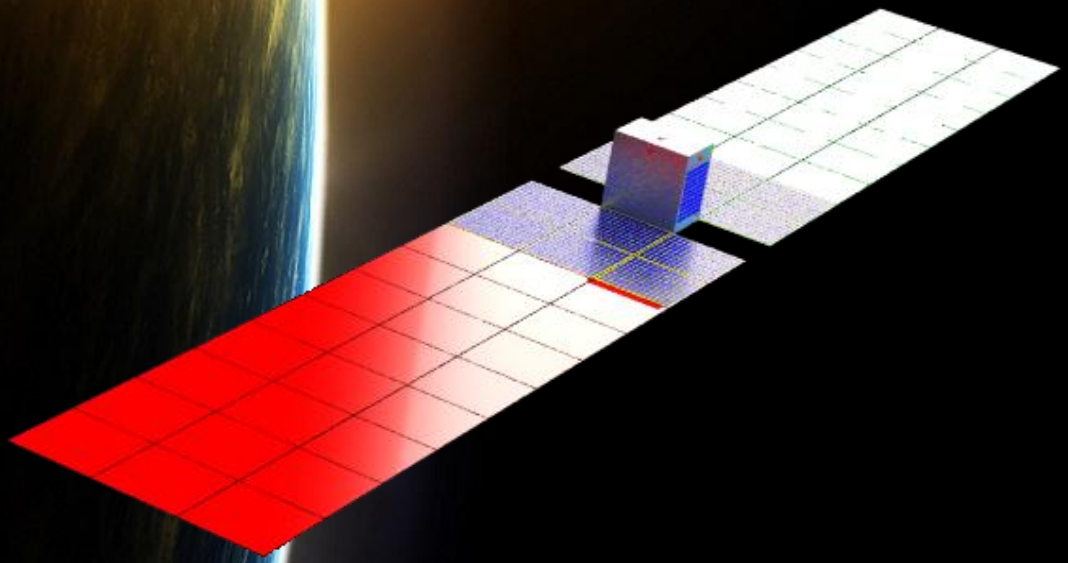

*Academic Link Center, University Library Complex*
*Nishi-Chiba Campus, Chiba University*
*1-33 Yayoi-cho, Inage-ku, Chiba-shi 263-8522 Japan*
*August 8 – 9 , 2013*

*ISBN : 978-4-901404-07-5*

# Program

## SOMIRES 2013 and 231th RISH

The 20th CEReS International Symposium or ***The Symposium on Microsatellites for Remote Sensing (SOMIRES 2013)*** is kick-off event of Chiba University microsatellite project and co-organized by Research Institute for Sustainable Humanosphere (RISH), Kyoto University (The 231th RISH Symposium): ***The International Workshop on GPS Radio Occultation Mission with a Microsatellite***. This symposium will provide an opportunity for researchers and system engineers to discuss new and viable technical topics of microsatellites, payload and spaceborne system, missions, analysis technique and applications for remote sensing.

## Organized and Sponsored by

- Center for Environmental Remote Sensing (CEReS), Chiba University
- Research Institute for Sustainable Humanosphere (RISH), Kyoto University
- Department Electrical and Computer Engineering, Ajou University, Korea.

## Contact Persons & Secretary :

**Contact Persons** :

**Prof. Josaphat Tetuko Sri Sumantyo**
Center for Environmental Remote Sensing (CEReS), Chiba University
1-33, Yayoi, Inage, Chiba 263 - 8522 Japan
Phone +81 43 290 3840 Fax +81 43 290 3857
Email : jtetukoss@faculty.chiba-u.jp

**Prof. Toshitaka Tsuda**
Research Institute for Sustainable Humanosphere (RISH)
Kyoto University, Uji, Kyoto 611-0011, JAPAN
Phone: +81-774-38-3804, FAX: +81-774-31-8463
E-mail: tsuda@rish.kyoto-u.ac.jp

**Secretary** :

**Dr. Yohandri**
Center for Environmental Remote Sensing (CEReS), Chiba University
1-33, Yayoi, Inage, Chiba 263 - 8522 Japan
Phone +81 43 290 3868 Fax +81 43 290 3857
Email : andri_unp@yahoo.com

## Collaborators:

# Symposium site

## Venue

1F, Contents Studio “Hikari”, Academic Link Center, University Library Complex, Nishi Chiba Campus, Chiba University, 1-33 Yayoi, Inage, Chiba 263-8522 Japan.

## Maps to access Symposium site:

- 3-min walk from JR Nishi-Chiba Station to the South Gate of Nishi-Chiba Campus
- 7-min walk from Keisei Midoridai Station to the Center Gate of Nishi-Chiba Campus

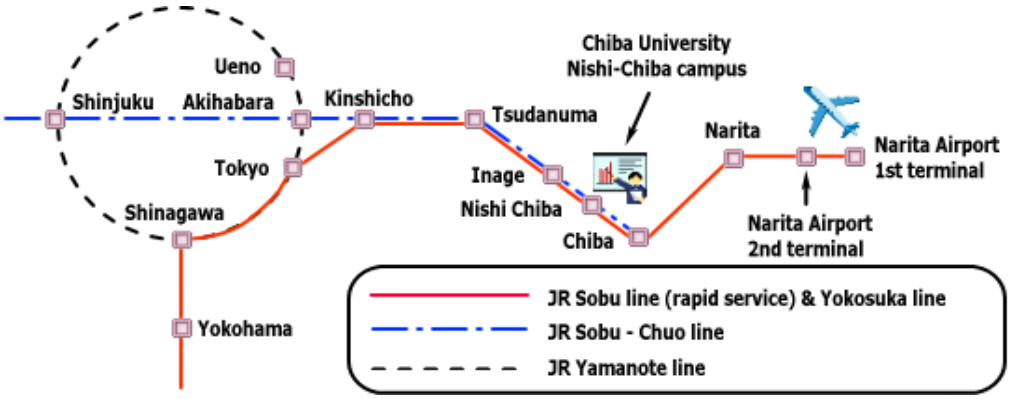


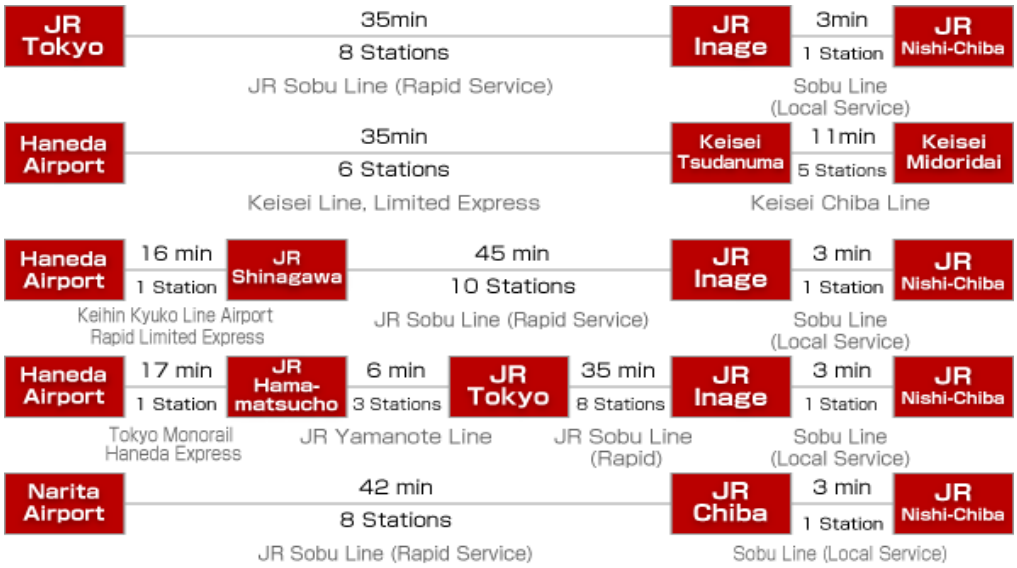

# Chiba University Map
# Nishi-Chiba Campus

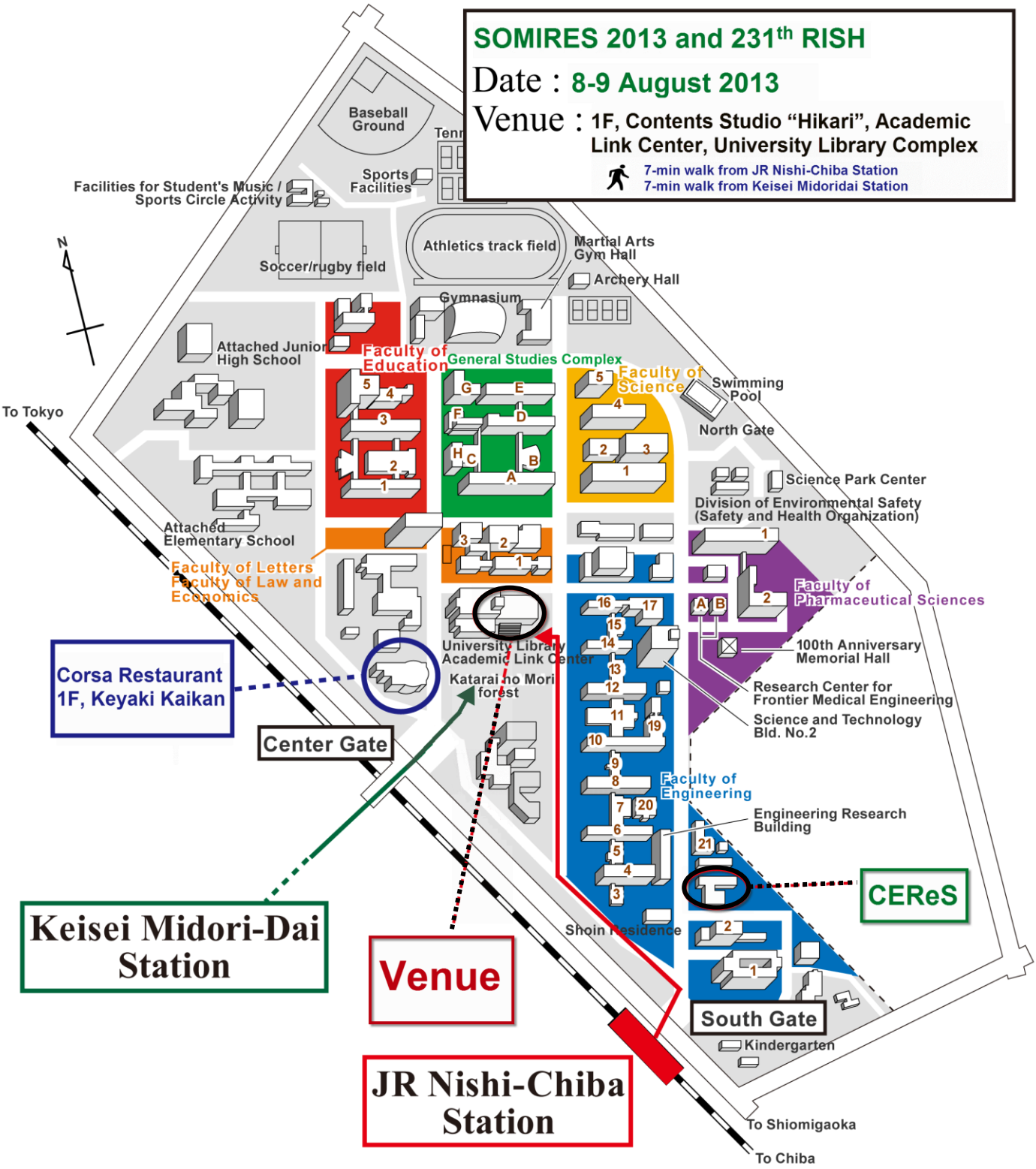

# Contents

# Event Schedule

## Thursday, August 8, 2013
### The International Workshop on GPS Radio Occultation Mission with a Microsatellite

| | |
|---|---|
| 09:00 – 09:30 | Registration |
| 09:30 – 10:00 | Opening Ceremony<br>Prof. Hiroaki Kuze, Director of CEReS, Chiba University<br>Prof. Toshitaka Tsuda, Director of RISH, Kyoto University<br>Prof. Josaphat Tetuko Sri Sumantyo, Microsatellites Project<br>Photograph Session<br>Break |
| **Session A1** | **Moderator : Prof. Josaphat Tetuko Sri Sumantyo** |
| 10:00 – 10:30 | Development of UAV and Microsatellites for Remote Sensing<br>*Josaphat Tetuko Sri Sumantyo (Chiba University), Koo Voon Chet (MMU Malaysia), and Robertus Heru Triharjanto (LAPAN Indonesia)* |
| 10:30 – 11:15 | GPS Radio Occultation Measurement Technique and Its Science Applications<br>*Bill Kuo and William Schreiner (University Corporation for Atmospheric Research USA)* |
| 11:15 – 11:35 | Experience from a GPS-RO mission on EQUARS<br>*Toshitaka Tsuda (Kyoto University), Hisao Takahashi(Instituto Nacional de Pesquisas Espaciais), and Yuichi Aoyama (National Institute for Polar Research)* |
| 11:35 – 12:00 | Impacts of RO Data on Rainfall Forecasts of Heavy Rainfalls and Typhoon Developments<br>*Hiromu Seko, Yoshinori Shoji, Masaru Kunii, and Hiromi Owada (Meteorological Research Institute/JAMSTEC)* |
| 12:00 – 13:00 | **Lunch** |
| **Session A2** | **Moderator : Prof. Koh-ichiro Oyama** |
| 13:00 – 13:25 | Science Accommodation for Space Missions with a focus on Radio Occultation Sensors and Transmitter Sources<br>*Chris McCormick (Moog), Brian Holz (Golden CO), Dr. Rob Kursinski (Moog), Erin Griggs (Moog)* |
| 13:25 – 13:50 | A distinct stronger warming in the tropical tropopause layer during 2001-2010 using GPS radio occultation: Association with minor volcanic eruptions<br>*Sanjay Kumar Mehta (Kyoto University), Masatomo Fujiwara (Hokkaido University), Toshitaka Tsuda (Kyoto University), Jean-Paul Vernier (Science Systems and Applications, USA)* |
| 13:50 – 14:15 | Electron Temperature Probe (ETP) for Microsatellite<br>*Koh-ichiro Oyama, C. Z. Cheng, Yu-Wei, Hsue (National Cheng Kung University, Taiwan)* |
| **Session A3** | **Moderator : Prof. Katsumi Hattori** |
| 14:20 – 14:45 | ELMOS Constellation: Lithosphere, Atmosphere and Ionosphere Monitoring by Small and Microsatellites<br>*Tetsuya Kodama (JAXA)* |
| 14:45 – 15:10 | GPS Total Electron Content (TEC) for Ionospheric Observation<br>*Katsumi Hattori, Shinji Hirooka, Chie Yoshino, (Chiba University) , Yuichi Otsuka(Nagoya University)* |
| 15:10 - 15:35 | Ionospheric Observations of FORMOSAT-3 and follow-on FORMOSAT-7<br>*Tiger J. Y. Liu (National Space Organization TAIWAN), (National Central University), G. S. Chang, S. J. Yu, T. Y. Liu (National Space Organization TAIWAN)* |
| 15:45 – 16:45 | **Visit facilities of Center for Environmental Remote Sensing, Chiba University** |
| 17:00 – 19:00 | **Banquet : Corsa Restaurant, Keyaki Kaikan (University Convention Hall), Chiba University** |

## Friday, August 9, 2013
## Spaceborne SAR Mission

**Session B1** **Moderator : Dr. Takuji Ebinuma**

10:00 – 10:25 Development of Space borne X Band SAR for 100 kg Satellite
*Hirobumi Saito, Atsushi Tomiki, Prilando Rizki Akbar (ISAS-JAXA), Takashi Ohtani, Kunitoshi Nishijo (JAXA), Jiro Hirokawa and Makoto Ando (Tokyo Institute of Technology)*

10:25 – 10:50 SAR Antenna Development in the UK
*Steven Gao (University of Kent), Yohandri and Josaphat Tetuko Sri Sumantyo (Chiba University)*

10:50 – 11:15 Korean Microsatellite Mission and VLBI Mission
*Tu-Hwan Kim, Dal-guen Lee, Jae-Hyun Kim, Hee-In Yang (Ajou University, Korea)*

11:15 – 11:40 Development of Bistatic GPS-SAR Image Processing Algorithm
*Takuji Ebinuma and Yoshinori Mikawa (University of Tokyo)*

12:00 – 13:00 **Lunch**

**Poster Session**

13:00 – 14:00

P01 Implementation of CP-SAR signal processing system on Virtex-6 FPGA
*Kei Iizuka, Kazuteru Namba, Josaphat Tetuko Sri Sumantyo (Chiba University)*

P02 Monitoring Land Subsidence by TerraSAR-X in Cengkareng, Jakarta City, Indonesia
*Ratih Fitria Putri, Luhur Bayuaji, Josaphat Tetuko Sri Sumantyo and Hiroaki Kuze, (Chiba University)*

P03 Three-dimensional electromagnetic-field distribution measurement system
*Satoshi Hasumi (Device Co).*

P04 Possibilities of Approach Integrating RS Multi-Data Analysis and GIS for Water Resources Management and Environmental Monitoring (The case study of Bili-Bili Irrigation System, Indonesia)
*Yaqien Gisno Ogalelano, Takao NAKAGIRI, Hiroki OUE, Dorotea Agnes RAMPISELA, Sartika LABAN (Ehime University)*

P05 Preliminary Study of Concrete Surface Temperature Mapping on Structure Problems in Makassar City with Airbone Thermal Remote Sensing
*Arwin Amiruddin(Hasanuddin University), Josaphat Tetuko Sri Sumantyo(Chiba University), Ilham Alimuddin, Merna Baharuddin (Hasanuddin University)*

P06 Array of Triangular Microstrip Antenna and Combined Triple Rectangular Microstrip Antenna for Radio Altimeter and Ground Penetrating Radar
*Merna Baharuddin, Elyas Palantei, Zulfajri B. Hasanuddin, Rusli, Andi Azizah (Hasanuddin University), Josaphat T. Sri Sumantyo (Chiba university)*

P07 FPGA Based Multiple Preset Chirp Pulse Generator for Synthetic Aperture Radar Onboard Unmanned Aerialvehicle System
*Kyohei Suto, Josaphat Tetuko Sri Sumantyo (Chiba University), CheawWen Guey, Koo Voon Chet (MMU)*

P08 Microwave dielectric constant measurement of arid soil in the 0.3-3 GHz frequency range and interrelationship with land cover and soil types
*Saeid Gharechelou, Ryutaro Tateishi, Josaphat Tetuko Sri Sumantyo (Chiba University)*

P09 The COTS-based Micro Earth Sensor(MESA) for small satelliteto The Symposium on Microsatellites for Remote Sensing (SOMIRES 2013) and The 231th RISH Symposium
*Kazuo Tanimoto, Takanobu Omoto(Meisei Electric), Hiroshi Tachihara(JAXA)*

P10 Allometric modeling for biomass estimation in remote sensing
*Ali Reza Sharifi and Jalal Amini (University of Tehran)*

P11 Doppler Centroid Ambiguity Analysis for High Resolution SAR Imagery Sensors
*Salar Gharibi and Jalal Amini (University of Tehran)*

| **Session B2** | **Moderator : Prof Koo Voon Chet** |
|---|---|
| 14:00 – 14:25 | UAVSAR Development Programme in Malaysia<br>*Koo Voon Chet (Multimedia University Malaysia), Hean-Teik Chuah (Universiti Tunku Abdul Rahman)* |
| 14:25 – 14:50 | Hyperspectral Camera for Microsatellite and UAV<br>*Yukihiro Takahashi (Hokkaido University)* |
| 14:50 – 15:15 | Modular and Compact Command & Data handling System with Fault-Tolerant Function for Microsatellite<br>*Dae-soo Oh and Myeong -Ryong Nam (JNM Korea)* |
| 15:20 – 15:30 | **Closing Ceremony** |

# DEVELOPMENT OF UAV AND MICROSATELLITES FOR REMOTE SENSING

*Josaphat Tetuko Sri Sumantyo1), Koo Voon Chet 2), Robertus Heru Triharjanto 3)*

1) Center for Environmental Remote Sensing, Chiba University, Japan
2) Faculty of Engineering & Technology, Multimedia University, Malaysia
3) Center for Satellite Technology, Indonesian Aeronautics and Space Agency (LAPAN), Indonesia

## ABSTRACT

Synthetic Aperture Radar (SAR) is well-known as a multi-purpose sensor in all-weather and day-night time. In this research, we are developing Circularly Polarized Synthetic Aperture Radar (CP-SAR) onboard microsatellite to observe land deformation on Earth surface under Japanese Ministry of Education and Technology (MEXT) program etc. The CP-SAR employs elliptical wave propagation and scattering phenomenon by radiating and receiving the elliptically polarized wave, including the specific polarization as circular and linear polarizations. The sensor is designed as a low cost, light, low profile of configuration to transmit and receive left-handed circular polarization (LHCP) and right-handed circular polarization (RHCP). Then these circularly polarized waves are employed to investigate relationship of physical information of scatterer and axial ratio, ellipticity, tilt angle etc. This sensor is also considered to reduce the effect of ionosphere's Faraday rotation. For ground experiment of CP-SAR, we also develop the CP-SAR onboard unmanned aerial vehicle (UAV CP-SAR) that is discussed in this paper.

***Index Terms***— Synthetic Aperture Radar, UAV, CP-SAR, microsatellite

## 1. INTRODUCTION OF CP-SAR MISSION

In this research, we propose Circularly Polarized Synthetic Aperture Radar (CP-SAR) sensor to retrieve the physical information of land surface and disaster monitoring. The sensor is designed as a low cost, light, low profile of configuration to transmit and receive left-handed circular polarization (LHCP) and right-handed circular polarization (RHCP). For this purpose, we also develop unmanned aerial vehicle (UAV) for ground experiment of this sensor [1]-[2], see Fig. 1 and Fig. 2.

The main mission of CP-SAR is to hold the basic research on elliptically polarized scattering and its applications. In the basic research, we will investigate the elliptical (including circular and linear polarizations)


Fig. 1. Successful first flight of Josaphat Laboratory Experimental Unmanned Aerial Vehicle (JX-1) at Fujikawa Airport, Japan on 7 June 2012.

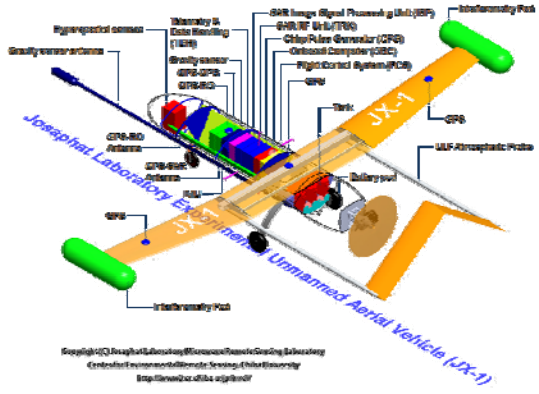


Fig. 2. Structure of Josaphat Laboratory Experimental Unmanned Aerial Vehicle (JX-1)

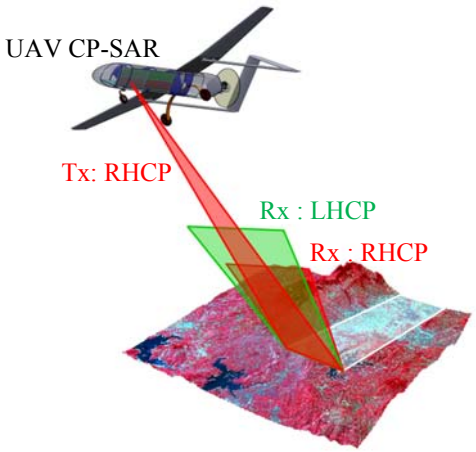


Fig. 3. Principle of CP-SAR sensor onboard UAV

scattering wave from the land surface, generation of axial ratio image, ellipticity and tilted angle images etc. We will hold the analysis and experiment of circularly polarized wave scattering on vegetation, snow, ice, soil, rock, sand, grass etc to investigate the elliptical scattering wave. These images will be extracted by using the received RHCP and LHCP wave. The principle of CP-SAR onboard UAV (UAV CP-SAR) is shown in see Fig. 3. This figure shows CP-SAR sensor transmits only one polarization, RHCP or LCHP, then this sensor will receive RHCP and LHCP scattering waves simultaneously. Then this image is employed to investigate the relationship of CP waves and physical characteristics of vegetation, soils, snow etc. The image of tilted angle as the response of land surface also will be extracted to mapping the physical information of the surface, i.e. geological matters, contour, tree trunk structure and its characteristics, snow-ice classification, vegetation characteristics etc.

In the application development, CP-SAR sensor will be implemented for land cover mapping, disaster monitoring, Cryosphere monitoring, oceanographic monitoring etc. Especially, land cover mapping will classify the forest and non-forest area, estimation of tree trunk height, mangrove area monitoring, Arctic and Antarctic environment monitoring etc. In disaster monitoring, CP-SAR sensor will be employed for monitoring of earthquake area, volcano activity, landslide etc. Especially, this L band CP-SAR sensor for UAV is being developed in our laboratory under Japan - Malaysia joint project (JICA-JST ODA program) in 2011 to 2014 to monitor landslide at Malay Peninsula and Southeast Asian countries in the future.

## 2. CP-SAR SYSTEM

The UAV CP-SAR (Fig. 1 and Fig. 4) is mainly composed by Flight Control System, Onboard Computer, Telemetry and Command Data Handling, Attitude Controller, and Sensors. Flight Control System is composed by manual and automatic flight module. Onboard Computer is employed

TABLE I. SPECIFICATION OF UAV CP-SAR

| Parameter | Value |
|---|---|
| Altitude | 1 to 4 km |
| Frequency range | 1270 MHz ± 150 MHz |
| Baseband range | DC to 150 MHz |
| Pulse transmission output power | 50 W, Pulse width 10 μs (max), Duty circle 2% (max) |
| Polarization | TX & RX : RHCP+LHCP |
| Transmission system gain | + 47 dB (min) |
| Receiver system gain | + 60 dB (min) |
| Gain flatness | ± 1.5 dB (max) |
| Receiver noise ratio | 3.5 dB (max) @+25ºC |
| Modulator | (RX and TX) QPSK |
| Output higher harmonic wave | -30 dBc (max) |
| Output spurious | -60 dBc (max) |
| Transmission system gain tuning function | 1/2/3/8/16 dB (0 to -31 dB) |
| Receiver system gain tuning function | 1/2/3/8/16 dB x 2 (0 to -62 dB) |
| Impedance | 50 Ω |
| Transmission system output VSWR | 1.5 : 1 (typ.) |
| Receiver system input VSWR | 1.5 : 1 (typ) |
| Transmission system antenna switching speed | 1μs (typ.) / 2 μs (max) |
| Receiver system antenna switching speed | 1μs (typ.) / 2 μs (max) |
| Transmission system On/Off speed | 100 ns (max) |
| Receiver system On/Off speed | 100 ns (max) |
| Power voltage | DC +28 V (DC +25 to + 35 V switchable) |
| Current consumption | 5A (max) |
| Temperature | +0ºC to 45ºC |
| Saving temperature | -20ºC to 80ºC |
| RF connector | SMA-Female |
| Power connector | N/MS3102A10SL-3P |
| Control connector | D-Sub-37P |
| Weight | 10 kg (max) |
| Size | W250mm x H100mm x D300mm |
| Pulse Length | 4.33 up to 47.63 μs |
| Off Nadir | 30° up to 60° |
| Resolution | Up to 1 m |
| Swath Width | 1 km |
| Antenna Size | 0.75 x 0.2 m (4 panels) |
| Axial Ratio | ≤3 dB |
| Antenna Gain | 14.32 dBic |

for controlling all sub-systems in UAV CP-SAR. Telemetry and Command Data Handling subsystems use S-band communications between UAV and ground station. Attitude Controller is composed by Inertial Measurement Unit (IMU) and four GPS units. Sensors are composed by CP-SAR as main mission sensor, and other sensors. CP-SAR sub-system itself is composed by chirp pulse generator module, Transmitter and Receiver (Tx-Rx) module, and Image Signal Processing module. Fig. 4 shows block

diagram of UAV CP-SAR that composed by UAV segment, ground station 1 and 2 segments. Especially, CP-SAR is mainly composed by RF system, chirp pulse generator, and image processing systems. Ground control segment has two units, where unit 1 for CP-SAR sensor monitoring and image processing. Unit 2 is employed for flight control and weather monitoring.

Fig. 5 shows the circuit of RF system or Tx-Rx module of CP-SAR. This system is composed by transmitter and receiver sub modules. The input of transmitter is In-phase (I) and Quadrature (Q) signal of chirp pulse generated by pulse generator with baseband range is DC to 150 MHz (normally 50 MHz). Then chirp pulse is modulated by frequency 1,270 MHz, where our Tx-Rx system has frequency range 1270 MHz ± 50 MHz (maximum ± 150 MHz). The transmission system has gain tuning function as 1, 2, 3, 8, 16 dB or 0 to -31 dB, and receiver has gain tuning function as 1, 2, 3, 8 and 16 x 2 or 0 to -62 dB. Power amplifier (PA) is available to control pulse transmission output power 50 W with pulse width maximum 10 μs, and maximum duty circle is 2%. The switching speed of transmission and receiver system antennas (RHCP and LHCP) is typically 1 μs and maximum 2 μs. The antenna is composed by two sets of CP microstrip array antenna (LHCP and RHCP panels), totally 4 panels to realize full polarimetric CP-SAR sensor. Size of Tx and Rx unit is W250 mm x H100 mm x D300 mm as one module in our CP-SAR system as shown in Fig. 4(b)-(c).

Fig. 5(d) shows our chirp pulse generator and image processing module. For the experiment, we could control the pulse length and bandwidth of chirp pulse (max 150 MHz). We save the data to SSD memory. We also plan to hold onboard processing for emergency mode and save raw data. Fig. 5(e) shows output of chirp pulse generator with bandwidth 50 MHz with center frequency 1.27 GHz.

## 3. CP-SAR ONBOARD UNMANNED AERIAL VEHICLE SYSTEM

In this research, the UAV CP-SAR as shown in Fig. 1 is developed for ground testing of CP-SAR. The platform called Josaphat Laboratory Experimental UAV (JX-1) has 25 kg of payload availability for various microwave sensors (CP-SAR, GPS-SAR etc) and optic sensors, i.e. hyper spectral camera. The operation altitude is 1,000 m to 4,000 m. The specification of CP-SAR sensor for UAV is center frequency 1,270 MHz, ground resolution up to 1 m, pulse length could be tuned from 4.5 to 48 μs, maximum pulse bandwidth 150 MHz, off nadir angle 30° to 60°, swath width 1 km, antenna size for 4 panels of CP-SAR 1.5 m x 0.4 m, PRF 1,000 Hz, and peak power 8.65 W (1 km) to 95 W (4 km). We plan to hold ground experiment with altitude less than 2 km with pulse transmission output power 50 W. The CP-SAR has receiver antenna composed by LHCP and

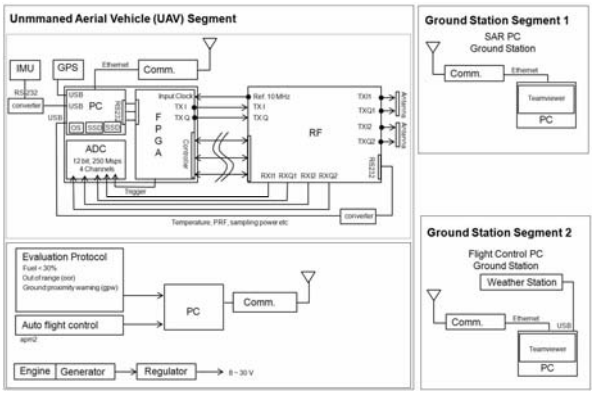


Fig. 4. Block diagram of UAV CP-SAR system

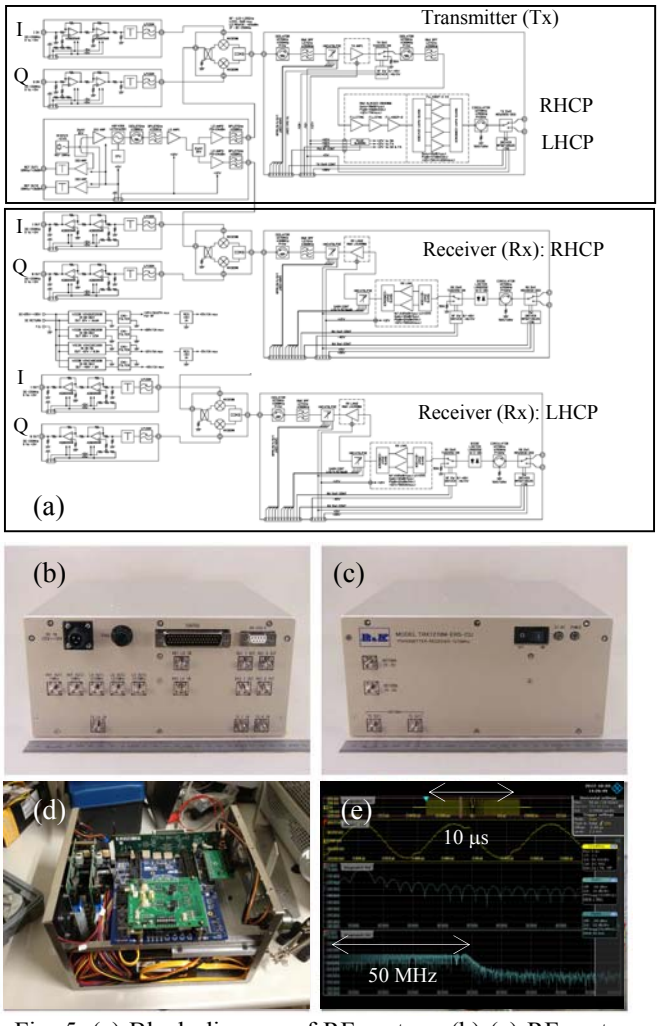


Fig. 5. (a) Block diagram of RF system, (b)-(c) RF system, (d) Signal Processing Module, and (e) Chirp pulse output

RHCP antenna. The data retrieved by LHCP and RHCP antenna [3] is employed to investigate the characteristics of elliptical polarization, including circular and linear polarizations.

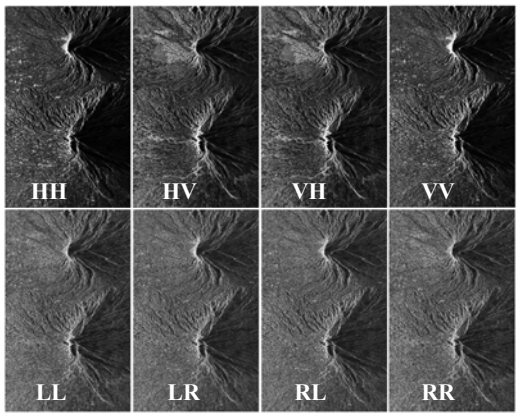

Fig.6. Images of linear and circular polarization

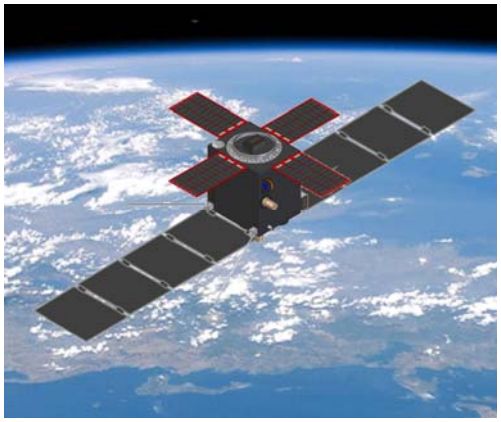
Fig.7. Illustration of CP-SAR onboard microsatellite

We have simulated circularly polarized waves with full polarization (LL, LR, RL and RR) as shown in Fig. 6 by using ALOS PALSAR polarimetric mode images. Where L and R is left handed circular polarization and right handed circular polarization, respectively. LR means LHCP transmission and RHCP receiving. In the future, further investigation of characteristics of circular polarization will be done by using our CP-SAR onboard UAV and microsatellite called LAPAN-Chibasat as shown on Fig. 7.

## 4. SUMMARY

In this paper, we introduce the progress of UAV development for ground experiment to investigate performance of our CP-SAR sensor. The CP-SAR is designed as small, light in weight and low power consumption system. The CP-SAR sensor is developed to radiate and receive elliptically polarized wave, including circularly and linearly polarized waves. In the near future, this sensor will be installed in our UAV and microsatellite that will be applicable for land cover mapping and disaster monitoring.

TABLE II. SPECIFICATION OF CP-SAR ONBOARD MICROSATELLITE

| Parameters | Values |
|---|---|
| Altitude | 550 km |
| Frequency | 1.27 GHz |
| Pulse length | 30 μs |
| Chirp bandwidth | 10 MHz |
| Off Nadir Angle | 30 degrees |
| Time Margin | 30 ms |
| Duty Cycle Maximum | 10% |
| Receiver Temperature | 300 K |
| Antenna Length | 6.0 m |
| Antenna Width | 1.8 m |
| Operational PRF | 1950 ~ 1880 Hz |
| Noise Figure | 3 dB |
| Normalized backscattering coefficient | -25 dB |
| Antenna Efficiency Loss | 2 dB |
| Single Antenna Panel Size | 500 x 500 x 3 mm |
| Transmit Peak Power | 687 Watts |
| Average Power | 39 Watts |
| Operational Duty Cycle | 5.85% |
| Operational Ground Swath Width | 67.08 km |
| Swath Width Time | 230 / 240 / 240 μs |
| Inclination angle | 97.591 degrees |
| Range Resolution | 15 m |
| Ground Resolution | 30 m |
| Azimuth Resolution | 3 m |
| Elevation Antenna Beamwidth | 4.8 degrees |
| Antenna Gain | 33.86 dB |

## ACKNOWLEDGEMENT

Thank to Japanese Ministry of Education and Technology (MEXT) for Integrated Earth Environment Diagnosis Program, JICA-JST ODA Program for Malaysia Peninsula landslide monitoring program, and Indonesian Aeronautics and Space Agency (LAPAN) for LAPAN-Chibasat program.

## REFERENCES

[1]J.T. Sri Sumantyo, "Microwave Remote Sensing Research and Education at Center for Environmental Remote Sensing, Chiba University," *IEEE Geoscience and Remote Sensing Society (GRSS) Newsletter*, Issue #159, pp. 32-38, June 2011.

[2] J.T. Sri Sumantyo, Chapter 11. Circularly Polarized Synthetic Aperture Radar onboard Unmanned Aerial Vehicle (CP-SAR UAV), Autonomous Control Systems and Vehicles, Kenzo Nonami edn., *Springer*, December 2012.

[3] Yohandri, V. Wissan, I. Firmansyah, P. Rizki Akbar, J.T. Sri Sumantyo, and H. Kuze, "Development of Circularly Polarized Array Antenna for Synthetic Aperture Radar Sensor Installed on UAV," *Progress in Electromagnetics Research C*, Vol. 19, pp. 119-133, January 2011.

# GPS Radio Occultation Measurement Technique and Its Science Applications

**Ying-Hwa Kuo[1] and William Schreiner**
*University Corporation for Atmospheric Research*
*[1]Email: kuo@ucar.edu*

## Abstract

The atmospheric limb sounding technique making use of radio signals transmitted by the Global Positioning System (GPS) satellites has emerged as a powerful and relatively inexpensive global observing system in all weather. As demonstrated by the proof-of-concept GPS Meteorology (GPS/MET) experiment and later by the CHAMP and SAC-C missions, the GPS radio occultation (RO) sounding data are shown to be of high accuracy and high vertical resolution. The GPS RO data provided by the joint U.S.-Taiwan COSMIC/FORMOSAT-3 mission, a constellation of six microsatellites launched in April 2006, have been shown to be extremely valuable for global numerical weather prediction, climate monitoring, and space weather forecasting. In this paper, we discuss the basic measurement technique of GPS radio occultation. We present the applications of RO data in weather, climate and space weather, based on the results from the COSMIC mission. We also discuss the development of the follow-on mission, COSMIC-2, which is expected to have an even greater impact on research and operation.

***Keywords:*** microsatellite, GPS, radio occultation, COSMIC

## 1. Introduction

The radio occultation (RO) technique, which makes use of radio signals transmitted by Global Position System (GPS) satellites, has emerged as a powerful and relatively inexpensive approach to sounding the global atmosphere with high precision, accuracy and vertical resolution in all weather, and the data are distributed uniformly over both land and ocean. This was first demonstrated by the proof-of-concept GPS/MET (GPS Meteorology) experiment in 1995-1997 (Ware et al. 1996), and further substantiated by the CHAMP (CHAllenging Minisatellite Payload, Wickert et al. 2001) and the SAC-C (Satellite de Aplicaciones Cientificas-C, Hajj et al. 2004) missions. In April 2006, the Formosa Satellite Mission #3/Constellation Observing System for Meteorology, Ionosphere and Climate (FORMOSAT-3/COSMIC, hereafter referred to as COSMIC) was successfully launched into initial orbits of 512 km from the Vandenberg Air Force Base. Within a year, the six COSMIC satellites are deployed to its final orbit of 800km. Anthes et al. (2008) summarized the early results of COSMIC mission. As of July 2013, COSMIC has produced 3.8 M GPS RO soundings, which have significant impact on operational weather prediction, climate monitoring, and space weather forecasting. Even though COSMIC has a mission life of five year, five out of the six microsatellites are still operating, producing 1,500 – 2,000 GPS RO soundings per day to support research and operation.

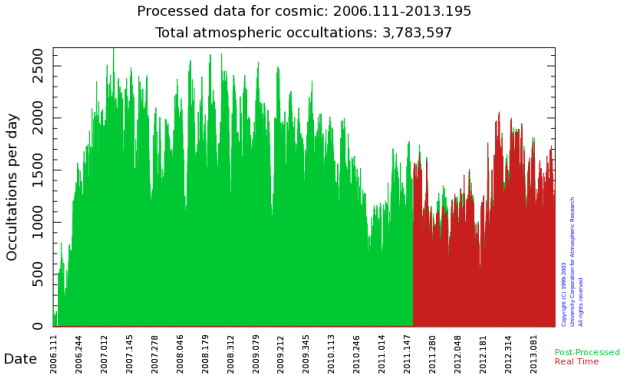


**Fig. 1. The number of COSMIC GPS RO soundings since launch. Red color indicates number of real-time soundings per day, and green color indicates number of soundings after post-processing.**

## 2. Radio Occultation Technique

The GPS RO measurements are based on the phase delay of GPS radio waves transmitted from a GPS satellite occulted behind the Earth as viewed from a low-Earth-orbiting satellite. The magnitude of the delay is related to the electron density in the ionosphere and the density of the neutral atmosphere. By tracking the signals transmitted from GPS we can obtain vertical profiles of bending angles, which can be used to retrieve information on electron density, atmosphere refractivity, temperature and water vapor (Kursinski et al. 1997).

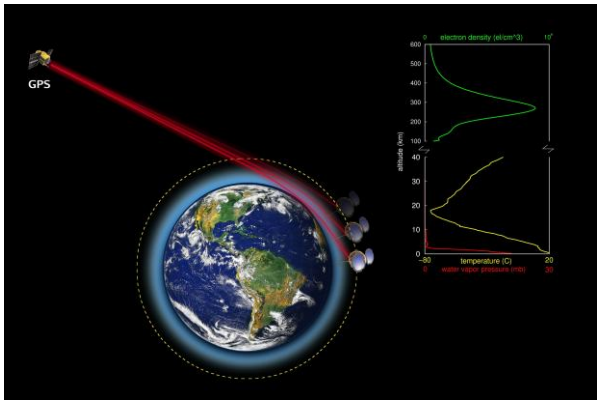


**Fig. 2. Schematic diagram illustrating the GPS RO measurement technique.**

## 3. COSMIC-2 Mission

Building upon the success of COSMIC, U.S. agencies and Taiwan are developing a follow-on RO mission (called FORMOSAT-7/COSMIC-2) that will launch six satellites into low-inclination (Equatorial) orbits in early 2016, and another six satellites into high-inclination (polar) orbits in early 2018. U.S. agencies, led by the National Oceanic and Atmospheric Administration (NOAA) and the U.S. Air Force and including NASA and NSF, are partnering with Taiwan's National Space Organization (NSPO) to execute the COSMIC-2 program. In comparison with the original COSMIC mission, COSMIC-2 will have several important advances. First, it will use the latest generation receiver, known as TriG, developed by the Jet Propulsion Laboratory (JPL), which can track radio signals from three global satellite navigation systems, including GPS (U.S.), GALILEO (Europe), and GLONASS (Russia). Second, an advanced antenna design will considerably boost the performance of radio signal tracking, resulting in considerably improved quality of radio occultation sounding. Third, through both tropical and polar constellation, COSMIC-2 will collectively produce more than 10,000 radio occultation soundings per day.

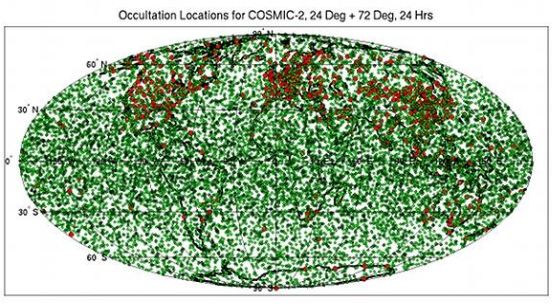


**Fig. 3. Global coverage of COSMIC-2 soundings in one day shown in green.**

## 4. Summary

With the continued operation of COSMIC through at least 2016 and the execution of the COSMIC-2 mission beginning with a first launch in early 2016 and a second launch in 2018, radio occultation data will continue to be freely available to support research and operations for many more years to come. With nearly an order of magnitude more RO data of higher quality expected to be available from COSMIC-2, unprecedented research opportunities will open up for weather, climate and space weather research, and the impact on operational NWP forecasting will be increased over the present, already significant, impact of COSMIC data (Anthes 2011).

## References

Anthes, R. A. and Coauthors (2008): The COSMIC/FORMOSAT-3 Mission: Early results. *Bull. Amer. Meteor. Soc.*, **89**, 313-333.

Anthes, R. A., 2011: Exploring earth's atmosphere with radio occultation: Contributions to weather, climate and space weather. *Atmospheric Measurement Techniques*, **4**, 1077-1103, DOI: 10.5194/amt-4-1077-2011.

Hajj, G., and Coauthors, 2004: CHAMP and SAC-C atmospheric occultation results and intercomparisons, *J. Geophys.Res.*, **109,** D06109, doi:10.1029/2003JD003909.

Kursinski, E. R., G. A. Hajj, S. T. Schofield, R. P. Linfield, and K. R. Hardy, 1997: Observing Earth's atmosphere with radio occultation measurements using the Global Positioning System. *J. Geophys. Res.*, **102**, 23429-23465.

Ware, R., and Coauthors 1996: GPS sounding of the atmosphere from low Earth orbit: Preliminary results. *Bull. Amer. Meteor. Soc.*, **77**, 19-40.

Wickert, J., and Coauthors, 2001: Atmosphere sounding by GPS radio occultation: First results from CHAMP. *Geophys. Res. Lett.*, **28**(17), 3263-3266

# Experience from a GPS-RO Mission on EQUARS

**Toshitaka Tsuda[1], Hisao Takahashi[2], and Yuichi Aoyama[3]**

[1]*Research Institute for Sustainable Humanosphere (RISH), Kyoto University,*
[2] *Instituto Nacional de Pesquisas Espaciais (INPE), Brazil,*
[2]*National Institute for Polar Research (NIPR),*
*tsuda@rish.kyoto-u.ac.jp*

## Abstract

In collaboration with INPE, we promoted a project on GPS radio occultation, aiming as a launch of a small LEO satellite named EQUARS (Equatorial Upper Atmosphere Research Satellite) in 2000s. We basically completed design of the satellite together with antenna and receiver system for the GPS RO mission. EQUARS was also planned to carry several sensors for optical airglow, in-situ measurements of ionospheric electron density, and plasma parameters. However, unfortunately, INPE has suspended the whole plan of EQUARS, whose launch was originally planned in 2006. We introduce here outline of the GPS RO mission proposed for EQUAS.

## 1. Background of GPS-RO Mission

From our recent knowledge of dynamical processes in the Earth's atmosphere, it is well known that the equatorial atmosphere plays an important role with respect to energy sources, transport, and global circulation. Atmospheric waves, such as gravity waves, tides and equatorial waves, generated in the tropical troposphere, play a significant part in transportation of wave energy and momentum flux to the middle atmosphere and ionosphere. Deposition of momentum and energy in the upper atmosphere drives the general circulation of the middle atmosphere. Gravity waves trigger ionospheric disturbances (Plasma bubbles). It is only in recent years that an integrated picture of the energy balance of the middle and upper atmosphere is beginning to emerge.

One of our special interests is to understand the dynamical and plasma characteristics of the equatorial atmosphere over Indonesia, South America and Africa where land-sea-ocean interactions are most active in the world. Plasma bubbles in the ionosphere directly affect satellite telecommunications. Changes in the global scale circulation of the lower atmosphere, such as those associated with El Niño and La Niña, greatly affect the climate not only in the tropics but also regions at middle and high latitudes.

Recent GPS RO mission; GPS/MET, CHAMP, SAC-C, GRACE, COSMIC, METOP, etc, have provided us a great opportunity to understand a global picture of the atmosphere dynamics and ionosphere irregularities. Further observations with more GPS RO missions are needed. For this reason we encourage the GPS-RO mission promoted by CEReS of Chiba University.

## 2. GPS-RO on EQUARS

For observations of atmospheric and ionospheric characteristics, the Brazilian space agency (INPE) announced a plan of a small LEO satellite named EQUARS (Equatorial Atmosphere Research Satellite). Then, we proposed a GPS RO measurement on EQUARS. Inclination angle of the EQUARS orbit was less than $20^{o}$ so it can obtain a dense data-set of temperature, humidity and electron density in the equatorial atmosphere. GPS-RO data are also useful to improve weather forecast at low latitudes through a real-time assimilation for a numerical weather prediction model.

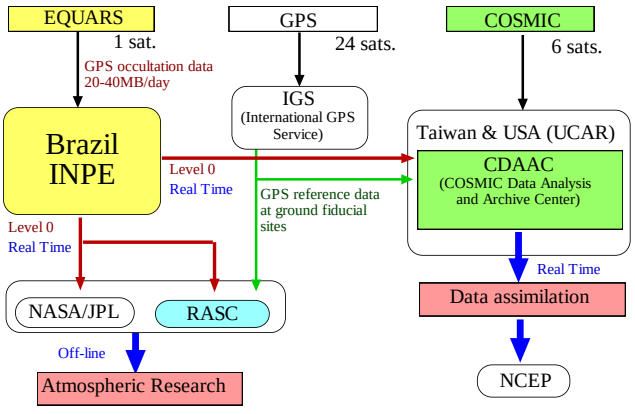


Figure 1 Data acquisition, transfer and analysis system for GPS RO mission of EQAURS

Figure 1 shows our proposal for a data transfer and analysis system of GPS occultation data that was considered for EQUARS. Raw data will be down-loaded to the

Brazilian ground station at Natal (7S, 60W), which, however, misses some orbits in the case that the inclination angle of EQUARS is larger than about 15 degrees. For a real-time data transfer, we needed to find another ground-based tracking station in the East Asia, such as Biak in Indonesia, Darwin in Northern Australia, and Bangalore in India.

We planned to transfer the Level-0 to Japan (RASC) on a real-time basis. The data was also planned to transfer to CDAAC at UCAR for distribution to a wider user community, including meteorological agencies for data assimilation into a numerical weather prediction model.

It is necessary for CEReS to establish a similar data transfer and analysis system for the new LEO experiment. GPS RO data is most useful when they are processed on a real-time basis and transferred to a meteorological agency with latency not longer than a few hours.

## 3. Antenna Design for EQUARS

For a GPS RO mission, two types of antennas are normally installed on a LEO satellite. One antenna with a high-gain (about 15 dB) is attached on the side panel of a satellite in the orbit direction. And, it is pointed about 20-25 degrees downward so as to observe limb of the Earth. The other antenna can be a small omnidirectional one for conventional positioning. Two sets of the antenna pairs could be installed on the fore and rear sides of the LEO satellite in order to measure both rising and setting occultation events. Figure 2 shows two examples of the occultation antenna that were considered for EQUARS; phased array with patched antenna and a high-gain antenna.

## 4. Summary

GPS RO data is useful not only for atmospheric science but also operational meteorology. GPS RO mission needs a careful design for both instruments/firmware on board a satellite and ground-based data analysis system. We hope the new GPS-RO experiment promoted by CEReS will be successful by obtaining intensive supports from international community.

**(a)**

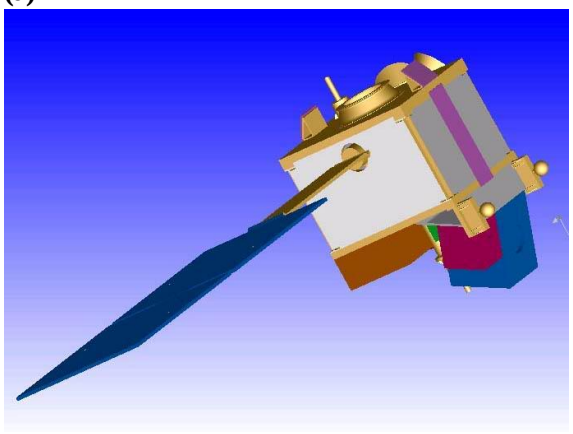

**(b)**

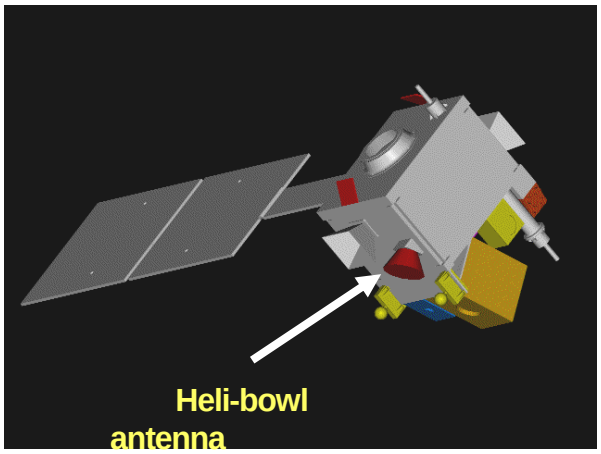


Figure 2 Two examples of antenna for occultation. (a) A phased array consisting of four micro-strip patch panels. Although the antenna is attached to the satellite, antenna core-sight is tilted about 20-30 degrees downward relative to the satellite orbit for pointing toward limb of the Earth. (b) a heli-bowl antenna with high-gain, which was used for CHAMP.

# Impacts of RO Data on Rainfall Forecasts of Heavy Rainfalls and Typhoon Developments

**Hiromu Seko[1], Yoshinori Shoji[2], Masaru Kunii[2], and Hiromi Owada[3]**
[1] *Meteorological Research Institute/JAMSTEC,* [2]*Meteorological Research Institute,*
[3]*Numerical Prediction Division/Japan Meteorological Agency, E-mail hseko@mri-jma.go.jp*

## Abstract
Radio waves (RWs) that are transmitted from satellites of the Global Navigation Satellite System (GNSS) are delayed and bent by atmosphere in which the paths of the RWs pass before reaching low earth orbit (LEO) satellites. In radio occultation (RO) observations of GNSS satellites, information of water vapor and temperature is obtained from the bending angle or delay of the RWs. In this presentation, the results of data assimilation (DA) experiments of GNSS RO data in the Meteorological Research Institute (MRI) and the recent usage progress of GNSS RO data in the operational global DA system of the Japan Meteorological Agency (JMA) are explained.
***Keywords*** **:** Radio Occultation, Data Assimilation, Rainfall Forecast, Heavy Rainfall.

## 1. Introduction
In the Japan, humid airflows supplied from the sea often cause heavy rainfalls. Middle-level dry layers also enhance heavy rainfalls, because they increase convective instability. Thus, water vapor distribution over the sea and its vertical profiles are needed to increase accuracy of the numerical forecasts. Global Navigation Satellite System (GNSS) radio occultation (RO) data were used as data assimilation (DA) data because it provides vertical profiles of refractivity. To show the impact of the RO data on the numerical forecasts, it was applied to events of heavy rainfalls and typhoons. Apart from RO, ground-based GNSS data, such as precipitable water vapor (PWV) or slant water vapor (SWV) (Fig. 1), are also expected to improve water vapor distributions in the analyzed fields. To show synergy effects of RO and ground-based GNSS data, simultaneous assimilations of these data was also performed. RO data was also expected to be a useful data that improves temperature distributions. The 'Yamase' phenomenon, in which cold airflows cause stratus clouds east of the northern Japan, was also adopted as a target of RO DA experiments.

## 2. Data assimilation experiments of RO data
DA methods of RO data and PWV, SWV have been developed so far (Seko et al., 2010; Seko et al., 2004), and their impacts on rainfall forecasts were investigated with the Mesoscale 4-dimensional Variational DA system (Meso-4DVar) of the Japan Meteorological Agency (JMA). These methods were applied to a heavy rainfall that occurred at the northern Japan on 16 July 2004 (Seko et al., 2010). Figures 2-4 show the distributions of predicted rainfall regions and increments of the analyzed water vapor fields. When PWV data were assimilated, water vapor in the rainfall region was increased and on the northern sides was decreased, and then the shape of the rainfall region became similar to the observed one. However, the reproduced rainfall amount remained smaller than the observed one. When the RO data were assimilated, the low-level water vapor was increased so that the rainfall amount was largely increased. When PWV and RO data were assimilated simultaneously, low-level water vapor in the rainfall region and on its southern side was increased, and then shapes of rainfall region and the rainfall amount became similar to the observed ones.

RO data was also used to investigate impacts on the development of a tropical cyclone (TC), 'Usagi' that occurred in July 2007 (Kunii et al., 2012). Impacts of the RO refractivity are compared against the JMA's global analysis (GA) by conducting forecasts using the JMA non-hydrostatic model (Fig. 5). When the GA was used for the initial field, no typhoon was formed in the forecast model. In contrast, when the GA was replaced by the Meso-4DVar analysis (MA), the generation of the TC was successfully simulated. When RO data was assimilated, the intensity forecast was significantly improved (MA_RO). The results indicate that RO data is beneficial for the TC forecast.

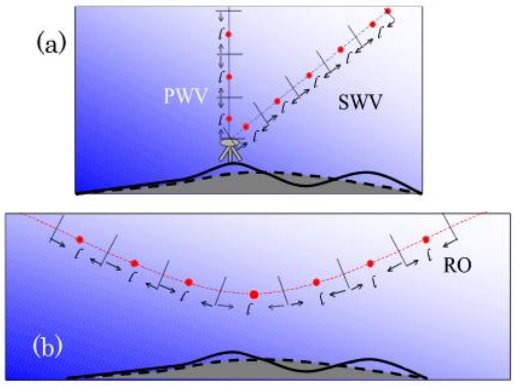

Fig. 1. Schematic illustrations of the observation operators of (a) PWV and SWV, and (b) RO data. Thick solid and broken lines indicate actual topography and model topography, respectively.

Third target is a cold weather (Yamase) in summer over the northeastern Japan, which is produced by a cool polar maritime air mass that develops over the North Pacific, including the Bering Sea and the Sea of Okhotsk. It usually accompanies boundary layer clouds (Yamase clouds) on east of the northern Japan. Yamase also influences the agricultural crops. It is needed to predict Yamase accurately. In this study, RO data was assimilated by the nested Local Ensemble Transform Kalman Filter (LETKF) system (Miyoshi and Aranami, 2006). When conventional data of the JMA was assimilated by the LETKF system, Yamase clouds were reproduced in all of the ensemble members. However, impacts of RO data on the Yamase clouds remained relatively small because the positions of RO data were far from the Yamase clouds. The number of Yamase events to which RO assimilation experiments are applied should be increased in order to show the impact of RO data more clearly.

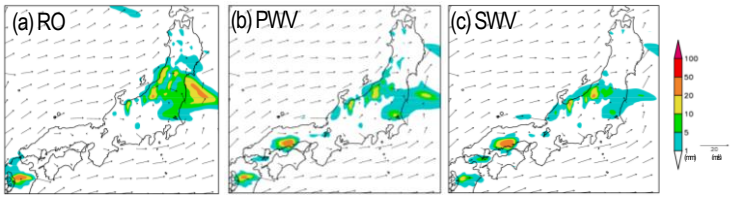

Fig.2 Reproduced 3-hour rainfall of forecast time from 0 to 3 hours reproduced from the analyzed fields. Valid time is 15 to 18 JST 16 July 2004.

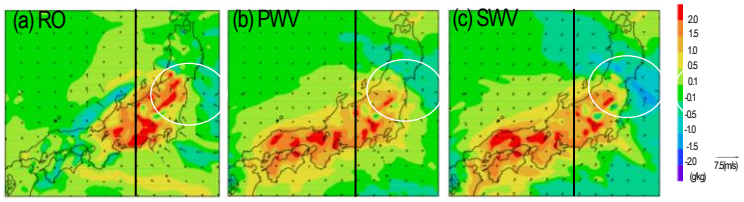

Fig.3 Horizontal distributions of the difference of water vapor from 'CNTL' at the height of 21 m. Black lines indicate the position of the vertical cross sections of Fig. 4.

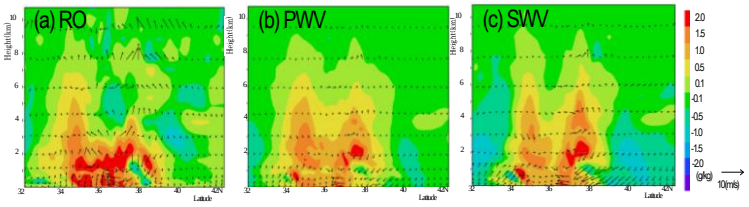

Fig.4 Vertical distribution of the difference of water vapor from 'CNTL' at the latitude of 138 deg. Vectors represent horizontal wind direction and velocity.

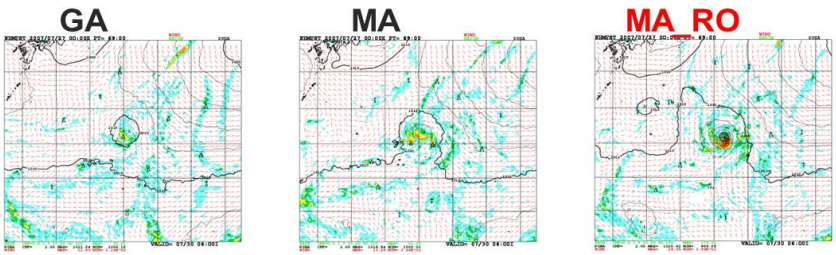

Fig.5 Distributions of sea-level pressure (contour, hPa), surface wind (vector, $ms^{-1}$), and 3 h accumulated precipitation (color, mm) at 1800 UTC 29 July 2007 predicted by NHM using different initial fields. (a) GA, (b) MA, and (c) MA _RO.

## 3. Recent usage progress of RO data in the operational global DA system of the JMA

The JMA began assimilating RO refractivity data into its operational global NWP system on March 22, 2007, and revisions to this process were implemented in the system on December 18, 2012. A bias correction procedure had been implemented in the preprocessing of RO data due to the presence of systematic biases in the tropical and polar regions (Owada et al. 2012). As the biases were reduced via updates of the observation operators, the correction procedure was eliminated. Observation system experiments for the new assimilation configuration, which includes these updates, showed that analyses and forecasting of temperature and sea surface pressure were improved, especially in the Southern Hemisphere. Most of the improvements were brought about by the observation operator updates.

### Acknowledgements

The CHAMP data and ground-based GPS data were provided from the GFZ and GSI. The COSMIC refractivity we used was calculated at the COSMIC Data Analysis and Archive Center. The Meso-4DVar system was developed by the Numerical Prediction Division of the JMA.

### References

1) Kunii, M., H. Seko, M. Ueno, Y. Shoji, and T. Tsuda, Impact of Assimilation of GPS Radio Occultation Refractivity on the Forecast of Typhoon Usagi in 2007, *J. Met. Soc. Japan*, **90**, 255-273 (2012).
2) Miyoshi, T., and K. Aranami, Applying a Four-dimensional Local Ensemble Transform Kalman Filter (4D-LETKF) to the JMA Nonhydrostatic Model (NHM), *SOLA*, **2**, 128-131 (2006).
3) Owada, H., and K. Yoshimoto, Recent Updates on the Usage of GNSS RO Data in JMA's Operational Global Data Assimilation System, *CAS/JSC WGNE Res. Activ. Atmos. Oceanic Modell*. **42**, 1-11 (2012).
4) Seko, H., M. Kunii, Y. Shoji, and K. Saito, Improvement of Rainfall Forecast by Assimilations of Ground- Based GPS Data and Radio Occultation Data, *SOLA*, **6**, 33-36 (2010).
5) Seko, H., T. Kawabata, T. Tsuyuki, H. Nakamura, and K. Koizumi, Impacts of GPS-derived Water Vapor and Radial Wind Measured by Doppler Radar on Numerical Prediction of Precipitation. *J. Met. Soc. Japan*, **82**, 473-489 (2004).

# Science Accommodation for Space Missions with a focus on Radio Occultation Sensors and Transmitter Sources For The Symposium on Microsatellites for Remote Sensing (SOMIRES 2013) and The 231th RISH Symposium

**Chris McCormick[1], Brian Holz[2], Dr. Rob Kursinski[1], Erin Griggs[1]**
[1]*Moog, Golden CO,* [2]*O3B Networks*

## Abstract

Science Accommodation and Science Instrument hosting from a space mission and space resources design "Total Systems & Science Engineering" perspective. This paper will present a short end-to-end science coordination mission, along with first introduction of the Ka-Band occulting system in the planning stages using the newly launched O3B Networks medium Earth Orbit equatorial communication spacecraft as the Ka Band source.

## 1. Introduction

Radio Occultation has been used on many of the planets to date, generally at higher frequencies than L-Band, in the S- to Ka-Bands (2.3 to 30+ GHz). General RO methods at Earth, has been used with the L-Band due to the prominence of 'free' transmitters with the GNSS systems. An extension of this method into the Ka-Bands (~20 GHz) on a newer system launched in 2013 system is described. The information to be presented is twofold, one on the mission and payload description for Ka-Band radio occultation, and two, on the process of designing spacecraft for science missions, with this Ka-Band mission being the example.

## 2. Methods

The O3B satellites are orbiting roughly 8000 km altitude over the equator with coverage ~ +/-45 degrees of Latitude, see **Figure 1**. There are 12 satellites in the first constellation, with a plan for a total of 24; with 4 in orbit now, and 4 more launching September 2013. The downlink frequencies that are available are mostly from 17.8 to 19.3 GHz with some higher to 20.2 GHz. It is possible for their satellites to have some of their dishes pointing at the Earth Limb. These would transmit two or more pure carrier frequencies to use for occulting signal reception. The antennas on the O3B spacecraft are approximately 30 cm, and at 19 GHz, that is 44 dB of gain, and ~ 3 degree beam width. See **Figure 2**. For the receiver spacecraft, we can have larger antennas if desired, but a 30 cm one is used for analysis, both from the science perspective, and for its impact on pointing requirements and platform stability requirements levied on the spacecraft design.

The Receiving spacecraft orbits will be modeled after the COSMIC system, though with 12 to 24 spacecraft in 72 degrees inclination and 800 km circular orbits. Real time communications can also be performed with the O3B spacecraft, or alternately with Inmarsat. Standard ground stations can be used to collect the resultant occultation data for store and forward methods.

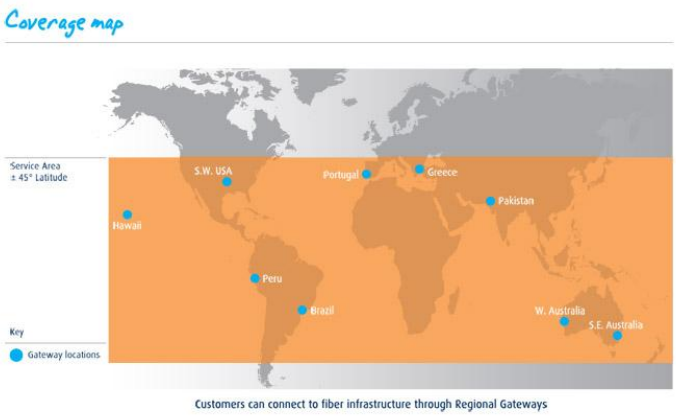


**Fig. 1 Occulting Coverage in Ka-Band (1)**

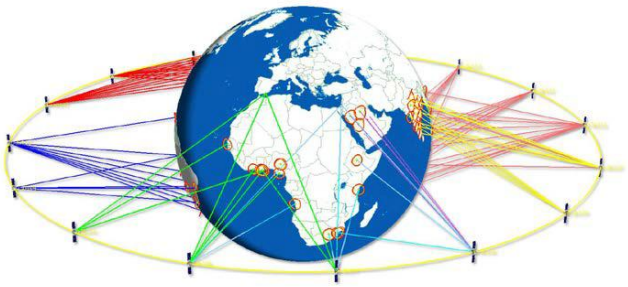

**Figure 2. Spacecraft steerable spot beams (1)**

## 3. Results and Discussion

Results will be shown for Occulting statistics if Ka band receivers were on board 12 to 24 higher inclination satellites, with a discussion of similar data products with

higher energy carriers and shorter wavelengths of ~1.6 cm plausible for ingestion into forecasting models. **Figure 3** below are estimate of standard deviation of water vapor error for clear sky tropical profile retrieved tracking four O3B signals at 17.8, 18.6, 19.3 and 20.2 GHz.

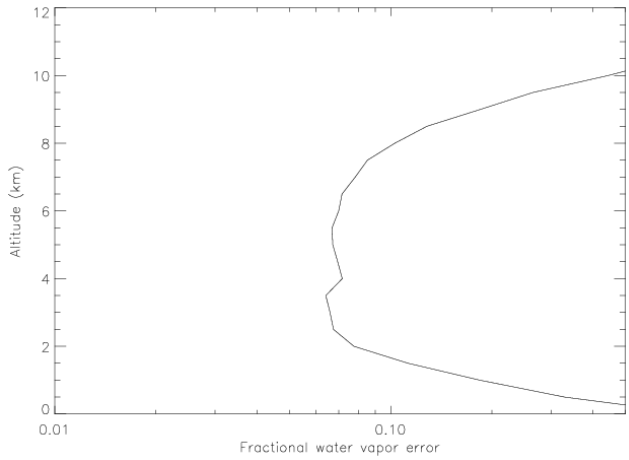


**Figure 3** Tropical water vapor error (2)

Suggestions and first level design constraints are also shown for hosting occulting receivers at these frequencies, and their proposed antenna design gain patterns and pointing control. Spacecraft accommodation system engineering is addressed and interactions of the classical spacecraft subsystem trades are presented, for spacecraft and instrument for GNSS-RO and Ka-RO for spacecraft such as depicted in Figure 4.

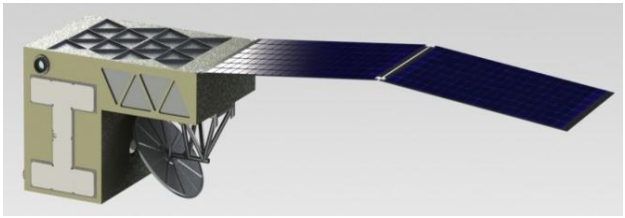

**Figure 4 – GNSS & Ka Radio Occultation spacecraft concept (2)**

## 4. Summary

Radio Occultation information content is not restricted to GNSS-RO; and should be investigated in most all available *stable* frequency sources. This describes one current Ka-Band radio source and how an RO system could be implemented, as well as some projected data quantity and data utility for ingesting into the forecast models.

## Acknowledgements

This symposium is sponsored by Center for Environmental Remote Sensing (CEReS), Chiba University and Research Institute for Sustainable Humanosphere (RISH), Kyoto University.

## References

1) O3B Networks, www.o3bnetworks.com
2) Moog, www.Moog.com

## Contacts

1) Chris McCormick; cmccormick@moog.com
2) Rob Kursinski; rkursinski@moog.com

# A distinct stronger warming in the tropical tropopause layer during 2001-2010 using GPS radio occultation: Association with minor volcanic eruptions

**Sanjay Kumar Mehta[1], Masatomo Fujiwara[2], Toshitaka Tsuda[1], Jean-Paul Vernier[3]**
[1]Research Institute for Sustainable Humanosphere (RISH), Kyoto University, Japan; [2]Faculty of Environmental Earth Science, Hokkaido University, Japan; [3]Science Systems and Applications, Inc., Hampton, VA 23666, United States.

## Abstract

The trends and various interannual variability components in the tropical tropopause layer (TTL) over the tropics (15°S-15°N) were examined by employing upper air data from GPS radio occultation (RO), radiosondes (IGRA, RICH, and HadAT2), and ERA-Interim during the period 2001-2010. The detection capability of the GPS RO, though with limited data coverage, has been shown in previous studies. A detailed analysis of the warming observed in the TTL from 2001 to 2010 using both standard linear and multiple regressions is carried out. The temperature trends estimated using standard linear regression analysis (with only constant and linear trend terms) reveals a strong warming of about 0.5-1.5 K/decade in the TTL in each dataset during 2001-2010. This strong warming in the TTL is not explained by the global warming. The contribution from various interannual variability components such as quasi-biennial oscillation (QBO), El Niño southern oscillation (ENSO), and stratospheric aerosol optical depth (AOD) is separated using multiple regression analysis techniques. We performed two types of multiple regression analysis that do not consider and that consider seasonal modulation of the interannual components. The distinct warming in the TTL is found to be partly associated with the minor volcanic eruptions during the first decade of the 21st century. Positive and significant AOD responses to the temperatures of about 0.1-0.2 K are observed in the TTL region, explaining about 5% to 15% of the total variance during 2001-2010.

***Keywords*** **:** Tropical tropopause layer, temperature trend, minor volcanic eruptions

## 1. Introduction

GPS radio occultation (RO) measurements are independent and calibration free, and they provide high-quality observations to monitor the TTL with global coverage and essentially all-weather capability and consistency [Kussinski et al., 1997]. The climate utility of GPS RO has been demonstrated in several earlier studies and more recently Steiner et al. [2009] observed that even short GPS RO records show tropospheric warming and stratospheric cooling, and pointed out the capability of GPS RO to become the future climate benchmark, reported warming in the tropical tropopause region for the period February 1997-2008. Recently, an increased amount of stratospheric aerosol due to minor volcanic eruptions was observed about 17-21 km during the first decade of the 21st century [see Vernier et al., 2010], which might have had some influence on this stronger warming from 2001 to 2010. The central objective is to discuss the impact of minor volcanic eruptions on the distinct stronger warming observed in the TTL during the period 2001-2010.

## 2. Methods

To isolate and extract each specific signal quantitatively so as to estimate trends, a simple multiple regression analysis was applied to the smoothed temperature anomalies ($T_s$) of GPS RO, adjusted and unadjusted radiosondes and ERA-Interim at each altitude and pressure level, which can be expressed as [*Randel and Cobb*, 1994]:

$$T_s(t) = \beta_0 + \beta_1 . t + \beta_2 QBO(t-\tau_1) + \beta_3 . ENSO(t-\tau_2) + \beta_4 . AOD(t) + e(t), \quad (1)$$

where t is the month index (t=1,2,…,112, for September 2001 to December 2010), $\beta_0$ is the constant term, $\beta_1$ is the linear trend, and $\beta_2$, $\beta_3$, and $\beta_4$ are regression coefficients for QBO, ENSO, and AOD, respectively. The term $e(t)$ denotes the residual time series, representing the regression error, whereas $\tau_1$ and $\tau_2$ are the time lags of the temperatures at given altitude or pressure levels with the QBO and ENSO, respectively. In this study, we do two types of regression analysis by using equation (1); for the first type of regression, the coefficients $\beta_0$, $\beta_1$, $\beta_2$, $\beta_3$, and $\beta_4$ are treated as the constants (method-1 hereafter), and for the second type, these coefficients ($\beta's$) are allowed for the seasonal modulation (time-dependent) given by a constant ($A_1$) plus annual (12-month), semi-annual (6-month), and quarterly (4-month) expressed in the form $A_1 + A_2 cos\omega t + A_3 sin\omega t + A_4 cos2\omega t + A_5 sin2\omega t + A_6 cos3\omega t + A_7 sin3\omega t$ ,where $\omega = 2\pi(rad)/12(month)$ (method-2 hereafter).

## 3. Results and Discussion

We applied the standard linear regression method, regression method-1, and method-2 to the $T_s$ at pressure levels (altitudes) up to 30 hPa (25 km), and the annual mean temperature trends along with standard errors at 2-sigma level (95% confidence interval) were estimated in each dataset over September 2001-December 2010, as shown in Figure 1.

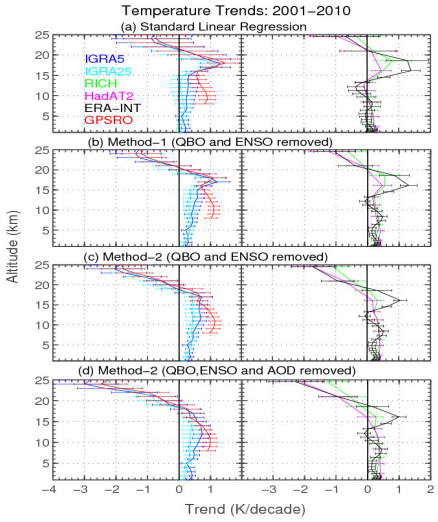


**Fig. 1** Altitude profile of temperature trends

The temperature trends from unadjusted radiosonde (IGRA5 and IGRA25) and GPS RO data while those from adjusted radiosonde (RICH and HadAT2) and ERA-Interim data are plotted separately, to avoid clumsiness due to their different vertical resolutions. Estimation of the trend using standard linear regression (Figure 1a), in fact, allows contribution from the potential interannual variability components in the troposphere and stratosphere besides the contributions from the anthropogenic variability. Each dataset, except for GPS RO, shows an insignificant warming trend in the troposphere up to 15 km and insignificant cooling above 20 km. There is a distinct and significantly strong warming layer in the TTL between 16 and 19 km (100-70 hPa), with a maxima at about 18 km in each dataset during the period 2001-2010. A comparison of Figures 1a and 1b reveals that the error bar becomes smaller due to better regression fits using method-1 when compared with standard linear regression. Between 16 and 19 km, the change in the temperature trends estimated with (Figure 1b) and without (Figure 1a) considering the QBO and ENSO are within statistical reliability. The temperature trend between 16 and 19 km from GPS RO and unadjusted data is about 0.84±0.39 K/decade and that from adjusted data is (0.52±0.37) K/decade after removal of the QBO and ENSO using method-1.

We further removed the seasonal dependence of the QBO and ENSO, if any, while using regression method-2 and estimated the temperature trends in each dataset over the period 2001-2010, as shown in Figure 1c. Figure 1c shows overall tropospheric warming and stratospheric cooling. A comparison of Figures 1c and 1b reveals that there is no change in the trend patterns except between 16 and 19 km. Thus, it appears that removing the seasonal dependence of the QBO and ENSO is important not only for the regression fits but also for the precise estimation of the temperature trends; otherwise the results will be contaminated with a large residual associated with the seasonality in the QBO and ENSO. We then applied method-2 while taking into account the AOD along with the QBO and ENSO, and estimated the temperature trends as shown in Figure 1d. Figure 1d also shows overall warming in the troposphere up to about 15 to 16 km and cooling in the stratosphere. The temperature trend pattern between 16 and 19 km, as evident from Figures 1a to 1c, changed significantly on removing the AOD.

## 4. Summary

The distinct stronger warming trend (0.5-0.8 K/decade) in the TTL between 16 and 19 km reported earlier and in the current study using method-1 is observed to be partly due to seasonality in the QBO and ENSO and partly due to the minor volcanic eruptions during the first decade of the 21st century. Removing them using method-2 results in an insignificant temperature trend due to anthropogenic climate change in the TTL between 16 and 19 km during 2001-2010. A positive and significant AOD temperature response of about 0.1-0.2 K is observed in the TTL between 16 and 19 km during 2001-2010, which explains about 5% to 15% of the total variability.

## Acknowledgements

This work is supported by the Japan Society for the Promotion of Science (JSPS) Foundation (ID No. P12025).

## References

Kursinski et al (1997), J. Geophys. Res., 102, 23,429–23,465, doi:10.1029/97JD01569.

Randel and Cobb (1994), J. Geophys. Res., 99(D3), 5433–5447, doi:10.1029/93JD03454.

Steiner, et al (2009), Geophys. Res. Lett., 36, L18702, doi:10.1029/2009GL039777.

Vernier, J. - P., et al. (2011), Geophys. Res. Lett., 38, L12807, doi:10.1029/2011GL047563.

# Development of Compact Plasma Instrument（TeNeP） for Nano and microsatellite

**K. -I. Oyama, C. Z. Cheng, Yu-Wei, Hsue**
Plasma and Space Science Center, National Cheng Kung University, Taiwan
*oyama@pssc.ncku.edu.tw*

## Abstract

The satellites for the educational purpose are being manufactured in many Universities in the world. Their weight ranges from several kg to 20 kg. However most of the satellite seems to be engineering oriented. For the scientists, these Nano/micro satellites constellation might provide excellent chances to conduct new sciences and to increase the research opportunities. In order for the science instruments to be accommodated in the Nano/microsatellite, the following factors need to be fulfilled; 1.The small dimension/low power consumption of the instrument, and data bit rate should be very small. 2. The sensor should be easily deployed or fixed without complex mechanism and, 3.The weight of the sensor should be right so that its deployment should not disturb the attitude of the satellite. These requirements are fundamentally important for the instrument to be accommodated in tiny satellites. It goes without saying that even small instrument should have a good performance in addition to provide accurate, and reliable information. Here we developed one plasma instrument to measure both electron temperature and plasma density simultaneously. Frequency sweep circuit is added to the conventional electron temperature probe [1]. The electron temperature probe which was developed more than about 30 years ago was accommodated in 5 earth orbiting satellites as well as Mars orbitor, and about 50 sounding rockets in Japan including the sounding rocket in Antarctica. The probe was used for the sounding rocket experiment in India, Brazil[2], Canada, U.S.A, and West Germany. The probe was also accommodated in Korean, Brazil, and Russian satellites.

The circular electrode (100 mm in diameter, and 1.6 mm in thickness) should be ram direction of the satellite, and it should be about 30 mm away from the satellite wall, to avoid the measurement in the satellite wake and in the sheath. The electronics consists of frequency sweep circuit (200 KHz-10 MHz), amplitude modulation circuit and conventional electron temperature probe. The total weight, and power is about 200 g and 500 mW respectively. The bit rate of 2kbits/sec allows us to calculate electron density from upper hybrid resonance. This amount of bit rate also makes it possible to calculate electron density and temperature from the output signal of the instrument in low frequency (200 KHz), which allows us to compare electron densities both from upper hybrid resonance and from the output signal of the electron temperature probe. The measurement duration is about 1 sec. The instrument can be accommodated in 10 kg satellite, that is, the instrument can be accommodated to all satellite of constellation. One of the research subjects by using satellite constellation is to study the precursor features associated with large earthquakes [3,4,5].

**Keyword:** Instrument**,** Ionosphere, Nano/Micro satellite,

## References

1) **Oyama, K.-I.,** Verification of IRI plasma temperature at great altitude by satellite data (INVITED), presented in COSPAR in Washington, *Adv. Space Res*., 14, (12)105-(12)113, 1994.
2) MURALIKRISHNA, P., M.A. ABDU, J.H.A. SOBRAL, KOH-ICHIRO OYAMA "Plasma Diagnostic Experiments on Board of the First Brazilian Scientific Micro satellite - SACI-1", *Geofísica Internacional*, 39,127-133, 2000.
3) **Oyama, K.-I.** ,Y.Kakinami, J.Y.Liu, and M.Kamogawa, and T.Kodama, Reduction of electron temperature in low latitude ionosphere at 600km before and after large earthquakes, *J.Geophys.R*es., doi:10.1029/2008JA013367,2008.
4) **Oyama, K. -I.,** Y.Kakinami, ,J.Y.Liu, T.Kodama, and C.Y.Chen, Micro/mini satellites for earthquake studies - toward international collaboration, *Advances in Geoscience*, 21, 251- 256, 2010.
5) **Oyama, K.-I.,** Y. Kakinami, J. Y. Liu, M. A. Abdu, and C. Z. Cheng, Anomalous Ion Density Latitudinal Distribution as a precursor of large earthquake, *J.Geophys. Res.*, 116, A04319, doi:10.1029/2010JA015948, 2011
6) **Oyama, K.-I**., T. Abe, K. Schlegel, A. Nagy, J. Kim, and K. Marubashi, Electron temperature measurement in Martian ionosphere, *Earth and Planetary Science*, 51, 1309-1317, 1999

# ELMOS Constellation: Lithosphere, Atmosphere and Ionosphere Monitoring by Small and Microsatellites

**Tetsuya Kodama**
*Earth Observation Research Center, JAXA, kodama.tetsuya@jaxa.jp*

## Abstract

GPS radio occultation is a simple and precise observation tool of the atmosphere and the ionosphere, particularly for improvements of the forecasting accuracy on the numerical weather prediction [ex. Formosat-3/COSMIC]. Recently, Global Navigation Satellite Systems(GNSS) have been established not only GPS Navstar but also GLONASS and Beidou, Galileo, QZSS and IRNSS are under development. This means that atmospheric and ionospheric data obtained by GNSS radio occultation will definitely increase in near future.

As conventional earth observation satellites are on sun-synchronous orbit, it is impossible to obtain diurnal variations of the atmosphere and the ionosphere, therefore small and microsatellite constellation is the solution within the realistic resources. Especially, the discrimination between seismo-origin and non seismo-origin perturbations of the atmosphere and ionosphere, it is necessary that comprehensive understand of atmospheric ionospheric phenomena by satellite constellation.

***Keywords*** **:** GPS occultation, lithosphere-atmosphere- ionosphere coupling, small satellite, microsatellite

## 1. ELMOS Constellation

We have already proposed the ELMOS small satellite constellation since 2010. All the satellite equip 3 common instruments; GPS occultation receiver, electron density and temperature probes which are internationally acclaimed. Its altitude is around 500～600km and the inclination is 40～50 deg.

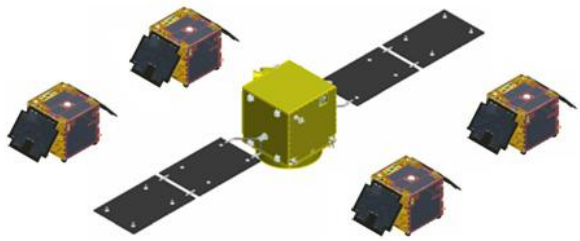

**Fig. 1 ELMOS Constellation**

## 2. Mission Objectives

Mission objectives of the ELMOS constellation are as follows;

1. Practical Utilization: improvement of the weather forecast accuracy by GPS occultation measurement
2. Scientific Research from the Ionosphere to the Lithosphere: contributions to the International Reference Ionosphere, ionosphere-atmosphere coupling, mesosphere, thermosphere, terrestrial gamma ray flash, transient luminous events, seismo-electromagnetics and oceanography etc.
3. Engineering Applications: space environment, space weather and ionosphere scintillation monitoring which is harmful for navigation communications

Mission instruments of the ELMOS main satellite as follows.

- GPS occultation receiver
- Plasma probes (electron density/temperature)
- VLF receiver
- Vector electric field probes
- 2D CCD camera
- Energetic charged particle analyzer
- Topside sounder
- Ion/neutral mass analyzer
- Neutral wind meter
- Plasma drift meter
- Atomic oxygen detector
- Magnetometer
- Technical Data Acquisition Equipment (TEDA)

Particularly, we expect promising results of seismo-electromagnetic research based on the reliable time and space ionospheric model by satellite constellation.

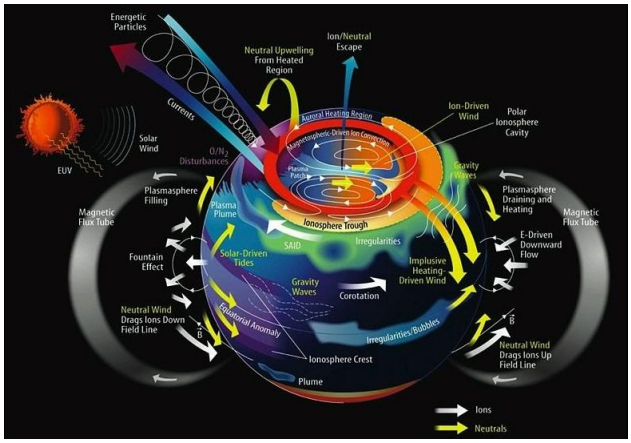


**Fig. 2 Ionospheric Dynamics (UCLA)**

## 3. Success Criteria

Success criteria of the ELMOS constellation is as follows.

| | Minimum | Nominal | Extra |
|---|---|---|---|
| Practical Utilization | Establishment of GPS RO technology | Improvement of weather forecast accuracy | Establishment of GPS Ocean reflection |
| Scientific Research | Data acquisition by onboard scientific instruments | Development of Reliable and accurate Ionospheric model | Establishing Proof of Pre-seismic Ionospheric Precursors |
| Engineering Applications | Data acquisition by TEDA | Space env. monitoring for JAXA Satellite Design Standards | Research of anomaly events by long-term operation |

## 4. Option Plan and Future Initiative

Since 2006, JAXA has been studying development of the Super Low Altitude Test Satellite (SLATS). If the SLATS become practical use, it is possible to observe various physical values directly in the F-layer of the ionosphere with ELMOS constellation.

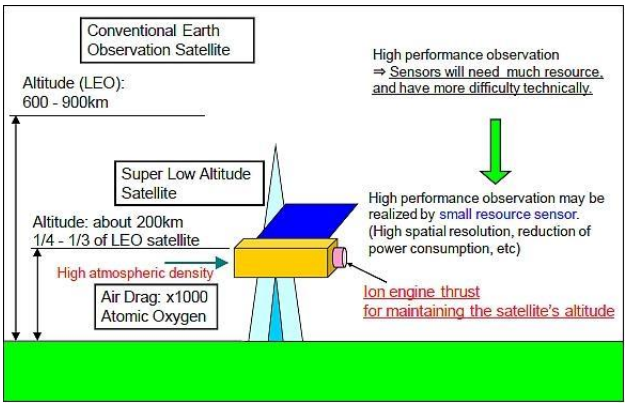


**Fig. 3 SLATS (JAXA)**

Japanese university-based microsatellite community dates back more than a decade, with most activities coordinated under the UNISEC that are steadily building increasingly functional satellites faster and cheaper nowadays.

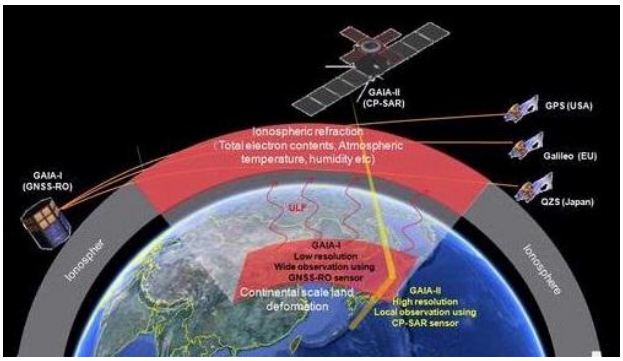


**Fig. 4 Microsatellite GAIA-I and-II (Kompass)**

At the Chiba university, two microsatellites named GAIA-I and GAIA-II are under development scheduled to launch in 2017 by Josaphat laboratory. The GAIA-I is installed GPS occultation receiver, electron density and temperature probes for seismo-ionospheric observation.

As an overseas activity, the Small Satellite Payload Task Group has been authorized under the Asia Oceania Geoscience Society in 2013. The task group is expected to provide an opportunity to discuss all aspects of the mission, from scientific goals that attract common interest such as earthquake precursors to candidate instruments as well as satellite systems.

Thus, it would be possible without increasing the program cost, thereby both an increase in the number of constellation satellites simultaneously with miniaturization of the satellite by the international cooperation.

In order to provide launch opportunities continuously for domestic and overseas microsatellite, it is strategically correct that JAXA have to reduce their own satellite program cost by small satellite for continuous launch of H-IIA or Epsilon.

## References

1) Kodama and Oyama, The ELMOS Small Satellite Constellation, The 28th ISTS, 2011.
2) Kodama et al., The ELMOS Small Satellite Constellation, The 43rd Annual Meeting of the Japan Society for Aeronautical and Space Sciences, 2012.
3) Uyeda et al., Proposal for Earthquake Prediction Program I: Short-term Prediction, Japan Geoscience Union Meeting, 2012.
4) Uyeda et al., Proposal for Earthquake Prediction Program II: Satellite Observation, ibid
5) Kodama, A Review of Seismo-Electromagnetic Satellite Missions - Recent Results and Prospects -, EMSEV 2012 in Japan, 2012.
6) Research and Development of an Ion Engine for a Super-Low-Altitude Satellite, Sora to Sora, No.42, 2011
7) Japan Advances University-led Microsatellite Constellation, Spacenews, Dec. 3, 2010
8) Microsatellite Powerful Earthquake Prediction 4 Days Before Happen, KOMPAS, June 26, 2012
9) Center for Environmental Remote Sensing Newsletter, No. 90, 2013
10) http://www.geocities.jp/s2ptg/
11) Kodama et al., Temporal and Spatial Observation of Atmosphere-Ionosphere by Small Satellite Constellation, The 44th Annual Meeting of the Japan Society for Aeronautical and Space Sciences, 2013

# GPS Total Electron Content (TEC) for Ionospheric Observation

**Katsumi Hattori[1], Shinji Hirooka[1], Chie Yoshino[1], Yuichi Otsuka[2]**
[1]*Graduate School of Science, Chiba University, Japan*
[2]*Solar-Terrestrail Environmental Laboratory,Nagoya University, Japan*
*E-mail hattori@earth.s.chiba-u.ac.jp*

## Abstract

Total electron content (TEC) investigation is one of the powerful tools in ionsopheric study. Several case studies and statistical studies on storms, tsunami, earthquakes, and so on have been performed. To understand the mechanism, monitoring of three-dimensional distributions of ionospheric electron density is effective. In order to investigate the three-dimensional structure of ionospheric electron density, the neural network based tomographic approach is adapted to GEONET and ionosonde data. However, it is an ill‐posed problem in the context of sparse data, and accurate electron density reconstruction is difficult. The Residual Minimization Training Neural Network (RMTNN) tomographic approach, a multilayer neural network trained by minimizing an objective function, allows reconstruction of sparse data. In this study, we validate the reconstruction performance of RMTNN using numerical simulations based on both sufficiently sampled and sparse data. First, we use a simple plasma‐bubble model representing the disturbed ionosphere and evaluate the reconstruction performance based on 40 GPS receivers in Japan. We subsequently apply our approach to a sparse data set obtained from 24 receivers in Indonesia. The reconstructed images from the disturbed and sparse data are consistent with the model data, except below 200 km altitude. To improve this performance and limit any discrepancies, we used information on the electron density in the lower ionosphere. The results suggest the restricted RMTNN‐tomography‐assisted approach is very promising for investigations of ionospheric electron density distributions, including studies of irregular structures in different regions. In particular, RMTNN constrained by low‐Earth‐orbit satellite data is effective in improving the reconstruction accuracy.

Many anomalous electromagnetic phenomena possibly associated with large earthquakes have been reported. TEC (Total Electron Contents) anomaly is one of the most promising phenomena preceding large earthquakes. In this study, TEC anomalies before large earthquakes have been investigated. TEC values are computed by using the GEONET and GIM (Global Ionosphere Maps). 15 days backward running average (TECmean(t)) and its standard deviation σ (t) at a specific time are taken for the normalization. The normalized TEC, GPS-TEC$*$(t) is defined as TEC$*$ (t) = (TEC(t)-TECmean(t))/σ(t). We investigate TEC anomalous changes in times and space from May1998 to May 2010 in case and statistical studies. Results show that positive anomalies significantly appear 1-5 days before M>=6.0 earthquakes in Japan area. In addition, we investigate the 2011 off the Pacific coast of Tohoku Earthquake. GIM-TEC$*$ anomalies exceeding +2σ appear 3-4 days before the earthquake. The duration is more than 20 hours. This result is consistent with the previous statistical results of positive anomalies for M>=6.0 earthquakes in Japan area.

To understand the mechanism, monitoring of 3D distributions of ionospheric electron density is considered to be effective. In this study, to investigate the three-dimensional structure of ionospheric electron density prior to large earthquake, the neural network based tomographic approach is adapted to GEONET and ionosonde data for the 2011 Off the Pacific Coast of Tohoku Earthquake (Mw9.0). As mentioned above, significant enhancements of TEC are found 1, 3-4 days prior to the earthquake. Especially, TEC increase of 3 days prior to the earthquake was remarkable. As a result of tomographic analysis, the reconstructed distribution of electron density was enhanced in sub-ionosphere to over F-region in comparison with 15 days backward median distribution. Moreover the enhanced area seems to be developed to upper ionosphere from sub-ionosphere with time. The rise velocity along magnetic field line was approximately 70 m/s. The tomographic results suggest the existence of some energy influx from the surface associated with seismic activity. Then, in order to understand the relationship of detected phenomenon and earthquake, we performed the tomographic analysis for other earthquakes occurred in Japan. The details will be shown in the presentation.

# Ionospheric Observations of FORMOSAT-3 and follow-on FORMOSAT-7

**Tiger J. Y. Liu[1,2], G. S. Chang[1], S. J. Yu[1], T. Y. Liu[1]**
[1]*National Space Organization (NSPO), TAIWAN*
[2]*Institute of Space Science, National Central University, TAIWAN*

## Abstract

The FORMOSAT-3/COSMIC (F3/C) constellation lunched on 15 April 2007, which consists of six micro-satellites in the low-earth orbit, is capable of monitoring the ionosphere by using the powerful technique of radio occultation. With more than 1500 observations per day, it provides an excellent opportunity to monitor three-dimensional structures and dynamics in the electron density and scintillation of the ionosphere. Many prominent features of equatorial ionization anomaly, plasma cave, middle latitude trough, the Weddell Sea anomaly, sudden stratospheric warming, irregularity, etc. in the ionosphere are observed. Finally, simulation results of ionospheric observations by the F3/C follow-on, FORMOSAT-7, are presented.

# Development of Space borne X Band SAR for 100kg Satellite

**Hirobumi Saito [1], Atsushi Tomiki [1], Prilando Rizki Akbar[1],**
**Takashi Ohtani[2], Kunitoshi Nishijo[2], Jiro Hirokawa[3], and Makoto Ando[3]**
*[1] Japan Aerospace Exploration Agency, Institute of Space and Astronautical Science,*
*[2]Aerospace Research & Development Directorate, JAXA, [3]Tokyo Institute of Technology*
*E-mail saito.hirobumi@jaxa.jp*

## Abstract
We have started development of small synthetic aperture radar (SAR) compatible to 100kg class small satellites with about 3m ground resolution and multi-polarization, aiming for constellation SAR observations. This technology enables us to realize high frequency SAR observations with only several hours observation interval. This paper describes key technologies of this development such as deployable slot array antennas, waveguide feeder with a small gap at a deployment point, and GaN HEMT X band amplifier. Also we show an integration design result of this SAR system to 100kg class bus system.
***Keywords*** **:** X band SAR, 100kg Small Satellite, slot array antenna, SAR constellation

## 1. Introduction
Synthetic Aperture Radar (SAR) is a well known remote sensing technique with reliable capabilities that offer advantages over an optical sensor. However, SAR sensors require relatively large antennas with several meters and high RF power of hundreds watts or more. Up to now, only large or medium size satellites with hundreds kilo-grams or more can afford SAR sensors. These large or medium satellites cost hundreds million US dollars including launching cost.

In this paper, we propose a synthetic aperture radar sensor compatible with 100kg class piggy-back satellites. A 100kg satellite may cost roughly ten million US dollars. Furthermore it can be injected into an orbit as a piggy-back, resulting in total mission cost of less than twenty million US dollars..

In the next section, we discuss on the system goal and specifications of SAR that is suitable for a small satellite. Finally, the conclusion and future research will be summarized in section 3.

## 2. Small SAR Compatible with Piggy-Back Satellite
### 2.1 System Goal of Small SAR
Piggy-back launch is inexpensive method to inject a small satellite to an orbit. We have started development of a small satellite with a SAR sensor, which is compatible to piggy-back launch. Japanese H2A vehicle afford a maximum piggy-back satellite with 70x70x70 $cm^3$ volume and around 100kg mass.

Recently a medium or large SAR sensor has a high resolution of 1 meter or less. However, in most cases, a SAR sensor can operate for 5-10minutes in an orbit period of around 100 minutes because of power constraint. At present, a few number of medium or large SAR satellites can observe the earth in a limited time for example less than 10%.

Therefore, an advantage of a piggy-back satellite with a SAR is to increase in observation frequency with relatively low resolution observations. Piggy-back launch is a cost saving way to inject in different orbits many piggy-back satellites with SARs. A system of 12 piggy-back satellites with SARs affords a short revisit time of less than 10 hours. Probably the total cost is less that one of single large SAR satellite.

Candidates of applications that require short revisit time are disaster managements and maritime security to observe objects exposed at earth surface without covering vegetation. It implies that X-band observation is adequate for a small SAR compatible with a piggy back satellite.

### 2.2 System Description of Small SAR
We have performed a preliminary parameter design of a piggy-back satellite with a SAR [1]. It is concluded that X band is a good choice for a compact SAR antenna. Also X-band is adequate to observe objects exposed on the ground, which is the main target of a small SAR with a short revisit time. A transmitting RF power is 573W.We are developing a high efficiency GaN RF power amplifier, in which we improve to increase operational duty ratio up to 20-30%. The ground resolution is 6.1m in a case of noise-equivalent sigma zero $\sigma^{\circ}_{NE}$= -20dB and the duty ratio 20%.

A key technology of the small SAR compatible with a piggy-back satellite is a deployable plane antenna array. Maximum envelop size of a piggy back satellite is 70 x70 x 70$cm^3$ and size of one antenna panel is selected to be 70

cmx70cm. Waveguides have the lowest transmission in this frequency region. Single layer slotted waveguide antennas are a good candidate for this application [2]. We are developing a RF feeder system based on waveguide, which is compatible with deployment and has low loss. The satellite deploys two wings each of which consist of three antenna panels. Antenna arrays are also on the satellite body and the total size of the antenna is 0.7m x 4.6m. Figure 1 shows a preliminary outlook of the satellite.

A SAR sensor radiates high RF power in a short observation time. Time profiles of power and heat of this satellite have a very high peak-average ratio. This satellite has to manage the issue of a high peak-average ratio under severe constraint of mass and volume. In addition to conventional satellite technologies, several advanced technologies would be applied to solve these issues. A solution of the power management is to apply olivine-type lithium-ion batteries compatible for high discharge rate.

## Conclusions

This paper describes the goal and system description of a piggy-back satellite with a small SAR. The system analysis shows that a ground resolution of several meters is possible with X-band. Possible applications are to form a constellation of several piggy-back SAR satellites for disaster managements and maritime security, which require short revisit time.

A preliminary satellite design is in progress. The total mass of satellite is 100kg mass and the satellite is zero-momentum 3-axis stabilized. The details will be reported in the conference.

## References

[1] P.R. Akbar, JT Sri Sumantyo, and H. Saito, "Design of synthetic aperture radar onboard small satellite," International Conference on Space, Aeronautical and Navigational Electronics 2012, SANE2012-80, Incheon, Korea, 2012.

[2] K. Sakakibara, J. Hirokawa, M. Ando, and N. Goto, "A high-gain and high-efficiency single layer slotted waveguide array for use in 22GHz band," IEE Electronics Letters, vol.32, no4, pp.283-284, 1996.

**Table 1 Main Parameters of Small SAR**

| Parameter | Value |
|---|---|
| Frequency (GHz) | 9.65 |
| Altitude (km) | 510 |
| Off Nadir (°) | 21 |
| Pulse Bandwidth (MHz) | 40 |
| $\sigma^{\circ}_{NE}$ (dB) | -25 |
| Resolution (m) (Number of look = 4) | 9.8 |
| Swath Width (km) | 23 |
| Antenna size (m) | 4.9 x 0.7 |
| Peak Power (W) | 573 |
| Average Power (W) | 230 |
| System Noise Temperature (K) | 589 |
| Noise Figure (dB) | 4.8 |
| System Loss (dB) | 4 |
| Antenna Efficiency | 0.6 |
| Transmitter Duty Cycle | 0.4 |
| SAR Battery Capacity (Wh) | 127 |
| SAR Battery Mass (kg) | 1.26 |
| Operational Battery Capacity (Wh) | 26.39 |
| Operational Battery Mass (kg) | 0.26 |
| Power Control & Converter Unit Mass(kg) | 5 |
| Operational | 9.57 |
| SAR Observation | >0.67 |
| Solar Paddle Area ($m^2$) | |

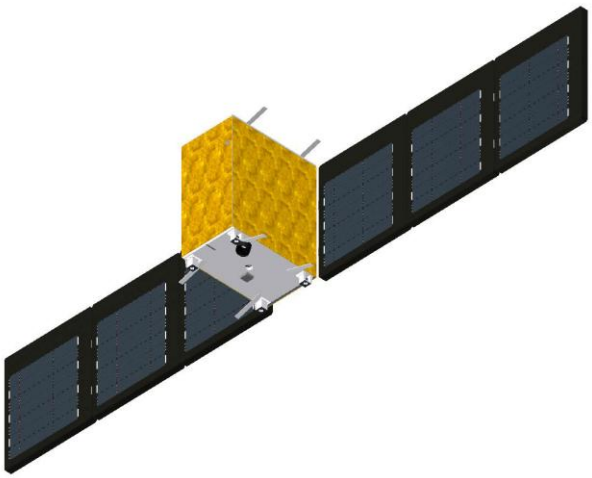

**Fig.1 Outlook of Piggy-back Satellite with Small Synthetic Aperture Radar. Mass is 100kg and body size is 0.7x0.7x0.4m3. Two wings of SAR antennas are deployed and each antenna panel is 0.7x0.7m2. Back side of SAR antenna is partially solar cell.**

# SAR Antenna Development in the UK

**Steven Gao[1], Yohandri[2,3] and Josaphat Sumantyo[2]**
[1]University of Kent, Canterbury, UK
Email: s.gao@kent.ac.uk
[2]Physic Department, State University of Padang, Indonesia
Email: yohandri@fmipa.unp.ac.id
[3]Centre for Environmental Remote Sensing, Chiba University, Japan
Email: jtetukoss@faculty.chiba-u.jp

**Abstract**
Antenna sub-system is one of the most critical and expensive sub-systems for Synthetic Aperture Radar (SAR) onboard aircraft or satellites. This paper provides a brief overview of SAR antenna development in the UK. Some results will be shown. The conclusion and future development of SAR antenna and systems in the UK are given in the end.
**Key words:** SAR, phased array, space antenna

## 1. Introduction

Due to the capabilities of day-and-night operation and penetration through clouds and rain, SAR has become an important tool for earth observation and environmental monitoring worldwide. Space-borne SAR systems are usually very expensive and take many years from the development to launch. One of the recent trends is to develop low-cost SAR systems onboard small satellites. In Europe, one of the recent examples is the COSMO-SkyMed (Constellation Of Small Satellites for Mediterranean basin Observation) is a four-satellite constellation funded by ASI (Agenzia Spaziale Italy) and the Italian Ministry of Defense. The four satellites, from Thales Alenia Space, Italy, were launched during 2007 and 2010, and each satellite is equipped with a SAR operating at X band with multiple operation modes (Spotlight, Stripmap and ScanSAR) and multi-polarization capabilities. The multi-mode and multi-polarization capability of SAR is achieved by using an active phased array for the SAR antenna onboard. The COSMO-SkyMed allows both the wide-area mapping (at low resolution, ScanSAR mode, X band) and the high-resolution imaging (in Spotlight SAR mode, X band) of the Mediterranean latitudes with repetition time of a few hours. A brief review of SAR antenna development will be given in the following.

## 2. Brief Review of SAR Antenna in the UK and Some Results of Low-Cost SAR

In the UK, many SAR systems have been developed during recent decades. These SAR systems mainly operate at S band, C band, X band, both S/X band, etc, for air-borne or space-borne applications. Key players in SAR systems and related technologies include companies such as EADS Astrium UK Ltd, Surrey Satellite Technology Ltd (SSTL), Selex, BAE Systems, Qinetiq, as well as academic institutes such as the University of Kent, University College London, University of Sheffield, University of Surrey, etc. Some examples of recent space-borne SAR systems include ERS-1 (C band), ASAR on ENViSAT (C band), NovaSAR-S (S band), Sentinel-1 (C band), AstroSAR-Lite (X band), etc. A variety of antenna technologies have been developed for SAR systems, including printed microstrip patch arrays, slotted waveguides, deployable antennas, horn antennas, annular slot arrays, active phased arrays, etc [1]. As an example, the antenna sub-systems for NovaSAR-S are explained below.

NovaSAR-S is a low-cost radar imaging satellite, recently developed by SSTL and Astrium UK Ltd [2-3]. One key drive of NovaSAR-S development is to significantly reduce the cost of space-borne SAR systems while improving the performance of imaging. This is made possible by adopting the modern small-satellite platform technology, new antenna technology and new RF sub-system technologies. NovaSAR-S operates in S-band (3.1-3.3 GHz) and has a design life of 7 years. The total mass of the satellite including SAR system is below 400 kg. It can operate in single (e.g., HH or VV) or multiple polarizations (HH, VV, HV and/or VH). The modes of operations are highly flexible, including ScanSAR (narrow), Stripmap, ScanSAR (wide swath width), and a maritime surveillance mode. In single-polar operations (e.g., HH or VV), spatial resolutions in the range 6-30m are achieved with corresponding swath widths ranging from 15-

150 km. The maritime surveillance mode is unique and it has a surveillance swath of 750 km width for detecting the ships or other targets in the ocean. The optimum orbital altitude for NovaSAR-S is 580km. The highly flexible modes of NovaSAR-S are enabled by using an active phased array antenna.

Figure 1 show the antenna array which is a microstrip-patch active phased array consisting of 18 sub-arrays. The total size of the antenna array is 3 m×1 m. The antenna can achieve multi-polarizations (VV, HH, VH, HV). To achieve electronic beam steering, the antenna is integrated with microwave phase shifters which are controlled by DC voltages. To reduce the size and mass (and cost) of SAR antenna system, it is integrated with GaN power amplifiers. The use of GaN technology is important here for significantly reducing the size and mass of active phased array, due to the high power density capability of GaN devices in comparison to conventional GaAs technologies.

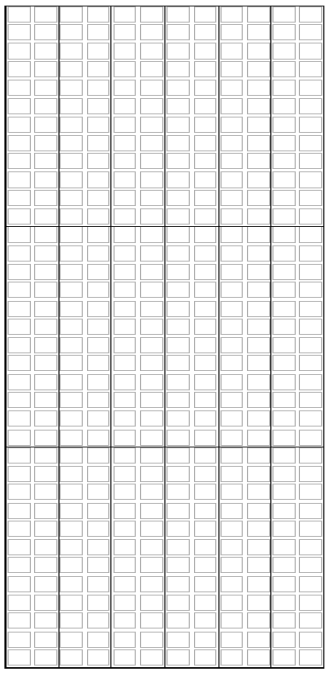

Figure 1 SAR antenna for NovaSAR-S [2,3]

One challenge of SAR antenna is to improve the polarization purity and increase the isolation between transmit and receive chains. This is achieved by using the "anti-phase technique". Figure 2 shows the configuration of one sub-array. As shown in Figure 2, the radiating elements (square microstrip patch) in the 1st row and the 2nd row are fed at opposite positions. This will excite electric currents following in opposite directions on the elements in the 1st and 2nd row. To compensate this, these two rows will be fed with 180° phase difference between them. Such an "anti-phase technique" enables the cancellation of high-order modes in the sub-array, leading to high polarization purity and high isolation between transmit and receive [1,4].

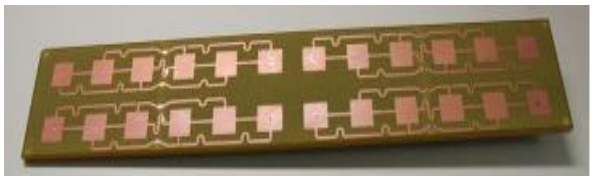

Figure 2 Sub-array of SAR antenna for NovaSAR-S [2,3]

## 3. Conclusion and Future

The above provides a brief overview of SAR antenna in the UK. One of important steps next is to develop digital beamforming (DBF) multi-static SAR. The University of Kent, teamed with DLR (Germany) and other European partners, is working on DBF multi-static SAR for a constellation of several micro-satellites in low earth orbits. Such a SAR system requires DBF array antennas and novel algorithms for antenna adaptive beamforming.

## Acknowledgement

The author thanks the support from Japan Society for Promotion Science (JSPS) fellowship programme, Japan.

## References

1) W. Imbriale, S. Gao and L. Boccia, Space Antenna Handbook, Wiley, UK, May 2012
2) Web: http://www.sstl.co.uk/NovaSAR-1
3) P. Davies, et al., NovaSAR – Bringing Radar Capability to the Disaster Monitoring Constellation, *Proceedings of The 4S Symposium 2012*, Slovenia, June 2012, pp.1-12
4) R. Di Bari, T. Brown, S. Gao, C. Underwood, et al., Dual-Polarized Printed S-Band Radar Array Antenna for Spacecraft Applications, *IEEE Antennas and Wireless Propagation Letters*, Vol. 10, 2011, pp. 987-990

# Micro SAR Satellite Development in Korea and a Plan of Space Observation Network in Southeast Asia

**Tu-Hwan Kim†, Dal-guen Lee†, Jae-Hyun Kim‡, Hee-In Yang‡**

*†Department of Space Survey Information Technology, Ajou University*

*San 5, Woncheon-dong, Yeongtong-gu, Suwon, 443-749 Korea*

*‡Department of Electronics Engineering, Ajou University*

*San 5, Woncheon-dong, Yeongtong-gu, Suwon, 443-749 Korea*

*E-mail : †{thkim@ajou.ac.kr, dalguen84@gmail.com}, ‡{ jhkim,@a jou. ac.kr, kfcddong@gmail.com*

**Abstract** Recently, Ajou University, Korea with Institute of Space and Astronautical Science (ISAS) and Chiba University, Japan has done the micro satellite project. Research topics are high speed downlink communication and synthetic aperture radar (SAR) system. Based on these technologies, Ajou University has a plan to offer small satellite for industries and other countries by cooperating with other companies. Especially micro satellites and ground stations for the micro satellite is offer for Southeast Asian countries that have natural disaster. The final goal is to construct earth observation network and the very long base-line interferometer (VLBI) system by cooperating with Korea and Japan.

***Keywords*** **:** Micro satellite, SAR, Korea-Japan space cooperation, Space observation network, VLBI

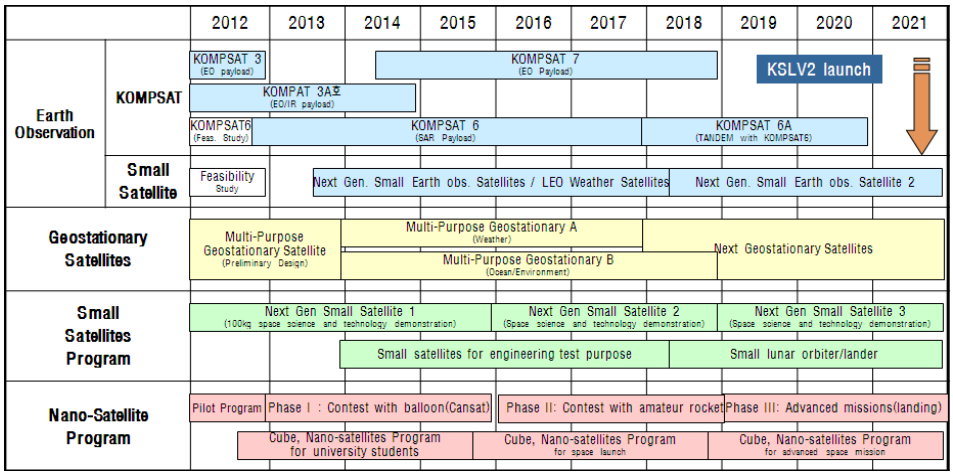


**Figure 1. Korea National Space Program Roadmap**

## 1. Korea-Japan joint development of next generation micro SAR satellites

The micro satellite can be developed at low cost in a short period of time while the large satellite development will take a long period of time to research and need a huge amount of investment. Therefore, the micro satellite development has an advantage in the development of space technology. As shown in Figure 1, this micro satellite development is included as part of the "Korea

National Space Development Program Roadmap" by detailed action plan. The proven technology in the micro satellite can be adapted to the large multi-purpose satellite in the future. The multi-purpose satellite can be made in Korea by the using the micro satellite technologies. And Korea government has a plan to launch a next generation micro satellite per 3~4 years. The core technologies for the micro satellite are an ultra-light and low-power X-band RF transmitter-receiver, wireless inner satellite networks for substituting instrumentation wired networks and etc. These technologies have been not studied in Korea before, Ajou university collaborate with Space science lab in JAXA, Japan which develops the high speed downlink transmission technology in satellite networks. And also Ajou University have made a MOU with professor Josaphat in National Chiba University, Japan who are excellent for development of the micro SAR satellite. The mirco SAR satellite is most popular as the utility of the micro satellite.

If the micro SAR satellite is developed by National Space Program, Ajou University will develop the standard satellite

for micro satellite with corporations and supply it to domestic and foreign countries. Then it will help to accelerate the space industry. Especially, it contributes to the advancement of science and economy of countries in Southeast Asia which have rich resources and many natural disasters.

## 2. A plan of Space observation network in Southeast Asia

Countries in Southeast Asia have rich natural resources but they have many natural disasters, too. Thus these countries have needs of earth observations with observing satellite and installing the small ground station to gather and utilize the desired observing data effectively. The space observation network can be utilized as the remote sensing exploration or the observation of natural disasters. Moreover, it is the benefits of the small ground station that the cost of a installing is much cheaper than that of the large ground station.

Meanwhile, in Southeast Asia, the geodetic VLBI observation network is not existed and the world geodetic system is not used. However, in these days, most countries commonly use the world geodetic system as a national geodetic system. To establish the world geodetic system of a country, the origin point of national geodetic system should be determined exactly.

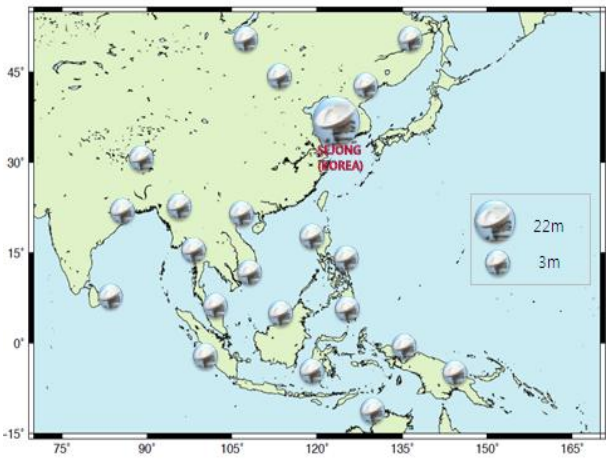


**Figure 2. A plan of observation network in Southeast Asia**

For determining the point, the country should install the geodetic VLBI observatory station and then do the international VLBI observation. The measured point becomes an origin point of the national geodetic system, and the new coordinates system of the whole country are determined based on it. Finally, the new national geodetic system is established based on the world geodetic system.

For the geodetic VLBI observation, if the diameter of an antenna at one side is more than 20m, then 3m is acceptable as a diameter of the other side antenna. As shown in Figure 2. if the space VLBI station (in Sejong-si, Korea) which has the 22m-diameter antenna play a role as the central station, then the geodetic VLBI observation can be possible by using the small ground station with the 3m-diameter antenna in Southeast Asia. For that, only requirement is that the replacement of the antenna receiver for the satellite communication with for the geodetic VLBI receiver.

When the geodetic VLBI observation is possible, each country can not only determine the origin point of the new national geodetic system, but also measure the variation of plate movements in Southeast Asia region. Therefore, they can minimize damages from the natural disaster such as earthquake and tsunami by predicting and simulating the plate movements of 10, 100 and 1000 years later.

# Development of Bistatic GPS-SAR Image Processing Algorithm

**Takuji Ebinuma and Yoshinori Mikawa**
*The University of Tokyo, ebinuma@nsat.t.u-tokyo.ac.jp*

## Abstract
Remote sensing using scattered or reflected GPS signals off the Earth's surface is a new category of satellite navigation applications. These multipath signals are usually considered to be undesirable signals since they degrade the accuracy of GPS positioning. However, scattered GPS signals can be utilized as signals of opportunity for passive remote sensing. This paper presents new synthetic aperture radar imaging process using scattered GPS signals in bistatic radar geometry and its validation through a field experiment.
***Keywords*** **:** Bistatic radar, SAR, GPS

## 1. Introduction
For positioning and navigation applications using GPS signals, the so-called multipath is one of the major error sources. In recent years, however, it has been recognized that reflected or scattered GPS signals off the Earth's surface can be applicable for remote sensing[1)]. This new technique is generally known as GPS reflectometry (GPS-R). Unlike most radar-based remote sensing systems that actively transmit microwave pulses and then detect their backscattered radiation, GPS-R utilizes the GPS satellites as non-cooperative transmitters in bistatic radar geometry.

The scattered GPS signals can also be applicable for Earth's surface imaging using synthetic aperture radar (SAR) approach. Space-surface bistatic SAR (SS-BSAR) is well-known bistatic SAR model, where it is supposed that a GPS transmitter is spaceborne and a receiver is located on or near the surface of the Earth[2)]. SS-BSAR utilizes both the scattered GPS signal and the line-of-sight (LOS) signal which is received directly from the corresponding GPS satellite. This approach assumes geometric similarity between the receiver and the scattering point so that the correlation process between the LOS and the scattered signal could eliminate the dynamics of the GPS satellite motion. This geometric similarity is, however, no longer valid for a high altitude receiver platform such as a low Earth orbit satellite.

In this paper, we introduce a newly developed GPS-SAR technique called the quasi-monostatic algorithm (QMA). In order to overcome the geometric restrictions in SS-BSAR approach, the range migration curve between the GPS satellite and the scattered point is modeled as a linear function. This approximation effectively eliminates the contribution of the GPS satellite motion in the aperture synthesis process. QMA is now able to analytically convert the bistatic geometry into monostatic without any geometric constraints, and the general range-Doppler algorithm can be applicable for GPS-SAR data processing. Thus we call this approach quasi-monostatic.

## 2. Quasi-Monostatic Algorithm
While the typical SAR system utilizes a chirp pulse signal in which the frequency changes linearly with time to realize a wide signal bandwidth, GPS signal is a continuous wave modulated by the so-called direct-sequence spread spectrum (DSSS) technique. For example, the typical civilian GPS L1 signal is modulated with the so-called C/A code. It can be considered as a pulse signal which has 100% duty cycle and repeats every one millisecond.

Similar to the general monostatic SAR algorithm, GPS-SAR time domains can be defined by the fast-time and the slow-time corresponding to the range and the azimuth directions, respectively. The range compression algorithm of GPS-SAR is identical to the auto-correlation process of the C/A code, and the resolution in the range direction is defined by the chip width of the C/A code, which is about 300 m. In the azimuth direction, the slow-time sampling rate is limited by less than 1 kHz because the fast-time sample bins should contain at least one millisecond of signal for auto-correlation process of the C/A code. This means that the Doppler frequency should be less than 500 Hz to satisfy the sampling theorem for the azimuth compression process.

It can also be assumed that the range between the GPS satellite and the receiver is constant in the fast-time domain. On the other hand, the effect of the GPS satellite motion is not negligible in the slow-time domain and appeared in the range migration curve. In QMA, the range between the GPS satellite and the scattering point is reasonably approximated by a linear function because the aperture synthesis time is much shorter than the orbital period of the GPS satellite. Therefore, the range rate due to the GPS satellite motion can be considered constant during the aperture synthesis. That means the aperture synthesis process in QMA is nearly

Fig 1. GPS-SAR UAV platform


Fig 2. Aerial photo of the observation field

identical to that of the typical monostatic SAR geometry. Detailed description on the point spread function (PSF) reconstruction in QMA can be found in our early work[3].

## 3. Flight Experiment

A field test of GPS-SAR imaging was conducted to evaluate the QMA performance. A small UAV shown in Fig. 1, equipped with a GPS L1 array antenna and signal capture instrument, flew over a border of the Ohtone River and its river bank. Fig. 2 shows the picture of the observation area taken by the onboard camera, and Fig. 3 shows the corresponding SAR image. Stronger scattering was successfully observed from the vegetation on the river bank, while the calm river surface behaved as a specular reflector and contributed less to the resulting SAR image.

There were a few scattered signals detected from different GPS satellites, and all of them where observed in the same range bins. This provided that the movement of each GPS satellite was removed properly, and the motion of the UAV was dominant in the QMA image formulation.

The range resolution of the resulting SAR image is limited to about 300 m, which corresponds the chip duration of the C/A code. This can be improved by using new wideband civil GSP signals, such as GPS L5. On the other hand, a much finer azimuth resolution can be achievable by the effect of the aperture synthesis.

## 4. Conclusions

We proposed a new bistatic GPS-SAR algorithm called QMA, which analytically resolves the constraints on the observation geometry in SS-BSAR. The field test result showed that QMA efficiently eliminates the effects of the

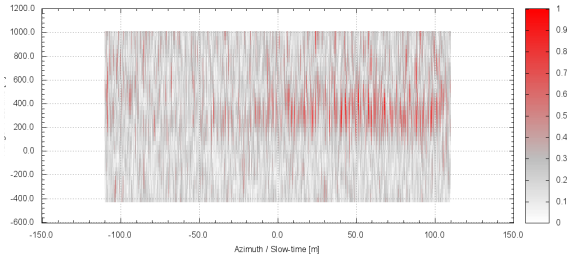


Fig 3. GPS-SAR image in the field test

motion of the non-cooperative transmitter from bistatic SAR image formulation and can be applied into wider range of observation scenarios.

## Acknowledgements

This research was supported by grant #22686083 from Japan Society for Promotion of Science (JSPS).

## References

1) A. Komjathy, *et al.*, "Developments in Using GPS for Oceanographic Remote Sensing: Retrieval of Ocean Surface Wind Speed and Wind Direction," ION 2001 Technical Meeting, pp. 753-761 2001.
2) M. Antoniou, M. Cherniakov, and C. Hu, "Space-Surface Bistatic SAR Image Formation Algorithm," IEEE Transactions on Geoscience and Remote Sensing, Vol. 47, pp. 1827-1843, 2009.
3) Y. Mikawa, T. Ebinuma, and S. Nakasuka, "The study of the remote sensing application using the GNSS reflected signal with the aperture synthesis," Proceedings of IGARSS 2012, pp. 400-403, 2012.

# UAVSAR Development Programme in Malaysia

**Voon-Chet Koo[1], Hean-Teik Chuah[2]**
[1]Multimedia University, Malaysia
[2]Universiti Tunku Abdul Rahman, Malaysia

## Abstract

The design and development of Synthetic Aperture Radar (SAR) is one of the focused research areas in Malaysia since early 2000s. The main objective of this research is to develop an all-weather instrument for earth resource monitoring. In the initial phase of development, a C-band (5.3 GHz) SAR prototype has been developed for ground-based experiments. Its enhanced version, a compact, light weight SAR has been successfully mounted onto a small unmanned aerial vehicle (UAV) in 2010. Since then, a series of flight missions have been carried out to acquire radar images for various remote sensing applications. In addition, two new UAVSAR sensors, operating at L-band (1.27 GHz) and S-band (3.125 GHz) frequency, respectively, have been proposed and currently under the final stage of development. The former sensor is targeted for landslide and flood monitoring, and the latter for deforestation monitoring. This paper presents the current progress and the future plan of the UAVSAR sensor development in Malaysia.

# Hyperspectral Camera for Microsatellite and UAV

**Yukihiro Takahashi [1] and Junichi Kurihara[1]**
[1]*Space Mission Center, Hokkaido University, yukihiro@mail.sci.hokudai.ac.jp*

## Abstract
Hokkaido University developed super multicolor imaging system, a kind of hyperspectral camera, using the LCTF (Liquid Crystal Tunable Filter) technology, which can select any colors with bandwidth of ~10-20 nm in 420-700 nm or 650-1059 nm at 1 nm step. This multispectral sensor can be applied to various subjects, such as measuring parameters essential parameters for tropical peatland carbon management, mineral exploration, fishery and so on. Thanks to its light weight and compact size, LCTF sensor is suitable for micro-satellite with weight of 50-100 kg. Our group will launch 50-kg satellites, namely, RISING-2 and RISESAT with LCTF telescopic camera in the period of 2013-2014.

***Keywords*** **:** microsatellite, UAV, payload, super-multicolor, spectral imaging

## 1. Introduction
Micro-satellite with weight of 50-100 kg has various merits compared to middle and large sized satellite, that is, 1) low cost fabrication compared to middle or large sized satellite, namely, few M USD including BUS and mission payloads. The launch cost will be 1-2 M USD as piggyback, 2) quick fabrication: about one or two years for flight model would be sufficient, enabling application of the latest technologies, 3) on-demand operation, taking detail information at a point of interest, and 4) the low cost and quick fabrication make us possible to launch not a small number of satellites and operate them as a network, which is called as constellation flight. In order to make the utilization of micro-satellite, the highly-functionable advanced optical sensors is essential, especially in conducting spectral imaging. On the other hand, UAV (uninhabited airborne vehicle) has a great potential in measuring local area with higher spatial resolution than satellite with lower cost as well as "test bed" of spacecraft equipment in developing phase. Hokkaido University is developing a kind of hyperspetral camera using LCTF (Liquid Crystal Tunable Filter) technology. Here we show the initial results of UAV campaign carried out in Jawa, 2012, and the scope of application to micro-satellite measurement.

## 2. UAV campaign
The tropical peatland is a significant carbon reservoir, but recently it has become a crucial $CO_2$ emission source due to the wild fire and rapid development works. Hokkaido University Group has conducted long-term research at Central Kalimantan's peatland in close cooperation with Indonesian experts by JSPS Core University Program (1997-2008). Following that, "Wild Fire and Carbon Management in Peat-Forest in Indonesia" project has been conducted supported by JST-JICA since 2010 until 2014, collaborated with Indonesian counterparts as LAPAN, LIPI, Ministry of Forestry, University of Palangka Raya/UNPAR and RISTEK. Furthermore, the collaboration between the Agency for the Assessment and Application of Technology (hereinafter referred to as "BPPT") and Hokkaido University, Japan have been established and signed on August 5th, 2012.

In the meantime, advanced sensors are developed in Hokkaido University. One of the examples is AMI (Airborne Multicolor Imager) using the LCTF (Liquid Crystal Tunable Filter) technology, which can select any colors with ~20 nm bandwidth in 420-700 nm at 1 nm step. This multispectral sensor is suitable for measuring parameters essential for tropical peatland carbon management. Other sensors using the LCTF technology are installed on the RISING-2 and RISESAT microsatellites and will be launched in 2013-2014. Therefore, AMI is positioned as a precursor to the future satellite remote sensing of the tropical peatland.

To demonstrate the performance of AMI, the airborne campaign was conducted on 29th-31th October 2012, in West Java, Indonesia, using un-manned aerial vehicle (UAV) of BPPT called PUNA. AMI was installed on PUNA "Wulung", which has capability to fly using autopilot to reach area in radius of 70 km and altitude of 8000 feet (2.4 km). In this campaign, Wulung flied over the target location in the peat swamp forest area, about 50 km east of Nusawiru airport. During the flight, AMI captured a total of 16625 digital images of 420-700 nm at

a 10-nm step with 2 images/sec. Parameters for classification of tree species in the peatland forest and other land-uses were measured in the area. AMI was proven to be suitable for Measurement, Reporting and Verification (MRV) using UAV, which is a cost-effective tool for remote-sensing.

**3. Potential of micro-satellite observation**

The constellation realizes a frequent monitoring from the low earth orbit. If we inserted 100 satellites into proper orbits, we can watch every location in the world about every 3 min. Here we suggest the establishment of such super micro-satellite constellation by Asian micro-satellite consortium. It's not easy to launch and operate more than several tens of satellites by single country. However, if each country launches 10+ satellites, the total number could be over 50. On the other hand, each owing countries would like to operate satellites for their own purposes. The idea is that the a certain percentage of machine time of the satellite, for example, 80 percent, is used for their own purposes, but 20 percent should be remained for public use, such as disaster monitoring or periodic survey planned by international committee. In order to construct the effective and practicable constellation, the key would be standardized remote-sensing payload. One of the examples is the 5-m resolution telescopic camera with LCTF, which can select any colors from 420-700 nm and/or 650-1050 nm at 1 nm step both onboard RISING-2 and RISESAT.

**Acknowledgements**

The research of UAV observation was carried out by "Wild Fire and Carbon Management in Peat-Forest in Indonesia" project supported by JST/JICA, SATREPS (Science and Technology Research Partnership for Sustainable Development), Japan. Microsatellite project is supported by Hodoyoshi project promoted by Cabinet Office and micro-satellite development project by MEXT and Kakenhi.

# Modular and Compact Command & Data handling System with Fault-Tolerant Function for Microsatellite

**Dae-soo Oh[1], Myeong-ryong Nam[1]**
[1] *JNM System, Korea, nam@jnmsystem.com*

## Abstract

This paper describes the design of modular and compact Command and Data handling System (CDS) for microsatellite. For SEU mitigation Triple Module Redundancy(TMR) and Hamming technology are applied to protect LEON3 and 8051 IP processors which are implemented in Field Programmable Gate Arrays (FPGAs). Error Detection and Correction (EDAC) algorithm and memory scrubbing algorithm are also applied to protect memories. This CDS is on-orbit reconfigurable by uploading FPGA images and Flight Software Code, so that modifying and upgrade the system during mission operation are possible.

***Keywords*** **:** Command & Data handling System, On-Board Computer, Fault Tolerant, Reconfiguration

## 1. Introduction

There is a trend for high-performance computing and on-board data processing while providing excellent reliability/SEU immunity.

JNM propose the Command and Data handling System (CDS) as a solution to the space industry's need for high-performance and reliable space data handling system. The CDS has a feature of a highly modular structure, such that it can be quickly and easily configured to most space applications, such as data processing, communication, and control of various spacecraft subsystems and payloads.

## 2. System Design

The CDS is composed of Leon3 Card, IO Card, Payload IO Card, Flash Memory Card, and LVPS (Low Voltage Power Supply) Card.

Leon3 Card manages the spacecraft bus and payloads according to the schedule set by Ground Station (GS) and provides environment for AOCS (Attitude and Obit Control Subsystem) Flight Software. Leon3 Card has three Leon-3 IP processors and TMR logic. Matrix multiplier for AOCS software is implemented in FPGA, which allows more stable and fast AOCS calculations.

IO Card has a 8051-FT IP processor which controls bi-level digital commands and collects onboard digital and analog sensors data. IO Card communicates with GS according to CCSDS Protocol and the Protocol IP is implemented in a IO Card FPGA.

Payload IO Card receives payloads data and transmit them to Flash Memory Card for onboard memory, and sends them to the GS via X-band RF

LVPS (Low Voltage Power Supply) Cards generates low voltage of +3.3V, +5V +15/-15V.

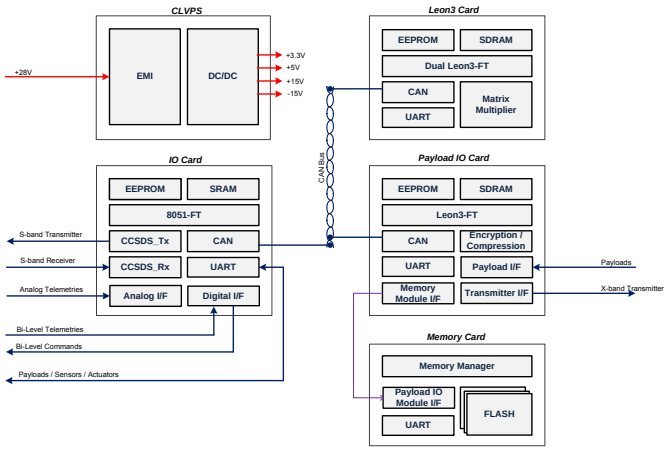


Fig 1. Configuration of CDS

Payload IO card receives data from payloads and process data such as RS Encoding, Encryption and Compression. Flash Memory card has non-volatile flash memories in which auto scrubbing algorithm is applied because of SEU mitigation in space environment

The main features of the proposed CDS are as follows.

(a) Modularity and Compactness
  A. Interchangeable Cards Assembly
  B. IP Cores of CPU and AMBA Bus in FPGAs
(b) Fault Tolerant CPU
  A. Three Leon3 processors and TMR Logic
  B. 8051 processors protected by Hamming codes
(c) Reconfigurability
  A. On-orbit FPGA Reconfiguration
  B. On-orbit Flight Software update

### 2.1. Modularity and Compactness

The CDS is designed to provide a high level of electrical and mechanical modularity, while resulting in a very

compact size. The system utilizes card-to-card stacking with PCI connectors as an electrical backplane allowing mix and match expansion, while CAN bus is used for communication between Cards. Each Card has aluminum frame for mechanical structure and thermal dissipation.

Each Card is designed on SOC concept for compactness. Most of important functions including CPUs and ARM's Advanced Microcontroller Bus Architecture (AMBA[1]) bus and peripherals as well as external memory controller are implemented in FPGAs.

The modularity and compactness result in the 3U (100 x 160 mm) size PCB of each Card.

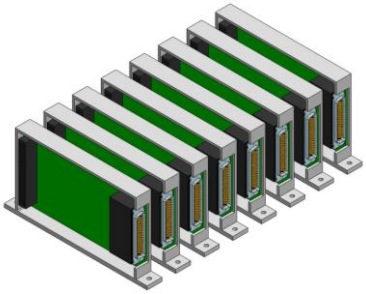

Fig 2. Card-to-Card Stacking type

### 2.2. Fault Tolerant Design

Fault tolerance techniques can improve reliability by reducing and correcting the faults. In Leon3 Card, three Leon3 IP cores are implemented in FPGA with TMR logic which performs voting about the results of the three Leon3 processors, and resynchronize and scrubs the processors.

In IO Cards, Payload IO Card, Flash Memory Card, 8051 micro-controllers are implemented in FPGAs with a VHDL description protected by the Hamming code technique. The choice of this micro-controller was based on the fact that it is widely used in space applications, and consequently, large amount of data about its behavior under radiation is available.

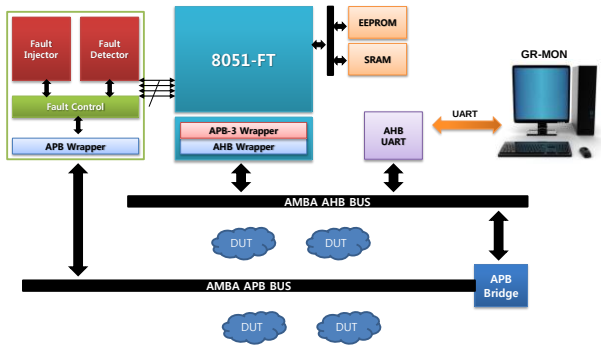


Fig 3. 8051-FT System

Besides, it makes possible the reuse and protection of all systems that are already running based on it. The SEU sensitive area of the micro-controller has been protected using the Hamming code technique. This technique is mainly based on the error detecting and correcting algorithm. In case of unrecoverable error occurrence, reset signal is automatically generated and all error event is recorded in non- volatile memory.

### 2.3. Reconfigurable Design

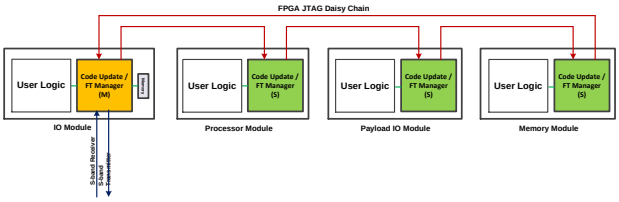


Fig 3. FPGA JTAG Daisy Chain

Small Satellite electronic components are not available for physical upgrade or repair after launch. Run-time Reconfigurable computing technology of SRAM or Flash based FPGAs allows to overcome this problem. This feature is good benefit for a new generation of low-cost commercial, scientific and military small satellites. For reconfiguration the IO Card receives FPGA images from GS and stores them to its memories and reprogram the other Card via FPGA JTAG which is connected in a daisy chain.

## 3. Results and Discussion

Modular CDS is a efficient system which can be configured to most space applications. It is particularly well suited for small satellites since Cards can be easily be removed or exchanged, resulting in a only necessary configuration. Fault tolerance feature can also ensure high reliability.

## 4. Summary

JNM proposed a modular and reliable CDS.

## Acknowledgements

This symposium is sponsored by Center for Environmental Remote Sensing (CEReS), Chiba University and Research Institute for Sustainable Humanosphere (RISH), Kyoto University

## References

1) "AMBA Specification, version 2.0", ARM Limited, 1999

# Implementation of CP-SAR signal processing system on Virtex-6 FPGA

**Kei Iizuka[1], Kazuteru Namba[2], Josaphat Tetuko Sri Sumantyo[3]**

[1 2] *Graduate School of Advanced Integration Science, Chiba University*
[3] *Center for Environmental Remote Sensing, Chiba University*
*1-33 Yayoi-cho, Inage-ku, Chiba-shi, Chiba, 263-8522 Japan*
[1]*k_iizuka@chiba-u.jp*, [2]*namba@faculty.chiba-u.jp*, [3]*jtetukoss@faculty.chiba-u.jp*

**Abstract**
We are developing a microsatellite with a circularly polarized synthetic aperture radar (CP-SAR). In this project an unmanned aerial vehicle (UAV) of CP-SAR loading is being developed for a preparation experiment prior to development of a micro satellite. To accomplish image processing on the image obtained by the radar, we are studying image processing system using Field Programmable Gate Array (FPGA). This paper presents a UAV on-board semi-real-time SAR image processing system. In addition, a sample raw data is processed in the implemented system and is compared to a data generated on PC, which gives evidence that the designed system provides processed image with sufficient high accuracy.
***Keywords*** **:** microsatellite, UAV, CP-SAR, FPGA

## 1. Introduction

We are developing a microsatellite with a circularly polarized synthetic aperture radar (CP-SAR). On the microsatellite, high-speed image processing for very large data is required. Image processing on the satellite is expected to reduce image data size and the communication time to the ground. From this view point, there are some works for image processing using Field Programmable gate Array (FPGA)[1].

In this project, we are developing an unmanned aerial vehicle (UAV) of CP-SAR loading for a preparation experiment prior to development of a micro satellite. This paper presents an image processing system designed for the preparation experiment. The system is implemented on two FPGA evaluation boards and PC.

## 2. Preliminary

### 2.1. Synthetic aperture radar

Synthetic Aperture Radar (SAR) uses microwave; it is operable in all-weather and day-night time. SAR accomplishes to obtain high resolution image; the SAR virtually made a large antenna by moving a small antenna.

### 2.2. SAR image processing

Raw image data obtained from CP-SAR is unclear; SAR image gives a clear image. SAR image processing is essential to analyze the image.

The proposed system uses Range-Doppler-Algorithm (RDA) which is a basic method for SAR image processing. The RDA processes SAR images with two steps of one-dimensional pulse compression, namely range and azimuth compressions.

The RDA performs FFT, IFFT, and compression using the reference signal for range and azimuth direction. In addition, the RDA corrects errors caused by the move of the platform [2].

## 3. Implemented system

Figure 1 illustrates the outline of the SAR image processing system implemented in this work. This system consists of two FPGA evaluation boards, ML605 and SP 605, and a PC. The ML605 has a Xilinx Virtex-6 FPGA and 2GB DDR3 DRAM. The SP605 has a Xilinx Spartan-6 FPGA.

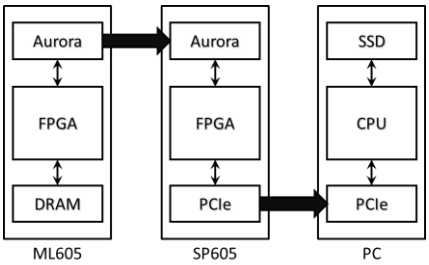


**Fig. 1 Outline of the SAR image processing system**

This system consists of two units: image processing unit and data storage unit. Raw image data obtained from CP-SAR are input to the image processing unit through an AD converter. The image processing unit processes SAR image processing using image processing system, and it is configured on the ML605. The processed data is output to the data storage unit, which is implemented on

the SP605 and the PC. Finally processed data is stored by the SSD in the PC.

Figure 2 shows the block diagram of the proposed SAR image processing circuit. The circuit consists of a calculation circuitry, a reference signal storage unit, a corner turn circuitry, a flow controller, a memory controller, an RX, and a TX. The image processing unit makes the RDA by performing processing, such as compression processing and correction processing, on the raw image data.

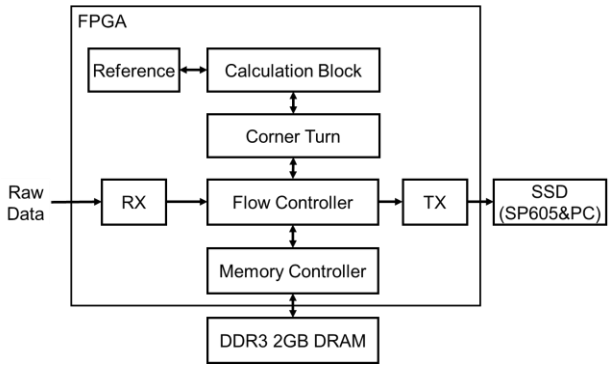


**Fig. 2 Block diagram on FPGA (Virtex-6 on ML605)**

First, data are input from external device, are processed on the calculation circuitry, and are stored in the DRAM. The data is read out from DRAM, is sent to the calculation circuitry, is processed, and stored in the DRAM. Subsequently SAR image data come and go between the DRAM and the calculation circuitry with being processed. During this, the data is processed along range and azimuth direction in the calculation circuitry, and reordered in the corner turn circuitry as needed. The processed data is output to the data storage unit. The RDA makes six times of range / azimuth FFT / IFFT; the proposed system performs the six by using one FFT circuit 8,192 points and one FFT circuit of 32,768 points. The six FFT operations shares two FFT circuitries, which reduces the amount of used FPGA resources.

## 4. Results and Discussion

A sample raw data was processed in the implemented system using FPGA in order to evaluate the system. The size of sample raw data is 2,048 x 1,024 pixels. In addition the processed data is compared to a data generated with MATLAB on PC in a proven manner.

Figure 3 shows the SAR image processed by the FPGA and the MATLAB. We can find that these images are almost the same; this means that the proposed system provides SAR image processing with enough accuracy for actual use.

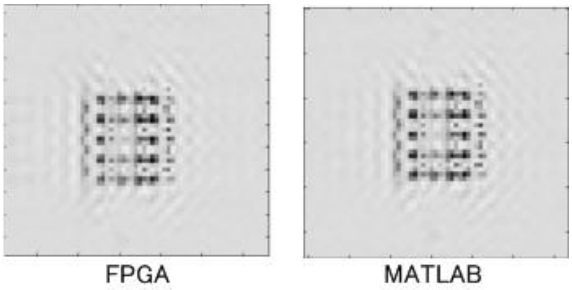


**Fig. 3 SAR image processed by the FPGA and the MATLAB**

## 5. Summary

This paper presented an image processing system, which is implemented on two FPGA evaluation boards and PC. In the implemented system, a sample raw data was actually processed and compared to a data generated on PC, the result of which gave evidence that the image processing system using FPGA has enough accuracy for actual use.

However, the implemented system is not capable of SAR image processing the raw data of 6,144 x 19,904 pixels due to a resource issue; we must resolve it.

**Acknowledgements**

This work was carried out by the joint research program of CEReS, Chiba university

**References**

1) Takuma Kusama, Kazuteru Namba, Josaphat Tetuko Sri Sumantyo, "Implementation to the Virtex-6 FPGA of the UAV with CP-SAR image processing system," Technical Report of IEICE, SANE2012-114, Nov. 2012. (in Japanese)
2) Kazuo Ouchi, "Principles of Synthetic Aperture Radar for Remote Sensing," Tokyo Denki University Press, 2004 (in Japanese)

# Monitoring Land Subsidence by TerraSAR-X in Cengkareng, Jakarta City, Indonesia

**RatihFitria Putri[1], Luhur Bayuaji[2], JosaphatTetuko Sri Sumantyo[1,3] and Hiroaki Kuze[1,3]**
*[1]Graduate School of Advanced Integration Science, Chiba University, Japan*
*[2]Faculty of Computer Science and Software Engineering, Malaysia Pahang University, Malaysia*
*[3]Center for Environmental Remote Sensing (CEReS), Chiba University, Japan*
*E-mail of contact person : ratihfp@chiba-u.jp*

## Abstract
Subsidence in urban area has the potential to cause severe damage in ecosystem. Therefore it is important to understand the subsidence phenomenon in urban area. The objective of this study is to investigate the land deformation in the metropolitan area of Jakarta, Indonesia using multiple satellite radar imagery. Differential synthetic aperture radar interferometry (DInSAR) is a technique useful for accurately detecting the ground displacement or land deformation in the antenna line-of-sight (slant-range) direction using synthetic aperture radar (SAR) data taken at two separate acquisition times. In this study the DInSAR technique was used to map the land subsidence in Jakarta region with X-band TerraSAR radar images. A total of 4 TerraSAR-X images acquired from 9 August 2010 to 1 March 2013 over Jakarta were used in this study. The results demonstrated that the land in the area of Cengkareng was deforming at different rates. Several subsidence bowls with peak displacement rates 10 – 17.5 cm/yr along the radar looking direction have been observed Cengkareng.
***Keywords*** **:** Land Subsidence, Monitoring, TerraSAR-X

## 1. Introduction
Land subsidence in urban areas may result in adverse impacts and can lead to serious problems. Urban subsidence can lead to increased risk of flooding of coastal areas, severe damage to the buildings and infrastructures, destruction to local groundwater systems, and also tension cracks and reactivated faults [1]. Differential synthetic aperture radar interferometry (DInSAR) is a technique useful for accurately detecting the ground displacement or land deformation in the antenna line-of-sight (slant-range) direction using synthetic aperture radar (SAR) data taken at two separate acquisition times [2,3].

Cengkareng is located between $6^0$7’9’’S latitude and $106^0$43’10’’E longitude, in the western part of Jakarta city. The sub district consists of six regions, covering an area of about 27.93 km2. Fig.1A shows map of Cengkareng district area on Jakarta City Map. The area is relatively flat: topographical slopes range between $0^0$ and $2^0$. The elevation of the southernmost area is about 20 m above sea level, with the other areas being lower (Figure 1B). Cengkareng, located in the Jakarta basin, has the following five main landforms: alluvial, marine origin, beach ridge, swamp (including mangrove), and former channel.

## 2. Methods
TerraSAR-X is a German high resolution radar satellite program which will be the first commercially launched on the 15th of June 2007. Until now there is no C-Band and L-Band has an operational of advanced SAR-satellite system for scientific and commercial application for public. Because of that, we used X-Band data to make continuously land deformation monitoring in Cengkareng. TerraSAR-X data provides high spatial resolution of about 3 m and has high geometric accuracy imagery. The advantage of X-Band than L-Band and C-Band is The X-Band has short wavelength (about 3.1 cm) and confers a high sensitivity to land deformation. The TERRASAR-X data is the only data that has descending orbit in this study. In this study we would like to investigate land subsidence by applying DInSAR technique. We processed one pair of TERRASAR-X data between 2010 and 2013. This is the newest available data in this study. The pair, spatial baseline and temporal baseline of TerraSAR-X can be found in Table 1.

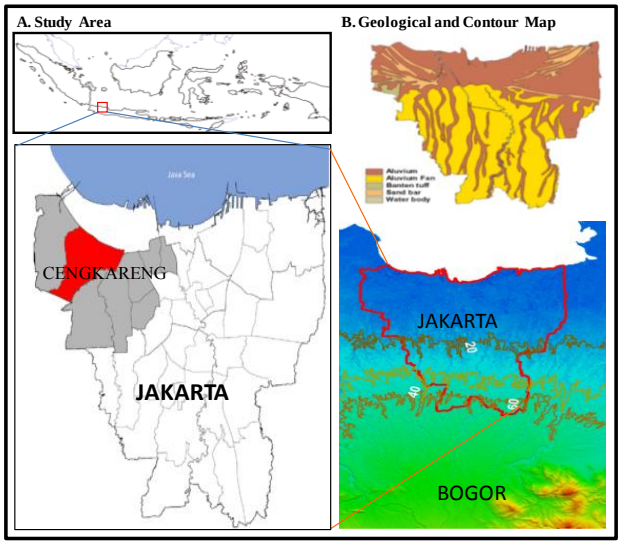


**Fig. 1. (A) Map of Jakarta basin and (B) Geological map of Jakarta urban area.**

**Table 1. TerraSAR-X pair and baseline information**

| | Acquisition Date | | Temporal Baseline | Spatial Baseline |
|---|---|---|---|---|
| Pair | Master | Slave | (week) | (meter) |
| 1 | 20100809 | 20110613 | 44 | 110.5 |
| 2 | 20100809 | 20121214 | 122 | 149.3 |
| 3 | 20100809 | 20130301 | 133 | 138 |
| 4 | 20110613 | 20121214 | 78 | 39.1 |
| 5 | 20110613 | 20130301 | 89 | 248.1 |
| 6 | 20121214 | 20130301 | 11 | 286.3 |

**Note:** Date are given as year, month, and a day (e.g., 20100809 denotes 9 August 2010)

## 3. Results and Discussion

The DInSAR technique result of TerraSAR-X data shows the land deformation is getting larger in terms of area and depth associate to longer interval time observation. The largest deformation rate estimation reach 17.5 cm/year in some points based on DInSAR calculation during 44-week interval times.

Cengkareng, is a settlement area that covers more than 23 km2. Since 2005, flat housing has been widely developed in this region to relocate the slum dwellers. The international airport and industrial area were built nearby. The maximum subsidence rates found during the time span of the study are 17.5, 11.8, 11.7, 11.5, 10.5 and 10 cm/year (Table 2).

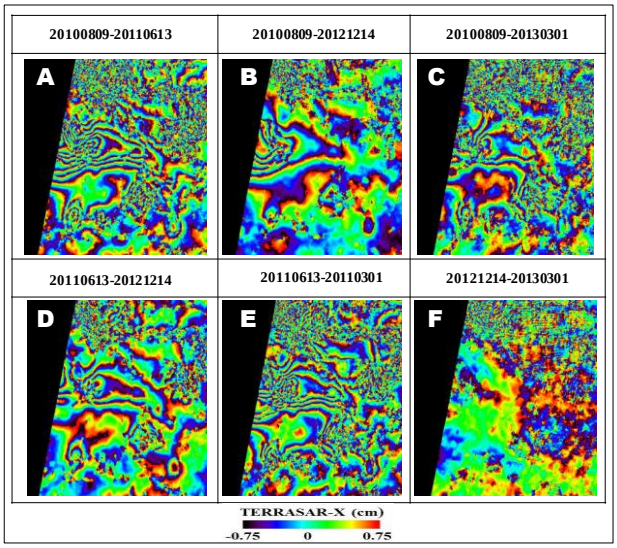


**Fig. 2. Cengkareng DInSAR result of TERRASAR-X data pair all pairs mentioned in Table 1. (a) Data pair on 20100809-20110613, (b) Data pair on 20100809-20121214, (c) Data pair on 20100809-20130301, (d) Data pair on 20110613-20121214, (e) Data pair on 20110613-20130301, (f) Data pair on 20121214-20130301.**

The study area is a newly developed residence area with more than 300 hundred households living over this area. The cause of subsidence was predicted as the result of ground water extraction, the building construction load and human activity over this area.

**Table 3. Maximum subsidence and subsidence rate estimation in Cengkareng by using DInSAR.**

| Pair Number | Acquisition Date | | Cengkareng Subsidence Rate (cm/year) |
|---|---|---|---|
| | Master | Slave | |
| 1 | 20100809 | 20110613 | 17.5 |
| 2 | 20100809 | 20121214 | 11.5 |
| 3 | 20100809 | 20130301 | 11.7 |
| 4 | 20110613 | 20121214 | 10.0 |
| 5 | 20110613 | 20130301 | 10.5 |
| 6 | 20121214 | 20130301 | 11.8 |

## 4. Summary

This study shows that DInSAR methods able to detect the ground deformation in Cengkareng sub district area. The DInSAR analysis can be considered as potential tool to monitor the land subsidence on disaster with low cost, especially to detect ground deformation as an impact of flood hazard area in 2013. The observation continuation becomes important to monitor the ground deformation and to prevent further human severe. In the future, multiple aperture technique and GPS measurement will be applied to get a better result and analysis.

## Acknowledgements

The authors would like to thank to PASCO and Center for Environmental Remote Sensing Chiba University for the financial support for the research.

## References

[1] A. Primanita, "Jakarta Areas Muara Baru, Cengkareng sinking Fast," in *Jakarta Globe*, ed. Jakarta, 2010.

[2] S. Stramondo, C. Bignami, M. Chini, N. Pierdicca and A. Tertulliani, "Satellite radar and optical remote sensing for earthquake damage detection: Results from different case studies", International Journal of Remote Sensing, vol.27, no.20, pp. 4433 - 4447 2006.

[3] D. M. Tralli, R. G. Blom, V. Zlotnicki, A. Donnellan and D. L. Evans, "Satellite remote sensing of earthquake, volcano, flood, landslide and coastal inundation hazards", ISPRS Journal of Photogrammetry and Remote Sensing, vol.59, no.4, pp. 185-198 2005.


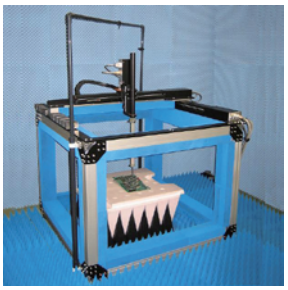

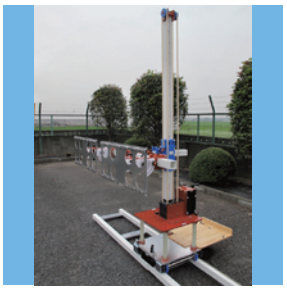
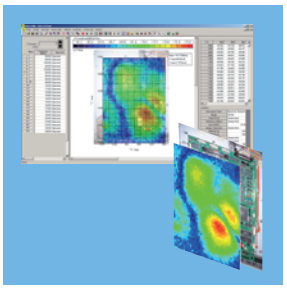

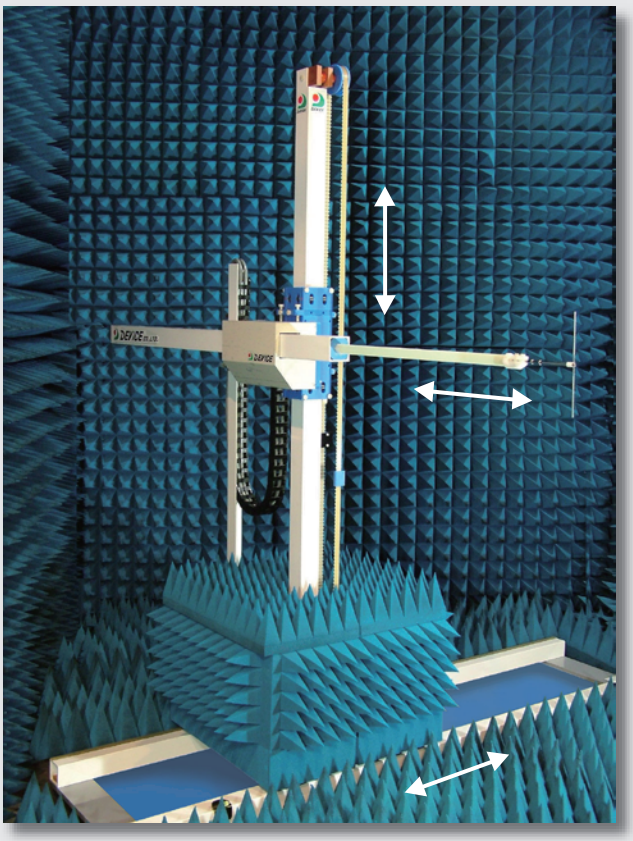

3D Scanner
DM3421AV1/O

# Three-dimensional electromagnetic-field distribution measurement system

## System

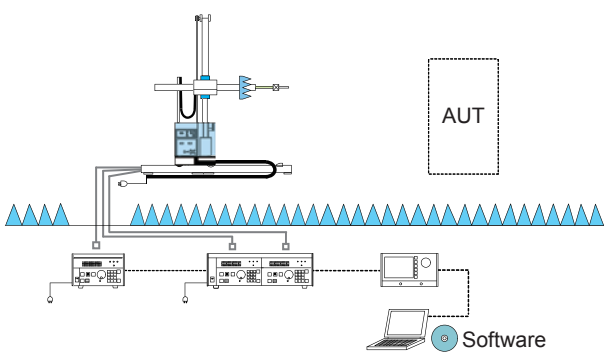


It is large activity to electromagnetic-field distribution measurement of area, and visualization measurement of equipment.
Good three-dimensional measurement and analysis of reproducibility are possible.

### ■ Three-dimensional vertical plane scanner & software

- X-Y-Z axes is controlled freely and wide range electromagnetic-field distribution measurement is possible.
- Various antennas can be attached.
- superposition of measurement data and a measurement thing photograph can be performed, it can check at a glance.
- Automatic measurement of a maximum of 24 waves is possible.


Elevation Positioner

Azimuth Table

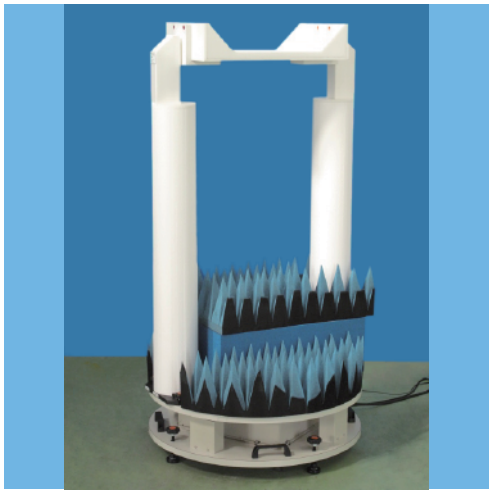

Great Circle Test System

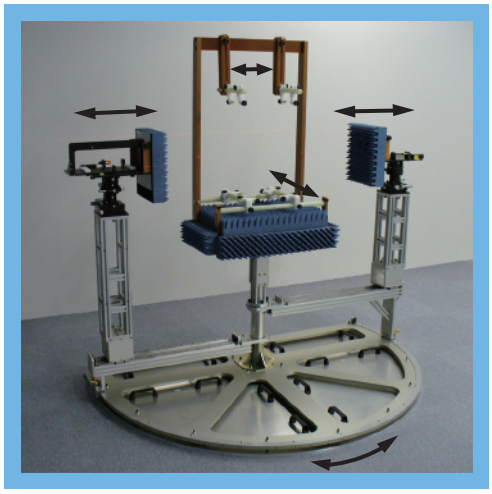

Reflective Transmission Measurement System

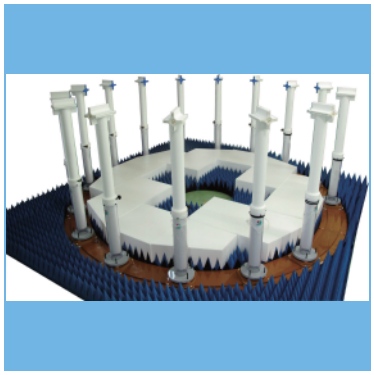

MIMO OTA System

Portable Anechoic Absorber Wall

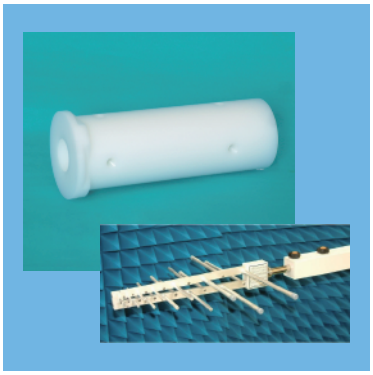

Antenna Adapter

# The 20th CEReS International Symposium on Microsatellites for Remote Sensing (SOMIRES 2013) and The 231th RISH Symposium Chiba, 8-9 August 2013

## Possibilities of Approach Integrating RS Multi-Data Analysis and GIS for Water Resources Management and Environmental Monitoring

### *The case study of Bili-Bili Irrigation System, Indonesia*

**Yaqien Gisno Ogalelano[1], Takao NAKAGIRI[2], Hiroki OUE[3], Dorotea Agnes RAMPISELA[4], Sartika LABAN[5], Hisaaki KATO[6]**

[1]*Ehime University, Hasanuddin University, E-mail: yaqien7@yahoo.com,* [2]*Graduate School of Osaka Pefectural University ,*[3]*Graduate School of Agriculture, Ehime University ,* [4]*Department of Soil Science, Hasanuddin University,* [5]*Ehime University,* [6]*Research Institute for Humanity and Nature.*

## Abstract

The use remote sensing and Geografic Information System (GIS) datas allow more efficient analysis because the temporal and spatial dimensions could be studied at once, especially to generate primary data on irrigated area, cropping pattern and crop yield at disaggregated level and to access the improvement in agricultural productivity and water management in canal irrigation schemes. Another issue in the spatial and temporal dimension of water productivity. A spatio–temporal analysis could broaden the role of models in exploring improved water use in agriculture. The GIS technique helps in integration of satellite data and ground information to evaluate the distribution water performance and to diagnose the inequality in the performance to aid in improving the water management. This paper aims to improve agricultural productivity, water productivity, and environmental monitoring through a predictable, equitable and reliable irrigation service.

***Keywords*** **:** Integration of RS and GIS, Multi data analysis, Water resources management, Environment, Monitoring

### 1. Introduction

According to Rampisela (2011) The Bili Bili Dam, which completed construction in 1999, has the capacity to store 375 million $m^3$ of water. Although the primary objectives of the dam are flood control and clean water supply for makassar urban area and its surrounding environs, the dam also proves capable of providing irrigation for 25,472.16 ha of rice fields (fig. 2(A).

Almost every year in irrigated areas of Bili-Bili especially in the lower reaches during the dry season, farmers didn't get water for irrigation. Many problems which is influence the insufficient water in irrigation canals, such as canals damage, water lost to pond (eks making brick), and water gate uncontrol).

The integration of remote sensing and Geographic Information Systems (GIS) has received considerable attention in the literature. Ehlers et al. (1991) first reviewed the necessity of integrating remote sensing with GIS, and discussed the potential of integration in water resource management and environmental monitoring.

In this paper we will discuss about possibilities approach integrating remote sensing multi data analysis and GIS to manage water resources and environment with 2 indicators, that is water availability and cropping patterns. Remote sensing multi data analysis means using variety of resolution data analysis from different sensors (fig. 1).

### 2. Methods

This research will survey (ground truth; observation, interviews, crop photos time series from few location), spatial analysis, time series analysis, statistical analysis, and collecting data (weather data from on site meteorological station, secondary data from BPS and etc)

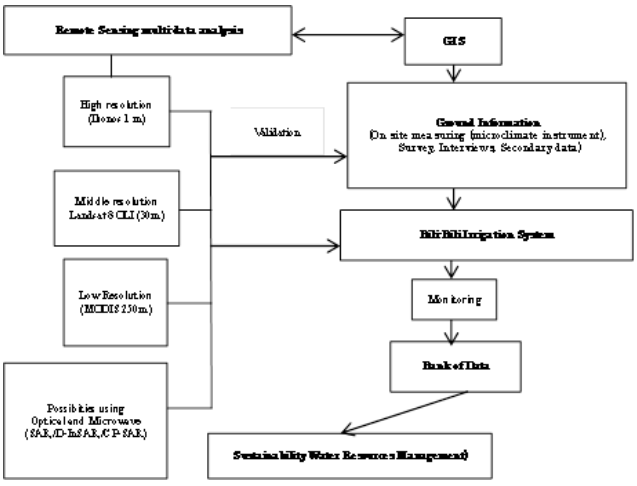


Fig.1. Approaches of integrating RS multi-data analysis and GIS Scheme

### 3. Results

We successfully to extract data from Ikonos (Fig.2) and Modis

data analysis (Fig.3) and now, we will try to Landsat 8 OLI and SAR data analysis to get more information about water resources and environment condition in Bili-Bili Irrigation System.

**Ikonos data analysis**

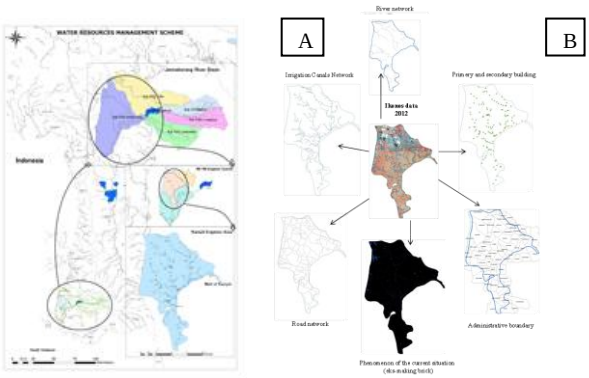


Fig.2 (A) Study site location, South Sulawesi, Indonesia. (B) Extraction of Ikonos data for spatial data analysis to observe the current situation with more accurate

**Modis data analysis**

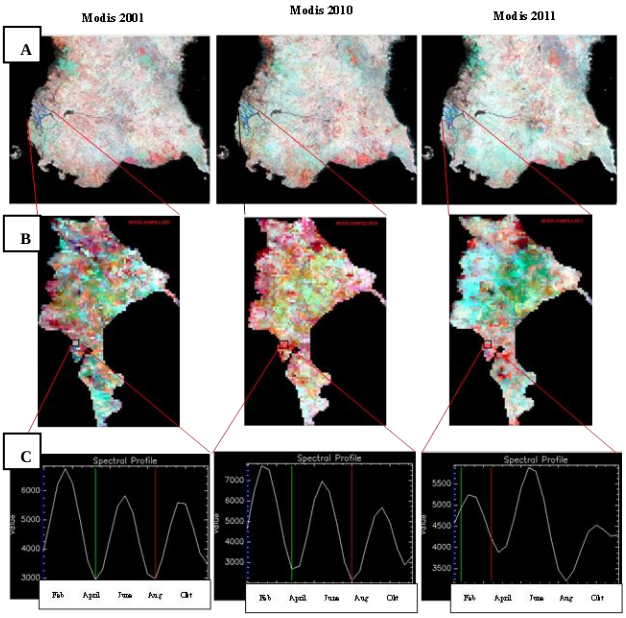


Fig .3. Validation of the underestimated number of crops in 2001, 2010 and 2011 in Bili-Bili Irrigation Area, South Sulawesi, Indonesia (A) EVI MODIS false-color image (R:G:B= Band 6: Band 2: Band 1). (B) Kampili Irrigation Area (MODEL). (C) Average monthly EVI MODIS data in areas where the almost every year insufficient water and number of crops per year decreased in 2010 to 2011 and also we compare within 2001 to 2010 which purpose to know about the copping pattern before and after landslide.

**Water use analysis**

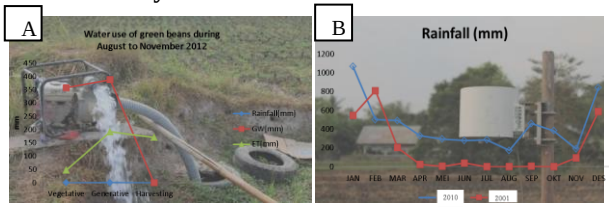


Source : Sartika & Oue data, 2012

Source: BPS data, 2011

Graph.1. On site measuring data and secondary data in Kampili Irrigation Area (A) Water use of green beans during Dry season (August to November). (B) Rainfall data in 2001 and 2010 from BPS (Central bureau of statistics).

After that, we will validation with ground information which extract from water use data analysis ,weather data (graph.1) and ground survey, then we collect all data in data bank using GIS analysis.

## 4. Discussion

One of the main advantages of this integrate is its capability to monitoring water resources and environment and easy to making the best management plan. The other hand, we want to try about using SAR and CP-SAR images from microsatellite to monitoring environment problem like the subsidence and ground water problem issue in irrigation area. This is the main problem issue for future because, we can see of human activity especially farmers exlore water from ground water in dry season to be increase every year.

## 5. Summary

In this paper, we proposed to develop a new approach integrating remote sensing data analysis from different resolution and sensor data. This is integrated will be applicable for irrigated area mapping, cropping pattern management, water requirement, and disaster monitoring. We also proposed the SAR image data for environmental monitoring at Bili-Bili Irrigation area..

## Acknowledgements

This Research is part of Water Resources Management Project (C-09-Init) funded by Research Institute for Humanity and Nature (RIHN), Kyoto, Japan. The authors would like to thank the Pelangi Agency of Makassar that provide the bili-bili irrigation system data

## References

[1] Ehlers, M., D. Greenlee, T. Smith, and J. Star, 1991. Integration of remote sensing and GIS Data and data access, Photogrammetric Engineering b Remote Sensing, 57(6):669-675.

[2] Rampisela D. A. 2011. Bili-Bili Irrigation system. Bili-Bili Irrigation Project. South Sulawesi, Indonesia.

[3] OUE H., Sartika L., D. Agnes Rampisela.. 2013. Evapotranspiration and Water Balance In A Water Use Association Block Area In South Sulawesi During The Dry Season. Water Management Project.

# Preliminary Study of Concrete Surface Temperature Mapping on Structure Problems in Makassar City with Airbone Thermal Remote Sensing

**Arwin Amiruddin[1], Josaphat Tetuko Sri Sumantyo[1], Ilham Alimuddin[2], Merna Baharuddin[3]**
[1]*Hasanuddin University,* [2]*Chiba University, a.arwinamiruddin@yahoo.com*

## Abstract
Nowadays, the corrosion of concrete structures has moved into attractive fast-growing research. Corrosion in concrete is influenced by water, air, and temperature. Especially for the influence of temperature, this preliminary research will focus on mapping the temperature of concrete surface. Objective of this study is to develop a temperature mapping on concrete structures through airborne thermal remote sensing. The research will located at Makassar city in South Sulawesi, eastern part of Indonesia. Due to the research is still preliminary so the study was limited to the characteristics of the existing concrete building in Makassar city related with a remote sensing perspective. Results of this study are expected to assist the local authorities for early detection of corrosion problems on concrete structures and possibly will prevent a significant amount of structural failure and loss. In future, the shadow effect on radiant temperature will analyzed. The statistical T-test will used as measure in detecting concrete surface and provided to be effective.
.

***Keywords*** **:** concrete surface, thermal, mapping, makassar city

## 1. Introduction
Makassar city is one of major cities in Indonesia and is located in eastern part of Indonesia. Based on data from the Meteorology, Climatology and Geophysics Region IV Makassar that rainfall in Makassar, South Sulawesi and other regions are generally categorized overcast-light rain with temperatures between 23-32$^{o}$C, humidity of 63-97%, and the average wind speed ranges from 2.9 knots. Because Makassar city is in the tropics region so the temperature is a few things to consider. Infrastructure in the city is an average made from concrete, therefore, the effect of temperature on the concrete / concrete surfaces need to be tested for early detection of damage of concrete structures and for the purpose of maintenance of them.

Figure 1 shows the Makassar city as the location of study. There are many concrete construction that stands such as hotels, offices, and others. In addition to temperature effects, the location of Makassar city is near the sea causing corrosion effects become important for concrete buildings.

A series of studies have been studied related to the corrosion problems in concrete buildings, such as the influence of sea water to coastal structure buildings (Arwin, et al, 2012). However, this research takes a long time so it needs to be done similar research through the perspective of remote sensing using airborne thermal remote sensing. Through this approach it is expected that it will be able to mapp the temperature on the concrete surface and early corrosion can be detected so that possibly will prevent a significant amount of structural failure and loss.

In this study, we investigate the applicability of airbone thermal remote sensing data for mapping concrete structure anomalies in detecting temperature differences.

## 2. Methods
Makassar city is located in the plains near the sea in eastern part of Indonesia. Recently, infrascture development using concrete material is incessant carried out in Makassar thi is consideration choosing this location as objects of study.

Thermal Airbone Broadband Imager 320 (TABI-320), a new airbone thermal sensor developed by ITRES Research Ltd. (Canada), was acquired by PASCO Corporation (Japan). The specifications of TABI are shown in Table 1.

The study will be divided into 2 (two) parts, namely, in early morning (EM) and in early afternoun (EA). The data will be recorded from flight record of TABI for acquiring the thermal data with 1.5m Ground Sampling Distance (GSD).

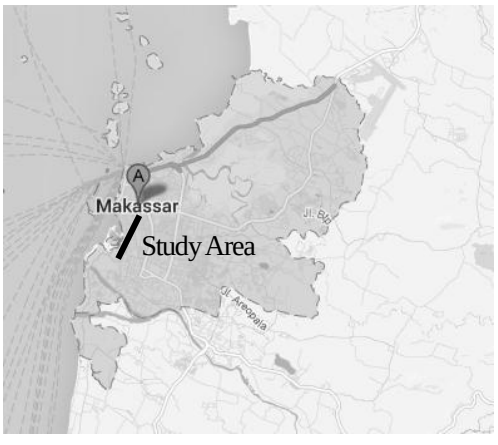


**Fig. 1** Makassar city as location of study

The study area covers 0.67 km * 7.2 km. These images were orthorectified with a 50 m resolution DEM (Digital Elevation Model) released by Geographical Survey Institute of Japan.

Table 1. Specifications of TABI-320

| | |
|---|---|
| Instrument Type | Pushbroom Thermal Imaging Microbolometer |
| Field of View (FoV) | 48 deg across-track across 320 pixels; ~f/1 |
| | 0.25 deg along-track |
| Instantaneous Field of View | 2.87 milliradians |
| Spectral Range | 8 – 12 μm (800 – 1200 mm) : 1 band |
| Dynamic Range | 4096 : 1 (12 bits) |
| Temperature Range | -20 to 110 ºC Nominal |
| NEΔt | 0.1 K |

In general, the temperature of each surface cover increases after sunrise, continues to increase until 2:00 PM, and then decreases gradually. The temperature deviation depends on surface cover type. Thermal image has a great possibility for concrete monitoring because the deviation of concrete surface temperature in one day is large. We assume that the irregular distribution of temperature occurs at the concrete anomaly points.

In general, the radiant temperature observed by spaceborne / airbone thermal sensors is easily affected by shadow, especially on the high resolution images. Therefore, a shadow simulation with DEM could be useful to estimate and remove its effect. However, the 50 m resolution DEM available in this study is unsufficient to simulate the shadow area of the 1.5 m GSD thermal images. Instead of DEM , 2 TABI images in early morning and in early afternoon were used to estimate the shadow effect.

The difference of the the radiant temperature (ΔT) was defined as below.

$$\Delta T = T_{EA} - T_{EM} \quad (1)$$

Where $T_{EA}$ is radiant temperature from the early afternoon (EA) image, TEM is radiant temperature from the early morning (EM) image.

For a statistical interpretation of concrete anomaly, the T-test is proposed to detect the temperature anomaly at peach pixel.

$$Z_{stnp} = X_{stnp} - M_{st} / \sigma_{st} \quad (2)$$

Where Z : statistical score
X : radiant temperature of the pixel of the pixel
M : mean value of the radiant temperature of normal concrete
σ : standard deviation (STD) of the radian temperature of normal concrete
s : shadow condition (N:NS, M:SM, A:SA, B:SB)
t : observation time (A:EA, M:EM)
n : number of line (1,2,3)
p : pixel position (-2, -1, 0, 1, 2)

if $|Z_{sAnp}|$ or $|Z_{sMnp}|$ is greater than 1.96 (95% confidence interval), the pixel will be discriminated as a concrete anomaly point.

## 3. Results and Discussion

Due to the study is still preliminary, the results have not been obtained yet. However, this preliminary study is the first step to start analyzing the effect of temperature changes on the concrete surfaces in Makassar city.

## 4. Summary

The temperature deviation depends on surface cover type. Thermal image has a great possibility for concrete monitoring because the deviation of concrete surface temperature in one day is large. We assume that the irregular distribution of temperature occurs at the concrete anomaly points.

## Acknowledgements

I would like to express my gratitude to Prof. Josaphat Tetuko Sri Sumantyo for his valuable help. Also, many thanks to Hasanuddin University through JIBIC Loan for financial support to participate in the short term research at Remote Sensing Laboratory, Chiba University for 3 (three) months (July – September 2013).

## References

1) F N. Karanja, S. Matara, 2013. *The Transformation From Green to Concrete Cities; A Remote Sensing Perspective*, International Archives of The Photogrammetry, Remote Sensing and Spatial Information Sciences, Volume XL-1/W1. ISPRS Hannover Workshop 2013, 21-24 May 2013, Hannover, Germany.
2) Karen Fletcher, 2007. *InSAR Principles: Guidelines for SAR Interferometry Processing and Interpretation*.

# Array of Triangular Microstrip Antenna and Combined Triple Rectangular Microstrip Antenna for Radio Altimeter and Ground Penetrating Radar

**Merna Baharuddin[1], Elyas Palantei[1], Zulfajri B. Hasanuddin[1], Rusli[1], Andi Azizah[1], Josaphat T. Sri Sumantyo[2]**

[1]*Dept. Of Electrical Engineering, Hasanuddin University, INDONESIA,*
[2]*Microwave Remote Sensing Laboratory, Chiba University, JAPAN,*
*merna@unhas.ac.id*

## Abstract

This study presents microstrip antenna developments for GPR and radio altimeter applications. An array of triangular antenna is designed for radio altimeter in the frequency of 4,25 GHz. A shape of combined triple rectangular microstrip antenna is designed for GPR appilication in the frequency of 1 GHz. Design and simulation was conducted using the software Ansoft High Frequency Structural Simulator (HFSS) V.13. Then the design is created in the form of prototypes by using Printed Circuit Board (PCB) made of FR4-Epoxy which has a thickness of 1.6 mm and a dielectric constant of 4.4. The measurement was done using a Vector Network Analyzer E5071C ENA and ED 3200.

***Keywords*** **:** microstrip antenna, radio altimeter, ground penetrating radar

## 1. Introduction

A radio altimeter [1] is a device, which is used to measure a low altitude or distance from an aircraft or spacecraft to ground surface or to a sea level. This distance is calculated under the craft in vertical direction. Radio altimeter is a part of radar. The working principle of radar is, it transmits radio waves towards ground level or sea level and receives an echo signal after time duration. This value of time is depending on speed of the vehicle and height between craft (air or space) and ground. Radio altimeter is working in the band of 4.2GHz to 4.4GHz

Ground Penetrating Radar (GPR) systems [2] are used for the subsurface investigation of earth. They are used in the detection of objects buried beneath the earth surface such as pipes, cables, land mines, and hidden tunnels. A GPR system consists of a transmitting antenna and a receiving antenna. The transmitting antenna is connected to a source and the receiving antenna is connected to a suitable signal processing device. It is required to develop efficient GPR antennas to satisfy a number of demands. A GPR system should have low and short coupling between transmitting and receiving antennas to avoid false detection. Since it operates very close to ground, its characteristics should not be affected strongly with ground properties

This study presents microstrip antenna developments for GPR and radio altimeter applications. An array of triangular antenna is designed for radio altimeter in the frequency of 4,25 GHz. A shape of triangular of a microstrip antenna previously has been investigated for CP SAR [3]. A shape of combined triple rectangular microstrip antenna is designed for GPR appilication in the frequency of 1 GHz.

## 2. Methods

The microstrip antennas have the form of triangular array and a combined triple rectangulars.. Design and simulation is done using HFSS V.13 software. By this software, then obtained shape and size dimensions desired of the microstrip antennas. Antenna prototype is made based on the shape and size dimensions of microstrip antennas that have been obtained from the HFSS v13 software. The design was done by making the antenna design in three dimensions. The dimensions of the designed antenna design are made in accordance with the results of mathematical calculations. After three dimensional antenna design has been established, next step is material selection. The patch, feed and ground plane, the materials is perfect-E, for substrate the material is FR4-Epoxy (relative permitivity ($\varepsilon_r$) 4.4, Dielectric loss tangent (tan $\delta$) 0.2, substrate thickness (h) 1.6 mm), while air is used for the boundary.

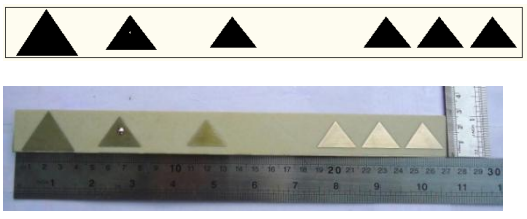

**Fig. 1 Designed Array of triangular microstrip antenna and the fabricated prototype.**

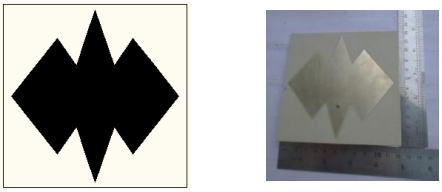

**Fig. 2 Designed Combined triple rectangular microstrip antenna and the fabricated prototype.**

Tabel 1 Microstrip Triangular Array Dimension

| | |
|---|---|
| Triangular patch driven element | Triangular side length (a) = 26,14 mm, Height (t) = 18,01 mm |
| Reflector Size | Longer 0,3 cm than the driven element , Triangular Side Length (a) = 32,14 mm, Height (t) = 21,01 mm |
| Director Size | Shorter 0,1 cm from the driven element, Triangular side length (a) = 24,14 mm, Height (t) = 17,01 mm |
| Distance between reflector and driven element | D1 = 0,2λ = 14,117 mm |
| Distance between 1 and driven element | D2 = 0,4λ = 28,235 mm |
| Distance between director 2 and director 1 | D3 = 0,8λ = 56,470 mm |
| Distance between director 3 and director 2 | D4 = 0,05λ = 3,529 mm |
| Distance between director 4 and director 3 | D1 = 0,05λ = 3,529 mm |

Tabel 2.Microstrip Combined Triple Rectangular Dimension

| Dimension Part | Size (mm) |
|---|---|
| *Wtrc* (wider side ) patch | 48,5 |
| $L_{MAX}$ patch | 113 |
| $W_g$ (width) groundplane | 120,71 |
| $L_g$ (length) groundplane | 120,54 |
| *d* (diameter) feed point hole | 1.27 |
| $X_f$ *(coaxial Feed)* | 16,61 |

The design of the antennas from the mathematic calculation of its dimension apparently not giving the desired results. Therefore, the optimization process is carried out by varying the dimensions of the components of Microstrip Antennas. Changes in patch dimensions, length and width of the feed, the dimensions of the ground plane and substrate dimensions provide significant changes to the antenna parameters.

Process optimization is done by numerical experimental to obtain the results as expected. From the optimization process final dimensions of designing an array antenna Microstrip Triangular and a combined triple rectangulars are obtained as shown in Table 1 and Table 2 . The final shape of the array triangular Microstrip Antenna and combined triple rectangular that are simulated in HFSS v13.0 are shown in Figure 1 and Figure 2.

## 3. Results and Discussion

Prototype microstrip antennas were measured using Antena Trainner System ED-3200 and Network Analyzer Agilent 5017C. This measurement is done in the Laboratorium of Telematika Electrical Engineering Department Hasanuddin University.

For the array of triangular microstrip antenna, the bandwidth obtained from the measurement is 270 MHz in the 4,25 GHz frequency. Further measurements are conducted to obtain the radiation pattern, and gain. Testing to measure height from certain position off the ground as this antenna will be applied for altimeter.

For the combined triple rectangular microstrip antennas, the bandwidth obtained from the measurement is 22 MHz in the 1 GHz frequency. Further measurements are conducted to obtain the radiation pattern, gain, and S21 parameters. As this antenna will be applied for GPR, the testing with certain soil depth using 2 antennas, one as transmitter and another as a receiver, will be conducted.

## 4. Summary

An array of triangular microstrip antennas (4,25 GHz) and a combined triple rectangular antenna (1 GHz) has been developed for radar altimeter and ground penetrating radar respectively. The simulation and measurement results have shown good results. Further measurement and testing will be conducted and more improvement on the antenna systems will be applied.

## Acknowledgement

Authors would like to express gratitude to Faculty of Engineering, Hasanuddin University, through the JBIC Loan for the opportunity to participate in the short term research program.

## References

[1] Wideband Partially-Covered Bowtie Antenna for Ground-Penetrating-Radars, G. E. Atteia, A. A. Shaalan, and K. F. A. Hussein, Progress In Electromagnetics Research, PIER 71, 211-226, 2007

[2] Asghar Keshtkar, Ahmad Keshtkar, and A. R. Dastkhosh, "Circular Microstrip Patch Array Antenna for C-Band Altimeter System". International Journal of Antennas and Propagation Volume 2008.

[3] Merna Baharuddin, Victor Wissan, Josaphat Tetuko Sri Sumantyo, and Hiroaki Kuze, "Equilateral Triangular Microstrip Antenna for Circularly-polarized Synthetic Aperture Radar," Progress in Electromagnetics Research (PIER) C, Vol. 8, pp. 107-120, June 2009.

# FPGA BASED MULTIPLE PRESET CHIRP PULSE GENERATOR FOR SYNTHETIC APERTURE RADAR ONBOARD UNMANNED AERIAL VEHICLE SYSTEM

**Kyohei Suto[1], Josaphat Tetuko Sri Sumantyo[1], Cheaw Wen Guey[2] , Koo Voon Chet[2]**

*[1]Center for Environmental Remote Sensing, Chiba University,*
*1-33 Yayoi, Inage, Chiba, 263-8522 Japan, z9t1541@students.chiba-u.jp*
*jtetukoss@faculty.chiba-u.jp*
*[2]Faculty of Engineering & Technology Multimedia University*
*Jalan Ayer Keroh Lama, Bukit Beruang 75450 Melaka, Malaysia, wengueyc@gmail.com*
*vckooo@gmail.com*

**Abstract**

Synthetic Aperture Radar (SAR) is one of active microwave radar sensor that could work all weather and day/night time. This system can transmit and receive the pulse to and from observe objects on ground surface, then its detailed figure or water vein location, output result as a microwave image could be obtained after some SAR image processing. SAR sensor needs special modulated signal especially chirp pulse for realization of high resolution and precise image. But, in the case of Unmanned Aerial Vehicle (UAV), Observation condition is always varying during flight or mission, therefore So some pulse parameter, like a i.e. bandwidth, and pulse duration, PRF etc, should be changed to adequate value each time simultaneously. This paper shows first step research of it, base chip pulse generator which can switch some preset output chirp signal. This paper discusses the proposed FPGA variable based Chirp pulse generator to solve the platform posture effect on our UAV SAR mission.

***Keywords*** **:** SAR, UAV, FPGA, Chirp pulse

## 1. Introduction

whole earth environment, including climate, temperature and land coverage is changing day by day. Recently, so called global warming problem accelerates these environmental changes. Of course this matter has potent influence on our human living, and sometimes appears as a disaster or any other environmental problem. So we must know two important factor about this environmental changes, precise detail of environmental changes and reason of it. Tectonic plate movement is key factor to understand environmental changes. Movement of tectonic plate never stop as long as all volcano on earth keep alive. It not only causes continual land deformation, but also has influence on our lives, land coverage, sea stream and climate. Earthquake is also one of the phenomenon caused by tectonic plate movement. As well known, earthquake gives serious damage to our lives in some country, especially located area called ring of fire around pacific ocean because the damage area is huge and we can't inhibit it. Therefore many researchers tried to manage to predict earthquake somehow. And recently, some method for earthquake prediction are still under research. We are also researching the relation between land deformation and earthquake. We use the microwave remote sensing technique to observe land deformation because microwave radar can get figure information which has only earth surface figure without any buildings and land coverage. Microwave radar which mounted on airplane or satellite can observe very vast area in short time so it's adequate for regular surveillance. Synthetic aperture radar called SAR is most popular system of microwave radar. SAR equips small and multiple separated antenna to improve resolution of observation, and generate one synthesis data from all data of small antenna as if getting from one huge antenna. In this system, resolution of range direction depends on signal characteristics used for observation. The more wide Frequency band become or the more higher pulse duration become, The more higher resolution also become. Therefore SAR system uses chirp signal which continuously changes its frequency as observation signal. When we use chirp signal for SAR system observation, we must consider to set some parameters of chirp signal because the most appropriate parameter of it depends on observation situation. Especially SAR which mounted on airplane is under very unstable condition, so we suggest to change the chirp signal parameters even during observation for more precise result. Therefore I tried developing chirp pulse generator which can change output signal parameters by using digital circuit which consists of FPGA and DAC. This device will use in

our SAR system to validate effectivity later, and in future I'll improve this to be able to change output in stand alone.

## 2. Methods

I designed chirp signal generator by using reconfigurable device, FPGA because it can make the time to configure and validate more shorter. I used two device, FPGA development board DE2-115 and data conversion card including DAC distributed by Terasic. (fig.1)

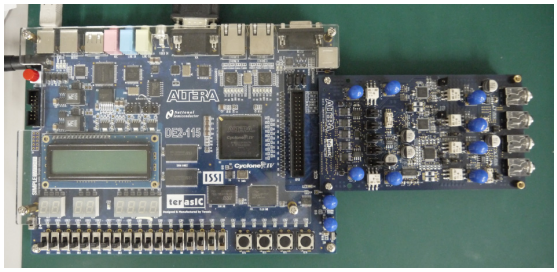

**Fig. 1 FPGA development board and DAC card**

I designed chirp signal generator by Direct Digital Synthesizer(DDS) method because this method is easy to change the output. This method uses both Tuning word LUT (Phase step value) and sine-wave LUT(amplitude value) to generate chirp signal. This time I set signal and DDS parameters as shown in Table 1 below. And whole logic structure is shown in Fig 2.

**Table. 1 Parameters of signal and DDS**

| Parameter | Preset-1 | Preset-2 | Preset-3 |
|---|---|---|---|
| Band width | 30MHz | 50MHz | 100MHz |
| Pulse duration | 0.5us | 2.0us | 4.0us |
| Number of sample | 125 | 500 | 1000 |
| Sampling rate | 250MHz | | |
| Quantization bit | 14bit | | |
| PRF | 1000 pulse /s | | |

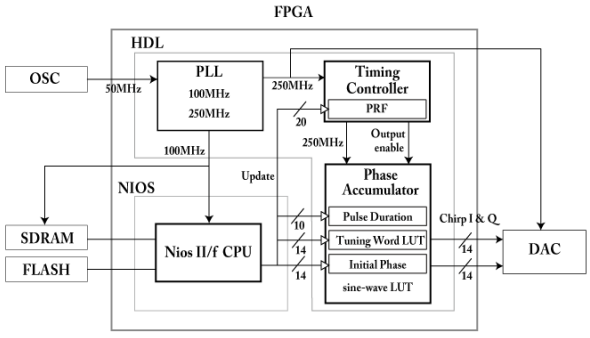


**Fig. 2 Block diagram of whole chirp generator**

## 3. Results and Discussion

Output signal waveform is shown in Fig 3 below.

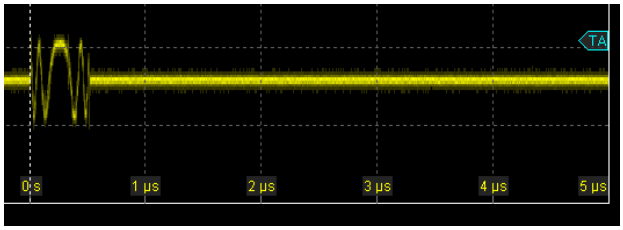


**(a) Preset-1 chirp signal**

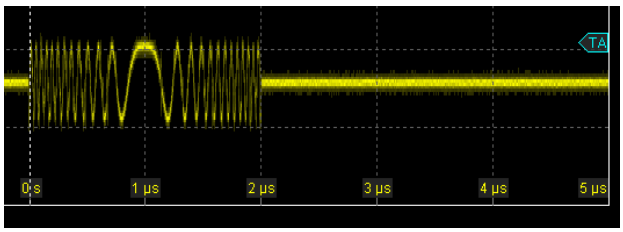


**(b) Preset-2 chirp signal**

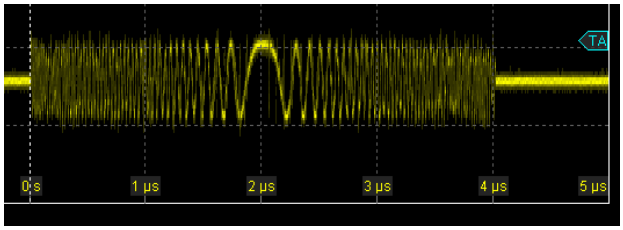


**(c) Preset-3 chirp signal**

**Fig. 3 Preset chirp signal on oscilloscope**

## 4. Summary

This is just result as a signal output. This means that the effectivity is not validated definitely. Therefore I must validate it by actual observation using SAR system and this device.

## Acknowledgements

I would like to express the deepest appreciation to my supervisor, Prof. J. T. Sri Sumantyo, Prof. V. C. Koo, Mr. W. G. Cheaw, and many researchers of Malaysia Multimedia University.

## References

1) J. T. Sri Sumantyo, V.C.Koo, 2012. Development of Circularly Polarized Synthetic Aperture Radar onboard UAV for Earth Diagnosis.

2) J. T. Sri Sumantyo, 2012. Development of Circularly Polarized Synthetic Aperture Radar Onboard Unmanned Aerial Vehicle (CP-SAR UAV).

3) M. Y. Chua, V. C. Koo, 2009. FPGA-Based Chirp Generator For High Resolution UAV SAR

# Microwave dielectric constant measurement of arid soil in the 0.3-3 GHz frequency range and interrelationship with land cover and soil types

Saeid Gharechelou[1], Ryutaro Tateishi[2], Josaphat Tetuko Sri Sumantyo[3]
1- PhD student, CEReS, Chiba University, Japan, e-mail: acfa3286@chiba-u.jp.
2- Professor, CEReS, Chiba University, Japan.
1-33 Yayoi-cho, Inage-ku, Chiba-shi, CEReS, Chiba University, Japan, post code: 263-8522.

## Abstract

Arid soils occupy around 12% of the Earth's ice-free land area. Aridisols are used mainly for range, wildlife, and recreation, because of the dry climate in which they are found. There are several methods to measurement the soil moisture in field and in laboratory experiment such as the dielectric constant and microwave remote sensing, the time domain reflectance (TDR) and gravimetric method. The purpose of this paper is to develop expressions for characterizing of the relative dielectric constant of arid soils in the 0.3-1.3-GHz frequency range and it interrelationship with soil types and land cover. In this study the first tried to took the field sample from top soil (0-15 cm) in homogeneous area in land unit map which provided in environmental GIS data base in arid region of Iran, and then measurement the dielectric constant at microwave remote sensing laboratory for investigation the characteristics and behaviors of dielectric constant of arid soil with variety of moisture content and soil fraction in 0.3 – 3 GHz frequency range. The result of dielectric constant properties has shown the soil types after the moisture content has most affected on the constant and then soil salinity. Land cover also has good agreement by dielectric constant in each level of soil moisture content even in same soil type, for example sparse vegetation and bare land both was in clay soil type but sparse vegetation recorded higher dielectric constant than bare soil. For soil salinity observed the in same soil type and moisture content saline soil has shown higher constant.

***Keywords*** **:** microsatellite, UAV, payload, mission

## 1. Introduction

Soil moisture plays the important role in environmental science such hydrology, agriculture, meteorology, etc. Arid soils occupy around 12% of the Earth's ice-free land area. Aridisols are used mainly for range, wildlife, and recreation, because of the dry climate in which they are found. There are several methods to measurement the soil moisture in field and in laboratory experiment such as the dielectric constant and microwave remote sensing, the time domain reflectance (TDR) and gravimetric method. In microwave soil moisture remote sensing determining the soil moisture by measured the value of dielectric constant is important, because the emissivity and back scattering coefficient of soil at each frequency is simulated and then driving the soil moisture on ground surface using satellite data. The dielectric constant depends on the type of material as well as its moisture state. The study area is located in arid area of Iran in northern part of central desert. The purpose of the study presented in this paper is to develop expressions for characterizing of the relative dielectric constant of arid soils in the 0.3-1.3-GHz frequency range and it interaction between soil moisture content, soil types and land cover.

## 2. Methods

In this study the first was tried to take the field sample from near top soil (0-15 cm) using GPS in homogeneous area in land unit map which provided in environmental GIS data base in arid region of Iran (Fig.1). Then measurement the dielectric constant of 40 soil samples at microwave remote sensing laboratory using dielectric constant tool kit of Agilent model. The measurement of dielectric constant down in 3 steps by change the moisture constant of each samples in the natural soil, dried soil and saturated soil finally oven soil (Fig.1). Thus, all data analyzed by integrated to other geo physical data in GIS such as land cover and soil type and soil salinity. Finally all data related to each sample position as spatial extracted in ArcGIS software and export to excel for statistical analysis.

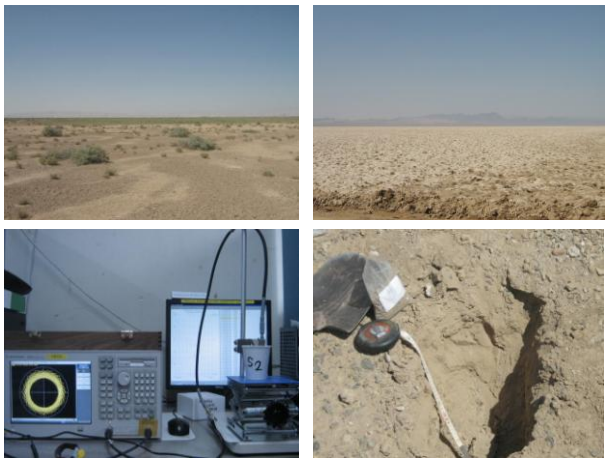

Fig.1. Field work in sparse vegetation, bare land for soil sampling and laboratory experiment

## 3. Results and Discussion

**I.** Dielectric measurement for the 0.3-1.3-GHz range

We was measurement more than 520 times for 40 samples of e' and the same for ***e"*** were made covering the range from 0.3 to 1.3 GHz especially for 1.27 GHz set on ALOS PALAR frequency for four soil types of sandy, silt, clay and loam under various moisture conditions. The first step in the analysis of the data was to compare the measured values with those calculated on the natural soil basis of the e' and e'' outlined the dielectric constant tool kit (Fig.2).

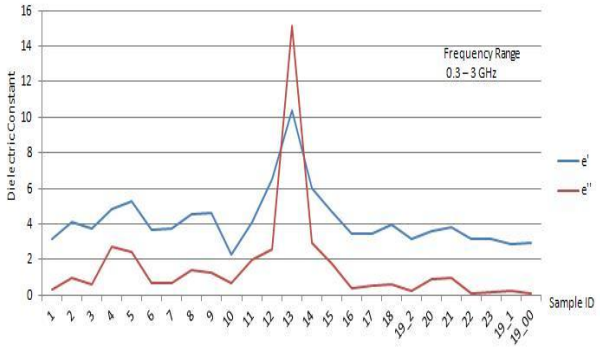


Fig.2. Shows measured values of e' and ***e"*** plotted at the 0.3-1.3-GHz range.

II. Dielectric dependency on soil types and land cover

The dependence of e' and e" on soil types composition (sand, silt, and clay) is a result of the role played by water storage in soil fraction particularly as boundary of soil particular. In the research, the soil types are comprised of four components: clay, silt, loam and sand and interrelationship with different land cover types and storage of water inside the soil that we could observed it. The total water volume fraction (m) which affected directly on dielectric constant between soil saturated condition and bound water in wilting point is administered by the specific surface area A (in m2 /g) of the soil particles. The surfaces (A) composed predominantly of clay that it depend directly to soil particle size and texture for example sandy soil has much more than clay soil. At result clay soil has more particle surface and could reserve much bound water and show the high dielectric constant than sandy soil, however other parameter such soil organic material and mineral are affected on it.

According to land cover types and interaction to soil types it seems the vegetation has important role to soil developing process and soil texture which it can influence to dielectric constant, for example sparse vegetation compare with bare land in study area show the higher dielectric constant (Fig.3) .

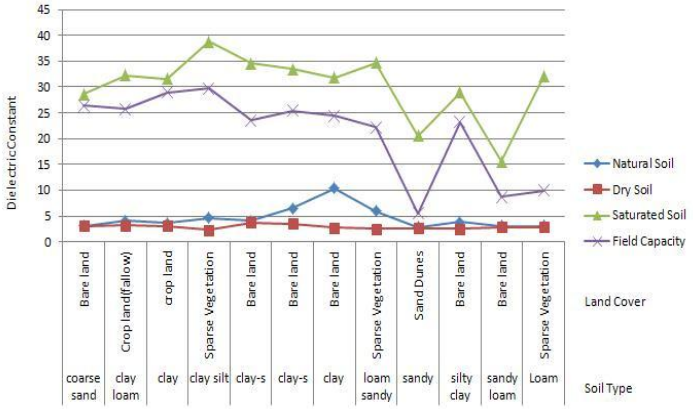


Fig.3. Dielectric constant properties and relationship in different moisture content, soil types and land cover.

## 4. Summary

The result of dielectric constant properties has shown the e' very sensitive than e" to soil moisture particularly for saline soil which could detect clearly. Soil types after the moisture content has most affected on the constant and then soil salinity, however the moisture content also dependent on soil texture and soil types. Land cover also has good agreement by dielectric constant in each level of soil moisture content even in same soil types. This information might be useful for backscattering simulation and modeling.

## References

1) E. Lee, T. N. Chase, B. Rajagopalan, R. G. Barry, T. W. Biggs, and P. J. Lawrence, Effects of irrigation and vegetation activity on early Indian summer monsoon variability, International Journal of Climatology, 573-581. 29 (2009).

2) Gadani . D. H., Vyas, A .D. Measurement of complex dielectric constant of soils of Gujarat at X- and C-band microwave frequencies, Indian Journal of Radio & Space Physics ,Vol. 37, June 2008, pp. 221-229.

3) Marttit, aillikainen, Fawwaz T. Ulaby, Myron C. Dobson, Mohamed A. El-Rayes, and Lin-Kunwu, Microwave Dielectric Behavior of Wet Soil-Part 1:Empirical Models and Experimental Observations, IEEE Transaction Geoscience and Remote Sensing, VOL. GE-23, NO. 1, January. 1985.

# The COTS-based Micro Earth Sensor(MESA) for small satellite to The Symposium on Microsatellites for Remote Sensing (SOMIRES 2013) and The 231th RISH Symposium

**Kazuo Tanimoto , Takanobu Omoto(Meisei Electric)**
**Hiroshi Tachihara(JAXA)**
**Takanobu Omoto ,omotot@meisei.co.jp**

## Abstract

We introduce the COTS thermopile –based Earth Sensor(MESA) for Small Satellite .It have been developed by Japan Aerospace Exploration Agency (JAXA) ,and We Meisei Electric co.,ltd have took charge of electronics .The thermopile sensor is very popular for security and hearth equipment ,then it can be used with low cost and short delivery time .MESA has I2C interface for space craft system ,the electronics is very simple ,verl low power and very small size . It make the developing for space use altitude sensor low cost ,minimized developing schedule and very low resource . The 4pieses of multi-pixel array of thermopile are used for MESA , In fundamental developing phase , MESA have been tested and verified that it's performance is fine to detect Erath edge for satellite altitude control , and also the Flight Model complete now ,The Flight model is now in integration for Small satellite "SOCRATES" and it will be launched in 2013 .

***Keywords*** **:**COTS thermopile ,Earth sensor, Small satellite

## 1. Introduction

The Earth sensor is one of altitude detection sensor for spacecraft and it is good performance sensor for Earth pointing satellite such as Earth Observation Mission . There are some Earth sensor for space use ,but all of them are large size and high cost because of these have been developed for large size space craft .The small satellite has possibility to make activation of use of space ,especially Erath observation .

The Erath sensor which is small size ,low cost and short delivery is required for Erath observation mission now.

## 2. Methods

The COTS thermopile sensor is very popular for security and hearth equipment ,then it can be used with low cost and short delivery time .MESA use the 4pieses of multi-pixel array of the COTS thermopile sensor .The points of MESA developing is follows .

(1) Selection of sensor device

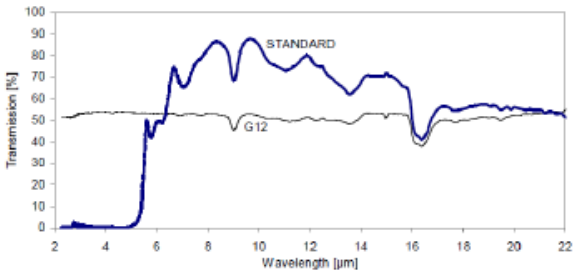


Fig2-1:Caracterlistics of Rends

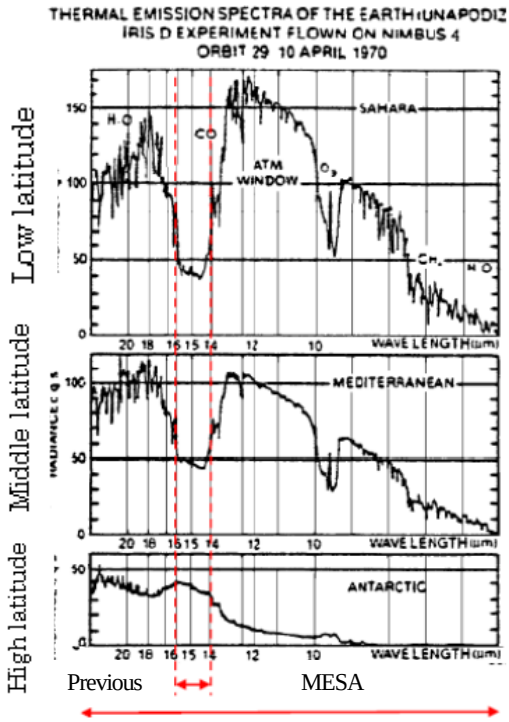


Fig2-2:Wave length distribution of infrared radiation

(2) Methods for Earth edge detection

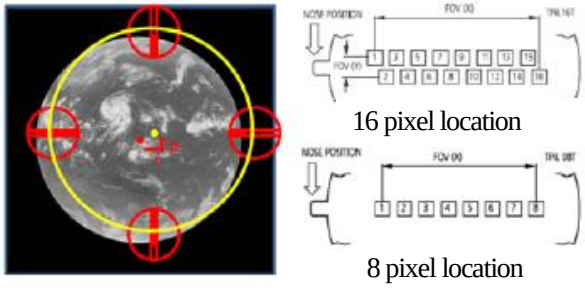


Fig2-3:Pixel location

(3) Study structure to minimize components size .

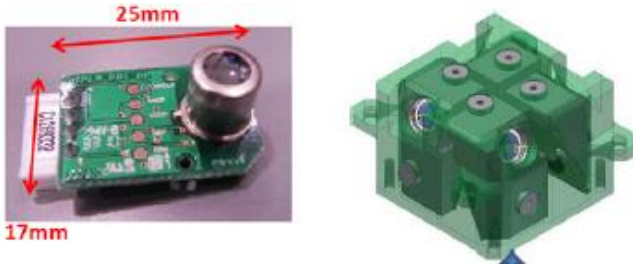


Fig2-3:Over view of thermopile device

## 3. Results and Discussion

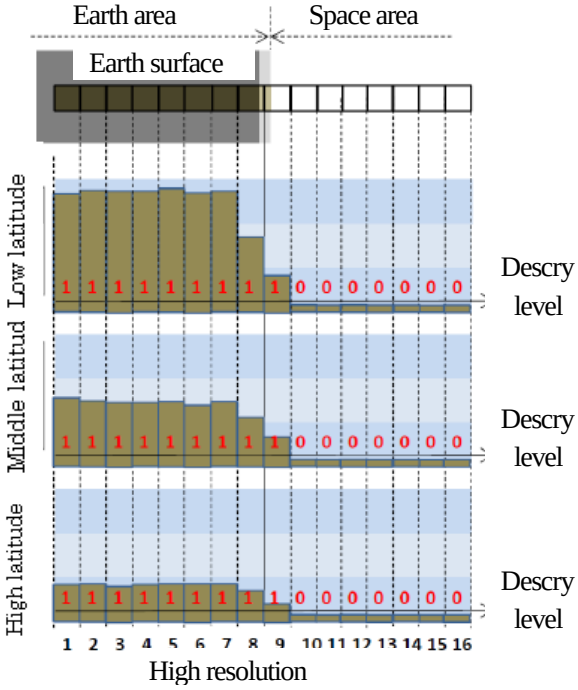


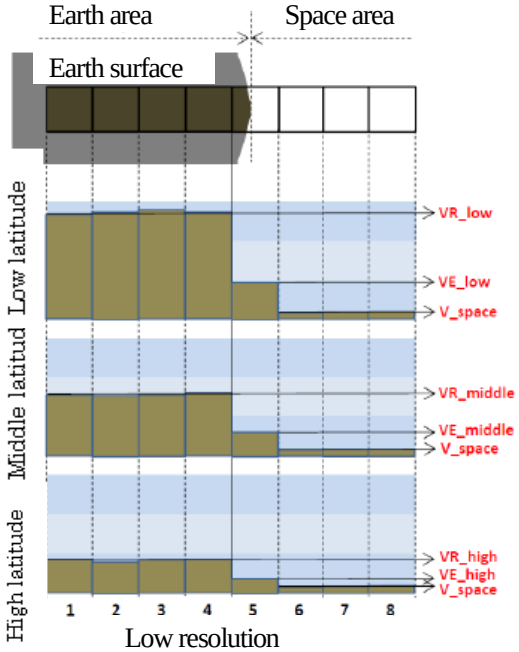


Fig3-1:Detection of Earth edge

## 4. Summary

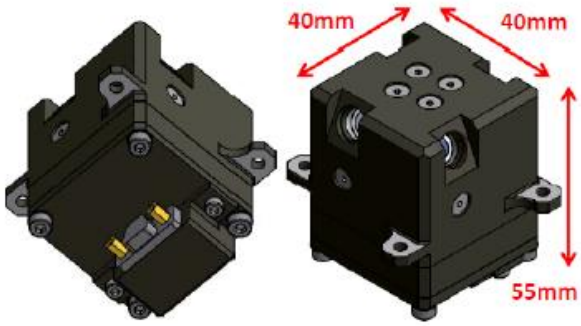


Fig4-1:Over view of Flight model

**Acknowledgements**

This symposium is sponsored by Center for Environmental Remote Sensing (CEReS), Chiba University and Research Institute for Sustainable Humanosphere (RISH), Kyoto University

**References**

1)3M14 Development of COTS thermopile based Earth Sensor for Small Satellite by JAXA

# Allometric modeling for biomass estimation in remote sensing

**Ali Reza Sharifi and Jalal Amini**
*Department of Geomatics Engineering, University of Tehran*
*Tehran, Iran*
*Email: jamini@ut.ac.ir*

## Abstract

This research develops an allometric model for estimation of biomass based on the height and DBH of trees in the forests of Iran. Without an accurate allometric model, we can't estimate true biomass from SAR images. After extensive field investigations, 124 trees are selected from the 4 different dominant tree species for the development of an allometric model covering the wide range of DBH and height classes. Twelve commonly used allometric models, three generic models and a proposed model are tested and the most suitable model is selected based on some of the commonly measured statistical parameters (coefficient of determination ($R^2$), RMSE, Mean Error, Underestimated Error, and Overestimated Error). We show that the biomass estimation accuracy is improved in a multilayer perceptron neural network (MLPNN) when the density of woods and the tree measurements are used in combination compared to estimating the biomass by classic allometric models.

## 1.Introduction

The most suitable method for biomass estimation is remote sensing, as this technique is usually better than traditional field-based methods when considering time, costs, and feasibility (Brown et al, 1989, Calama et al, 2008), although it is probably less accurate (Ketterings et al, 2001, Zianis and Mencuccini 2004). However, the problem of the remote sensing-based biomass estimation is that remotely sensed data do not directly estimate the amount of biomass present in a forest (Mette et al, 2004). Field AGB is necessary for comparing the result of remotely sensed methods in biomass estimation. In general, field AGB is calculated using the allometric equations based on the measured DBH and/or height or from the conversion of forest stocking volume. Regression models have commonly been used to relate field measurements to remotely sensed observations obtained via optical and radar sensors (Brown et al, 1989, Mette et al, 2004). Thus, field measurement of forest biomass remains necessary for remote sensing of biomass estimation, and the accuracy of remote sensing techniques largely depends on the accuracy of ground data (Brown et al, 1989).

The method of field based biomass measurement can be divided into two groups i.e. direct and indirect (Overman et al, 1994). The direct method involves the complete harvesting of sample plots and subsequent extrapolation to an area unit (Araujo et al, 1999, Charru et al, 2010). The indirect method aims to construct a functional relationship between tree biomass and other tree dimensions, such as stem diameter, height and wood density, by means of regression analysis (Brown et al, 1989, Henry et al, 2010, Knapic, 2011). Since the direct method is very time consuming, costly and completely destructive, and biomass expansion factors (BEFs) are complex in nature, field observations of biomass are normally based on allometric models that approximate the biomass of the tree component or the total biomass of single trees according to easily measured variables, such as diameter at breast height (DBH) or height (Ketterings et al, 2001, Pilli et al, 2006).

## 2.Modeling

The relationship between the physical parameters (DHB or/and height) and the AGB of all harvested sample trees needed to be established in order to estimate the AGB of non-harvested trees. Although there are several empirical methods available, this study established this relationship using allometric equations because an allometric model is a useful tool which can approximate the AGB of single trees according to easily measured variables, such as diameter at breast height (DBH) or height (H) (Overman et al, 1994, Brown, 1997, Araujo et al, 1999, Ketterings et al, 2001, Montagu et al, 2005, Pilli et al, 2006(.

The most common allometric model in biomass studies takes the form of the power function (Brown, 1997, Ketterings et al, 2001, Zianis and Mencuccini, 2004, Pilli et al, 2006) as follows:

$$AGB = a.\ (DBH)^b \qquad (1)$$

Where *AGB* is the total above-ground biomass, *DBH* is the diameter at breast height, *a* and *b* are the scaling coefficient and scaling exponent, respectively. In most cases, the variability of *AGB* is largely explained by the variability of *DBH*. However, the values of *a* and *b* are reported to vary with species, stand age, site quality, climate, and stocking of stands (Ketterings et al, 2001, Zianis and Mencuccini, 2004), and the most common problem with allometric equations as that the raw data are non-linear and tend to be heteroscedastic.

As such, the equation 1 cannot satisfy the relationship between AGB and the DBH. Hence, the standard method for obtaining estimates for the coefficients *a* and *b* ns by the least-squares regression for *D* and *M* measured from destructively sampled trees which represent the diameter range within the stands under investigation (Zianis and Mencuccini, 2004, Pilli et al, 2006), and the form of the model will be as follows (2):

$$ln\ (AGB) = In\ (a) + b.\ In\ (DBH) \qquad (2)$$

This transformation is appropriate when the standard deviation of *AGB* at and *DBH* increases in proportion to the value of *DBH* in many cases, log-transformation of real data results in homoscedasticity of the dependent variable *AGB*, a prerequisite for regression methods. However, even though the linear relationship of equation 2 mathematically equivalent to equation 1, they are not identical in a statistical sense (Zianis and Mencuccini, 2004) and this transformation introduces a systematic bias that is generally corrected using a correction factor estimated from the standard error, but it has become conventional practice in allometric studies (Niklas, 2006).

Different types of regression models and combinations of parameters have been used including ordinary least squares on log-transformed data (Overman et al, 1994, Montagu et al, 2005, Pilli et al, 2006, Arevalo et al, 2007), weighted least-squares regression on log-transformed variables (Arevalo et al, 2007), and non-Iinear regression (Saint-Andre et al, 2004, Murali et al, 2005, Arevalo et al, 2007). However, apparently there is no single optimal regression model that can give a good calibration function for the estimation of AGB because the values of coefficients are varied based on many factors (Ketterings et al, 2001 and Zianis and Mencuccini, 2004). Considering this situation, this paper tested different types of regression models for North of Iran including linear and non-linear, but most emphasis was placed on the methods of Brown et al, (1989), Brown et al, (1997) and Chave et al, (2005) as the work of these three researchers used in recently remote sensing researches for estimation of biomass from SAR images (Amini and Sumantyo, 2009, Englhart et al, 2011, Saatchi et al, 2011, Carreiras et al, 2012, Englhart et al, 2012). Finally, proposed method was done with an MLPNN. A multilayer neural network is made up of sets of neurons assembled in a logical way and constituting several layers.

**Refernces**

**Brown**, S, Gillespie, A J R, and Lugo, A E, (1989), Biomass Estimation Methods for Tropical Forests with Applications to Forest Inventory Data, Forest Science, 35, pp 881-902.

**Calama**, R., Barbeito, I., Pardos, M., del Río, M. and Montero, G. 2008. Adapting a model for even-aged Pinus pinea L. stands to complex multi-aged structures. For. Ecol. Manag., 256(6): 1390–1399.

**Ketterings,** Q M, Coe, R, van Noordwijk, M, Ambagau, Y, and Palm, C A, (2001), Reducing uncertainty in the use of allometric biomass equations for predicting above-ground tree biomass an maxed secondary forests, *Forest Ecology and Management*, 146, pp 199-209.

**Zianis, D** and Mencuccini, M, (2004), On simplifying allometric analyses of forest biomass, *Forest Ecology and Management*, 187, pp 311-332.

**Mette**, T, Papathanassiou, K, Hajnsek, I, Pretzsch, H and Biber, P, (2004), Applying a common allometric equation to convert forest height from Pol-InSAR data to forest biomass, *Geoscience and Remote Sensing Symposium, 2004 IGARSS 2004 Proceedings 2004 IEEE International*, 1, pp 269-272.

**Overman**, J P M, Watt, H J L, and Saldarriaga, J G, (1994), Evaluation of Regression Models for Above-Ground Biomass Determination an Amazon Rainforest, *Journal of Tropical Ecology*, 10, pp 207-218.

**Araujo**, T M, Hnguchn, N, and Junior J Ade C, (1999), Comparison of formulae for biomass content determination in a tropical ram forest site in the state of Para, Brazil Forest Ecology and Management, 117, pp 43-52.

**Niklas**, K J, (2006), A phyletic perspective on the algometry of plant biomass partitioning patterns and functionally equivalent organ-categories, *New Phytol*, 171, pp 27-40.

# Doppler Centroid Ambiguity Analysis for High Resolution SAR Imagery Sensors

Salar Gharibi , Jalal Amini
*Department of Geomatics Engineering, University of Tehran*
*Tehran, Iran*
*E-mail: salar.gharibi@ut.ac.ir*
*Email: jamini@ut.ac.ir*

**Abstract**
Attitude errors are significant for space borne SAR. The main effects of attitude errors are to decrease the SNR and increase the ambiguities in the image. To maximize the SNR and minimize the ambiguity ratio, it is desirable to centre the antenna beam on the target area being imaged. If there is an error in the knowledge of the antenna beam pointing direction (resulting from satellite attitude errors or any other cause), the target area being imaged will be shifted with respect to the antenna beam. This means that the image being formed is not centered about the centre of the antenna beam [1,2]. To solve these problems in azimuth, it is common to determine where the antenna is pointing after the fact using Doppler centroid techniques. In this paper, we show the maximum available standard deviation of yaw and pitch angles of local coordinate system of SAR for Unambiguous Doppler centroid frequency is a function of carrier frequency, look angle, altitude of satellite, PRF and squint angle. We also show when the satellite using yaw steering technique, errors in look angle and altitude do not affect Doppler centroid ambiguity and maximum available errors for yaw and pitch angles of local coordinate system of SAR sensor will be optimum.

**Material and Method**

Doppler centroid frequency for circular orbits [4].To satisfy the above condition (to avoid incorrect able ambiguity) Standard deviation of Doppler centroid frequency with confidential interval of %95 must be lesser than half of the PRF; thus we have:

$$\sigma_{Dop}(\%95) < \frac{PRF}{2} \qquad (1)$$

Doppler centroid frequency is the function of local attitude and altitude of SAR sensor. Having considered that these parameters are independent, standard deviation of Doppler centroid frequency will be:

$$\sigma_{f_{Dop}} = \sqrt{(\frac{\partial f_{Dop}}{\partial \gamma}\sigma_{\gamma})^2 + (\frac{\partial f_{Dop}}{\partial \delta_a}\sigma_{\delta_a})^2 + (\frac{\partial f_{Dop}}{\partial H}\sigma_H)^2} \qquad (2)$$

Where $\sigma_\gamma$ is standard deviation of look angle, $\sigma_{\delta a}$ is standard deviation of change of squint angle caused by yaw and pitch angle errors of local coordinate of SAR sensor and $\sigma_H$ is standard deviation of satellite altitude. The following conditions are considered in our simulation:

1) Satellite is sun synchronize

2) For eliminating earth rotation effect on Doppler centroid frequency, satellite pointing in Yaw Steering mode [4].

3) Squint angle (a) calculated by following equation: $a=a_0+\delta_{a0}-\delta_a$ where $a_0$ is squint angle in yaw steering mode, $\delta_{a0}$ is change of squint angle which is arbitrary, $\delta_a$ is change of squint angle caused by yaw and pitch angles of local coordinate angle of SAR sensor.

4) We know that yaw and pitch angles of local coordinate system of SAR sensor have only an influence on the along-track parameter $x_p$ [5] :

$$x_p = R.\left[\tan(\Psi).\sin(\gamma) + \tan(\delta).\cos(\gamma)\right] \qquad (3)$$

Where $\gamma$ is Look angle, R is slant range to middle of swath width, $\Psi$ and $\delta$ is yaw and pitch angle of local coordinate system of SAR sensor, respectively. If $\delta_a$ is a function of Yaw and Pitch angle of local coordinate system of SAR; thus:

$$\tan(\delta_a) = \frac{x_p}{R.\sin(\gamma)} = \tan(\Psi) + \frac{\tan(\delta)}{\tan(\gamma)} \qquad (4)$$

If: tan ($\delta_a$) ≈ $\delta_a$; tan ($\Psi$) ≈ $\Psi$; tan ($\delta$) ≈ $\delta$; thus, we have:

$$\delta_a = \Psi + \frac{\delta}{\tan(\gamma)} \quad (5)$$

$$\sigma_{\delta_a} = \sqrt{\sigma_\Psi{}^2 + (\frac{\sigma_\delta}{\tan(\gamma)})^2} \quad (6)$$

Having considered conditions mentioned above, we illustrate graphs (Fig. 1) of maximum available standard deviation of yaw and pitch angles of local coordinate system of SAR for Unambiguous Doppler centroid frequency as a function of carrier frequency, look angle, altitude of satellite, PRF and squint angle. We also conclude that when the satellite using yaw steering technique, errors in look angle and altitude do not affect Doppler centroid ambiguity and maximum available errors for yaw and pitch angles of local coordinate system of SAR sensor will be optimum.

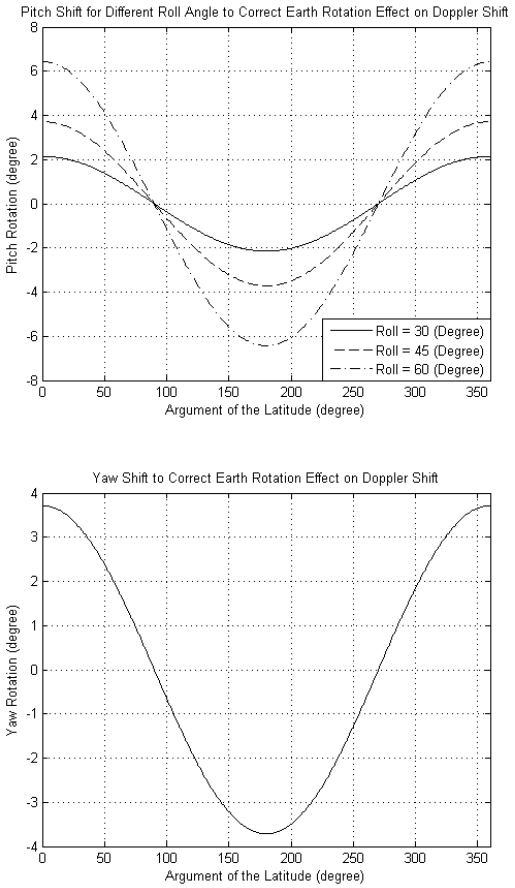


**Fig 1. Effects of Pith and Yaw angles on the Unambiguous Doppler centroid frequency**

# References

[1] D. Bickel, B. Brock, C. Allen, and S. N. Laboratories, *Spaceborne SAR Study: LDRD 92 Final Report*: Sandia National Laboratories, 1993.

[2] F. K. Li, D. N. Held, J. C. Curlander, and C. Wu, "Doppler parameter estimation for spaceborne synthetic-aperture radars," *Geoscience and Remote Sensing, IEEE Transactions on*, pp. 47-56, 1985.

[3] B. Barber, "Theory of digital imaging from orbital synthetic-aperture radar," *International Journal of Remote Sensing*, vol. 6, pp. 1009-1057, 1985.

[4] R. Raney, "Doppler properties of radars in circular orbits," *International Journal of Remote Sensing*, vol. 7, pp. 1153-1162, 1986.

[5] A. Hein, *Processing of SAR data: fundamentals, signal processing, interferometry*: Springer Verlag, 2004.